LA-5979-SR
Status Report

UC-38 and UC-66c

Issued: February 1977

Rapid Excavation by Rock Melting

-- LASL Subterrene Program --

September 1973—June 1976

Compiled by

R. J. Hanold

Contributors

J. H. Altseimer
P. E. Armstrong
H. N. Fisher
M. C. Krupka

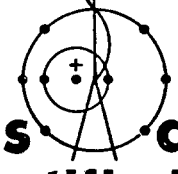

los alamos
scientific laboratory
of the University of California
LOS ALAMOS, NEW MEXICO 87545

Affirmative Action/Equal Opportunity Employer

UNITED STATES
ENERGY RESEARCH AND DEVELOPMENT ADMINISTRATION
CONTRACT W-7405-ENG. 36

DISCLAIMER

This work was supported by a grant from the National Science Foundation, Research Applied to National Needs (NSF-RANN) and by the US Energy Research and Development Administration, Division of Geothermal Energy.

Printed in the United States of America. Available from
National Technical Information Service
U.S. Department of Commerce
5285 Port Royal Road
Springfield, VA 22161
Price: Printed Copy $5.00 Microfiche $3.00

CONTENTS

RAPID EXCAVATION BY ROCK MELTING

-- LASL SUBTERRENE PROGRAM --

September 1973 — June 1976

Compiled by

R. J. Hanold

Contributors

J. H. Altseimer
P. E. Armstrong
H. N. Fisher
M. C. Krupka

ABSTRACT

Research has been directed at establishing the technical and economic feasibility of excavation systems based upon the rock-melting (Subterrene) concept. A series of electrically powered, small-diameter prototype melting penetrators has been developed and tested. Research activities include optimizing penetrator configurations, designing high-performance heater systems, and improving refractory metals technology. The properties of the glass linings that are automatically formed on the melted holes have been investigated for a variety of rocks and soils. Thermal and fluid-mechanics analyses of the melt flows have been conducted with the objective of optimizing penetrator designs. Field tests and demonstrations of the prototype devices continue to be performed in a wide range of rock and soil types.

Primary emphasis has been placed on the development of a penetrator designed for more economical extraction of geothermal energy and of small-diameter penetrators which can be utilized in support of geothermal energy exploration programs. The conceptual design of a geothermal energy rock-melting system will define the surface equipment, the stem, hole-forming assembly, and debris removal subsystems. Optimization of well design, the trade-off of advance rate with operating life, the advantages of using the melt-glass hole casing for well-bore seal-off, rig automation, and the benefits which result from the insensitivity of rock melting to formation temperatures and geologic variations have also been studied.

Subsystem hardware development has been directed toward resolution of critical technical questions related to penetrators for dense rock, debris handling, electrical heater configuration, and establishing penetrator life. Laboratory experiments and field tests provide data for final system design optimizations and indicate proof of applicability of the concept to a geothermal well hole-forming system. A field test unit to form relatively shallow vertical holes for heat flow surveys in support of geothermal exploration studies has been designed, fabricated, and field tested. Experience with this unit is intended to provide a basis for technology transfer to the drilling industry.

Practical applications to deep geothermal drilling will require an extensive development program in collaboration with the drilling industry. Progressive steps via smaller systems can potentially speed the transfer process.

I. INTRODUCTION AND SUMMARY

A. Objectives

The technical efforts and resources of the LASL rock-melting (Subterrene) program have been distributed to yield a balance of prototype hardware of increasing complexity and size, laboratory experiments, practical field-test experience, design and economic analyses, electric heater development, materials development and applications, and theoretical studies. The results of these technical activities were planned to yield:

- The demonstration of the basic feasibility of rock melting as a new excavation tool for applications up to 400 mm (16 in.) in diameter.
- Operational and field-test data from prototype devices of a range of sizes and configurations, and the verification of preliminary theoretical modeling needed to scale to larger diameters, predict performance, make cost estimates, and optimize advance rate and reliability.
- Refractory materials technology sufficiently established to permit predictions of component life and to generate materials selection criteria for prototype development needs and projections of service life for systems in practical applications.
- Field-test experience and operational demonstrations sufficient to exhibit the potential utility of smaller diameter prototype devices and to project commercial use in the important practical applications of geothermal energy exploration programs, economical extraction of geothermal energy, and shallow horizontal hole emplacements in loose or unconsolidated materials.
- Theoretical models and analytical techniques needed to describe the heat transfer and fluid mechanics of the rock-melting and penetration processes for the purposes of optimizing configurations, and predicting performance.

B. Technical Approach

The technical effort is organized into four technical activity areas whose functions are:

- Prototype Design and Test
- Power Source Design and Directed Research
- Field Test and Demonstrations
- Systems Analysis and Applications.

The significant results and achievements in the research and development program are summarized for each of these four technical activities in four major sections of this report for the period September 1973 to June 1976.

C. Summary

During the research period covered by this status report, a redirection of technical effort was initiated at the request of the program-sponsoring organizations. Efforts directed toward the application of rock melting to large-diameter tunneling systems were suspended. A vigorous research and development program leading to deep-drilling capability for geothermal energy systems was initiated including intermediate development of equipment for shallow exploratory holes, development of hole stabilization tools, development and test of hot rock penetrators for magma taps, and development of larger diameter shallow-hole devices for a variety of potential applications.

Extruding penetrator systems have demonstrated the basic features of rock-melt flow handling with debris produced in the form of chilled glass pellets, glass rods, or rock wool and carried out of the stem by the coolant gas flow. Two larger diameter (84- and 86-mm), higher advance rate, molybdenum extruding penetrator systems were designed, fabricated, and extensively tested in both laboratory and field tests. The first of these designs incorporates multiple heater stacks, multiple melt flow passages, and a penetrator configuration utilizing extended surfaces for enhanced heat transfer surface area. This penetrator was used with the new Experimental Field Unit (EFU) to produce a 30-m-deep hole in a basalt ledge near Los Alamos as a proof-of-concept experiment. The second design incorporates a more conventional melting body capable of producing thicker glass linings in dense rock, a single annular resistance heater which delivers a higher leading edge heat flux, and melt removal entirely through the central extrusion port. Significant improvements have been achieved in extruding penetrators, including improved coaxial-jet debris removal systems, higher

strength extractors, improved high-temperature operation and stability, and "designed in" instrumentation capability. The results from the successful testing of these extruding penetrator systems designed to investigate specific aspects of heater design, debris removal, and viscous rock-melt flow that will lead to higher penetration rates were analyzed to provide design considerations for future penetrator systems. Laboratory tests in Dresser basalt heated to 650 K confirmed the analytically predicted enhanced penetration rates in the hot basalt. Density consolidation penetrator designs have been developed to the stage where compressed-air-cooled, oxidation-resistant, easily replaceable penetrators are in satisfactory use for both laboratory experiments and field demonstrations in a wide variety of porous materials including tuff, alluvium, unconsolidated and layered sediments, saturated ground, and basaltic gravel. A high-temperature thermal stress rock fracturing probe based on rock-melting Subterrene technology has been developed and made available for rock mechanics and fracturing studies. A 114-mm-diam consolidating corer intended for use in porous alluvial soils has been designed, constructed, and laboratory tested. The core diameter is 64 mm, and the melting body, which is vacuum-arc-cast molybdenum, is fabricated as a single structural component.

The possibility of arranging the electric circuit of a rock-melting penetrator so that current passes through a molten region and deposits most of the melting power directly in the melt layer just adjacent to the melting interface has been recognized for a long time. This mode of rock melting has been investigated in recent laboratory experiments and analytical modeling calculations. The success of these preliminary experiments has initiated further experimental and analytical research to define the details of the heating mechanisms involved and the influence of the typical melt resistivity vs temperature behavior on the process. An experimental study of the feasibility of forming borehole plugs in underground salt deposits by melting and resolidifying salt similar to that found in the formation was conducted on the basis that a plug with physical and chemical properties close to those of the formation could be formed by this technique. Since melting and resolidification of rock salt causes practically no change in the chemical properties, emphasis was directed toward the resulting physical properties of the plugs prepared in this manner. Another technical approach investigated for Subterrene penetrators involves the application of plasma arc heating to increase penetration rates and handle the highest melting-point rocks. While the observation has been noted that a plasma torch readily melts a rock sample, little attention has been given to the task of providing a debris removal system for such a penetration device.

Resistively heated, pyrolytic-graphite heater elements, which radiate energy to the refractory metal penetrator body, have proven to be most satisfactory for the development efforts. With heater cavities filled with helium to enhance the radial heat transfer, heat fluxes of up to 2 MW/m^2 have been obtained from pyrolytic-graphite radiant-heater elements. Larger diameter annular-shaped pyrolytic-graphite heaters have been used to achieve higher leading edge heat fluxes in extruding penetrators, and heater stacks whose energy generation per unit length have been carefully matched to the penetrator requirements through the use of analytical modeling calculations are now routine. A new single-piece carbon cloth composite heater has been developed which allows greater flexibility in heater configuration and has been successfully tested in the thermal stress rock fracturing probe. Investigations of new designs have been initiated, including high-temperature liquid metal heat pipes, the direct melt-heating concept, and the use of higher resistance conduction heaters which would lead to solid penetrators of very high strength for use in deep wells. At the relatively high temperatures encountered by rock-melting penetrator systems, most materials react with one another to some extent, and thermodynamic and kinetic lifetime limitations have therefore been investigated. Static compatibility laboratory tests have been performed to determine the corrosion or dissolution reactions of molybdenum and tungsten with tuff, Jemez basalt, and granitic rocks at temperatures from 1700 to 2100 K. These experiments are designed to investigate quantitatively the effects of time and temperature on the reactions between refractory metals and rock-glass melts. Techniques for rock-glass property evaluation and optimization are under development with the goal of establishing rock-melt glass as an in situ structural element to serve as the hole

support during penetration. Laboratory experiments have confirmed a significant increase in crush strength and decrease in permeability for rock-glass liners when compared to the original porous materials from which they were formed in situ. Petrological examinations of parent rock and derived rock-glass samples have been performed. Correlation of petrographic information with physical properties and its extension to Subterrene design and performance is the desired goal. The melting ranges of approximately 15 different rock types were measured using hot-state microscopy. Penetrator fabrication technology has been vastly improved, particularly in the areas of refractory metal forming, the development of moderate-and high-temperature brazing techniques for dissimilar metals, and electron beam welding.

The field-test program was expanded with the design, construction, and utilization of two portable, modularized field-demonstration units (FDUs). These easily transportable units provided self-contained systems for demonstrating small-diameter rock-melting penetration system capabilities at locations away from the Los Alamos area and were mobilized for public demonstrations of the rock-melting process before large audiences in Washington, DC; Denver, CO; and Tacoma, WA. Such field evaluations of penetrator systems have served to acquaint excavation technologists with the potential of rock melting and have provided valuable data and experience on reliability and service life. Numerous penetrations into various unconsolidated soil samples, including layered samples formed from different loose materials, have been conducted to examine the resulting glass liners. The glass liners have been of good quality, and the smooth transition across the layered samples was particularly encouraging. The LASL-designed mobile experimental field unit (EFU) has been delivered, evaluated, and operated in the field on basalt penetration tests. This unit, which can be used with penetrators from 50 to 127 mm in diameter, consists of a trailer-mounted stem tower, hydraulic power supply, control functions, and a thruster that will support pipe stems 300 m long. The first field use of the EFU was in the production of a planned 30-m-deep hole in a basalt ledge at Ancho Canyon using 84-mm-diameter extruding penetrators. The basic concept of Subterrene systems for tunneling and excavating loosely compacted formations was demonstrated by an experiment conducted in the field using a field-demonstration unit. A prototype tunnel opening, 2 m high, 2 m deep, and 1 m wide, was formed in a loose alluvial dirt fill. The roof and side walls were formed by melting a series of parallel small-diameter horizontal holes in the loose soil fill using density consolidation penetrators. The holes were placed sufficiently close together that the glass linings fused and thus produced a double-walled lining reinforced by webs between the individual holes.

Efforts have been directed toward the development of new analytical and numerical techniques for analyzing the combined fluid dynamic and heat transfer performance of melting penetrators and the application of these techniques to specific penetrator designs and concepts. Numerical solutions of the coupled energy equation and the Navier-Stokes equations, including the strong temperature dependence of the rock-melt viscosity, have been obtained. Utilizing this viscous rock flow computer program, detailed calculations have been performed on a variety of consolidating and extruding penetrator systems. The validity of this powerful analytical tool has been established by comparisons with laboratory data, and design and scaling to larger diameters and different operating conditions can now be accomplished. Analytical techniques have also been extended to study the fluidized debris removal process in extruding penetrators. Calculations performed on extruding penetrator designs have also confirmed the significant penetration rate increases associated with increasing in situ rock temperatures and the general trend toward higher penetrator efficiencies with increasing penetration rate, both effects having been observed in the laboratory. Results from a two-dimensional heat conduction program have been instrumental in improving the thermal design of penetrator systems, particularly in the areas of desired heater performance, thermal control of the coaxial-jet debris removal zone, thermal control of the glass forming and conditioning zone, and in evaluating the thermal stress distributions and cooling requirements in critical penetrator regions. The development of analytical models has contributed to the basic understanding of specific relationships such as the leading edge flux limitations and the thrust-velocity dependence. Of major importance has been the theoretical calculation of material properties when the

experimental values were not appropriate or available. The application of these models and techniques to specific designs and the interpretation of test results have received the largest portion of the analysis program effort. Analytical calculations have also provided support for the laboratory experiments investigating new penetration techniques, including direct melt heating and plasma arc heating.

The number of novel and conventional potential applications of Subterrene technology that have been investigated continue to increase and range from deep hot rock penetrations for geothermal energy exploration and production to emplacements in arctic permafrost. The technology dissemination efforts expended by members of the Subterrene program have been extensive in both scope and depth. Of particular interest to the current program direction is a report entitled, "Geothermal Well Technology and Potential Applications of Subterrene Devices - A Status Review," which has been completed and distributed. This report reviews the past, present, and some future aspects of the geothermal energy industry with special attention given to geothermal well drilling problems.

A. Consolidation Penetrator Development

1. Introduction. For porous rock or soft ground, the density consolidation Subterrene can be used to simplify the excavation process. In these materials, the glass lining formed when the rock-melt cools, is significantly more dense and therefore occupies a smaller volume than did the original porous rock. By melting out to a diameter larger than that of the penetrator, the molten debris from the hole can be entirely consolidated in the dense glass lining, completely eliminating the necessity for removing debris. Density consolidation penetrator designs have been developed to the stage where compressed-air-cooled, oxidation-resistant, easily replaceable penetrators are used satisfactorily for both laboratory experiments and field demonstrations in a wide variety of porous materials, including tuff, alluvium, unconsolidated and layered sediments, saturated ground, and basaltic gravel.

2. Significant Technical Achievements.

- A prototype tunnel opening (described in detail in Sec. IV. A) was formed in loose alluvial fill using two different 50-mm-diam consolidating penetrator designs. These penetrator designs, which employ replaceable graphite glass formers, are illustrated in Fig. II-1. The solidified rock-melt layer which adheres to the molybdenum penetrator body and provides oxidation resistance is clearly visible. A considerable amount of operational field experience was obtained in this test as over 100 m of stabilized hole were formed in a loose fill including both vertical and horizontal penetrations.

- The ability of consolidating penetrators to produce glass-lined stabilized holes through variable, broken, and difficult rock samples was further verified by extensive testing in a wide variety of samples. Figure II-2 illustrates a hole melted in a conglomerate of Hanford alluvium containing basaltic gravel and large cobbles. Penetration of the largest cobbles without debris removal is achieved by thermal stress fracturing and extrusion of portions of the rock melt into the resulting cracks. The ability to provide a continuous glass lining across nonhomogeneous samples was demonstrated in tests in which samples comprised of layers of alluviums, shales, and tuff were penetrated and the resulting hole liners were removed and examined. A typical result from such a test is shown in Fig. II-3.

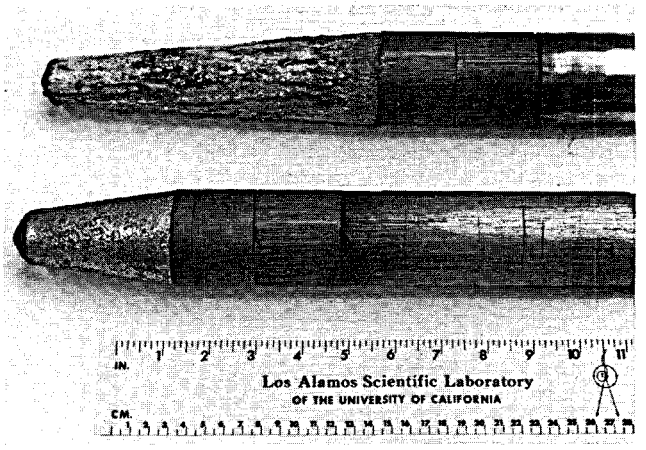

Fig. II-1. Consolidating penetrator designs used for melting prototype tunnel opening in loose alluvial fill.

Fig. II-2. Hole melted in a conglomerate of Hanford alluvium containing basaltic gravel and large cobbles with a consolidating penetrator.

Fig. II-3. Continuous glass liner produced through a layered sample of unconsolidated alluviums.

• A design study was conducted indicating the feasibility of an integrated 76-mm-diam extruder-consolidator hole-forming system. This proposed system would take advantage of the simplicity of consolidating penetrators, which eliminate the debris removal operation, for use in porous or low-density rocks and soils. If hard rock were encountered, the universal stem would permit changing to an extruding penetrator for hole advancement until soft ground conditions again prevailed. The emplacement of near-surface small-diameter utility lines represents the main application for such an integrated system.

• Detailed viscous flow calculations have led to the development of a penetrator geometry incorporating a parabolic leading edge segment joined to a cylindrical afterbody. The parabolic leading edge is designed to melt a hole out to the full radius of the penetrator while minimizing the necessary applied thrust for a given advance rate. The cylindrical afterbody melts the rock from the penetrator radius out to the radius required for complete debris disposal by density consolidation in the thick formed glass liner. This penetrator configuration is well suited for the use of high-temperature liquid metal heat pipes to increase the heat flux available at the leading edge for enhanced penetration rates. The conceptual design of a penetrator system incorporating these advanced features was completed.

• The analysis of consolidating penetrator performance has been extended to include the effect of mechanical compaction of the soil surrounding the melt zone. Calculations employing these methods show the dependence of consolidator penetration rates on soil density and mechanical compaction. Results indicate an extremely sharp drop in penetration rate with increasing soil density in the range of densities between 1.7 and 1.8 Mg/m^3. Penetration of soils with bulk densities greater than 1.8 by consolidating penetrators is very slow, and there is little possibility of significant mechanical compaction.

• Successful laboratory tests were conducted with a 50-mm-diam parabolic penetrator and a 60-mm-diam penetrator with a parabolic leading edge profile joined to a short cylindrical afterbody. Significant performance data were obtained from these tests, and penetration rates almost double the previous rates for the double cone configuration were achieved.

During the research period covered by this status report, technical effort was redirected at the request of the program-sponsoring organization. Efforts directed toward the development of density consolidation penetrators were terminated, and the program emphasis was placed on the development of hard rock extruding penetrator systems that could be applied to the exploration and production of geothermal energy.

B. Extruding Penetrator Development

1. Introduction. Extrusion penetrators are required in dense materials and are designed to continuously remove the debris from the borehole. As indicated in Fig. II-4, the melt flow, confined by the unmelted rock and the hot melting face of the penetrator, is continuously extruded through a nozzle in the melting face. This material is chilled and freezes shortly after the circulating cooling fluid impinges upon the extrudate exiting from the melt orifice. The flowing coolant then carries these small fragments up the stem to the exhaust section. Extruding penetrator systems have demonstrated the basic features of rock-melt flow handling with debris produced in the form of chilled glass pellets, glass rods, or rock wool. These penetrators have been operated in the laboratory and in the field, in vertical and horizontal orientations, and in both hard igneous rocks and porous tuffs and alluviums. Three larger diameter (84-to 89-mm), higher advance rate, molybdenum extruding penetrator systems were designed, fabricated, and tested. Significant improvements have been achieved in current extruding penetrators, including improved coaxial-jet debris removal systems,

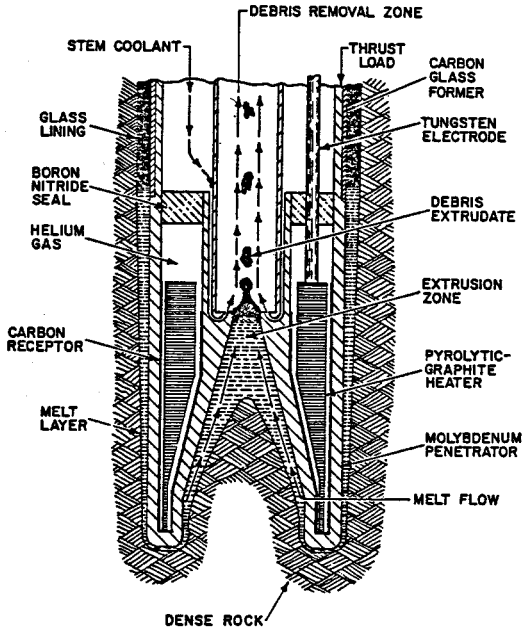

Fig. II-4. Extruding penetrator concept illustrating debris removal technique.

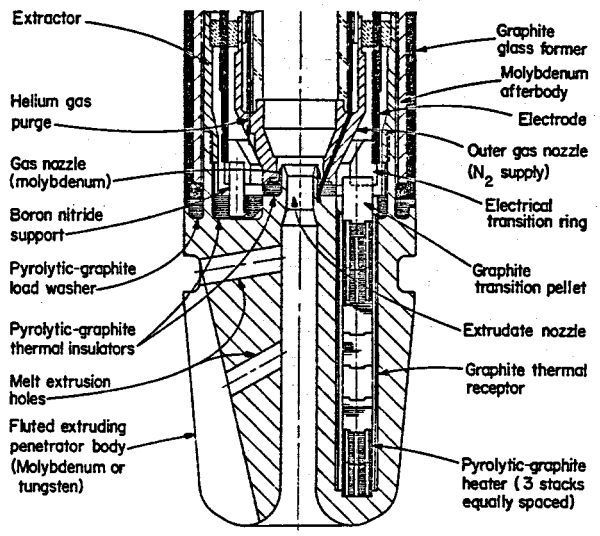

Fig. II-5. Cross section of the 84-mm-diam extended surface penetrator melting body.

improved high-temperature operation and stability, and "designed-in" instrumentation. A maximum penetration rate of 0.28 mm/s (3.31 ft/h) in dense basalt has been demonstrated in the laboratory.

2. 84-mm-diam Extended Surface Penetrator. This design introduced the concepts of multiple heater stacks, multiple melt flow passages, and a penetrator configuration using extended surfaces for enhanced heat transfer surface area. Based on the enhanced surface area, greater heater power, reduced operating melt layer thickness, and high thrust capability, this penetrator has melted hard rock at a significantly faster (~ 3X) rate than the earlier 66-mm design it replaces. Figure II-5 illustrates the major components of this penetrator design. The heater consists of three separate stacks of pyrographite resistance heater pellets and includes higher power density pellets near the leading edge to provide a higher heat flux in this critical region. Electrical power is supplied to the heaters by three tungsten electrodes. Energy distribution throughout the penetrator is accomplished by radiation from the surface of the heater stacks to the graphite receptors and then by conduction through the high thermal conductivity molybdenum melting body. Molten rock enters the rock nozzle from the axial and radial rock flow passages and is rapidly chilled by the high-velocity cooling gas exiting from the gas nozzle. The chilled debris is removed through the debris carry-off tube and transported to the surface by the gas stream. A portion of the cooling gas flow enters the debris carry-off tube through the gas orifices which provide a boundary layer of cool gas along the tube surface reducing its temperature and minimizing any tendency for the cooling rock melt to adhere to its surface. Actual 84-mm-diam hardware is illustrated in Fig. II-6. The upper penetrator is unused, whereas the lower unit was tested in basalt and retains its protective

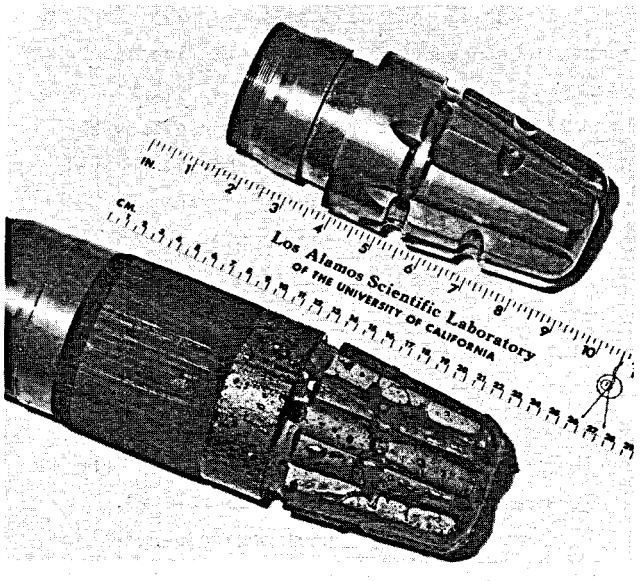

Fig. II-6. Extended surface penetrator hardware comparing an as-fabricated melting body with an assembly that was tested in basalt.

layer of solidified basalt melt. The fluted or extended surface configuration and the multiple melt removal passages are clearly visible in this photograph.

This 84-mm-diam extended surface penetrator was used to produce a 30-m-deep field hole in basalt (see Sec. IV. C. 3). Design changes based on field test experience have eliminated early difficulties encountered in the operation to produce this 30-m-deep hole. Rock intrusion has been eliminated by improved cooling of the glass-former region, and plugging of the debris carry-off tube has also been eliminated by improved cooling of the wall near the debris forming nozzle. The tube temperature is held below 650 K to prevent sticking of hot melt particles. This has been accomplished by a combination of increased gas flow and improved coolant passage design. Tests of this penetrator system incorporating a melt channel impedance, or surge suppressor, that increased the pressure in the molten layer have been successful in suppressing gas bubble production in the melt and have produced remarkably improved smooth glass borehole linings in addition to minimizing any tendency of the debris removal system to surge during transient operations. Surging occurs when a large melt pool is formed and the penetrator is suddenly pushed into it. This causes a large amount of liquid rock to extrude rapidly into the carry-off system. While the gas system can carry a considerable amount of rock in excess of the steady-state design, a severe surge can overload it. Successful operation of this debris removal system has been demonstrated in both vertical and horizontal orientations. In addition to operations in hard rock, this penetrator system has been tested in porous Bandelier tuff with encouraging results. The extrudate was ejected in short rods which were easily expelled from the system by the transport gas flow, and there was evidence that the penetration mode (i.e., extrusion or density consolidation) could be controlled by varying the gas flow rate to the extrusion nozzle and the heater power level.

3. High Advance Rate Extruder (HARE). The HARE design has a more conventional melting body capable of producing thicker glass linings in dense rock, a single annular resistance heater that delivers a higher leading edge heat flux, and melt removal entirely through the central extrusion port. The basic configuration of this penetrator corresponds to the design illustrated in Fig. II-4, depicting the concept of extruding penetrator operation. This design was based on the use of a large-diameter annular pyrographite heating element which would provide the maximum surface area for radiation heat transfer near the critical leading edge region. The annular design eliminates the azimuthal temperature variations present with the use of three separate heater stacks (as in the extended surface penetrator) and further enhances the leading edge heating since both the inner and outer surface of the heater can radiate with equal flux density. In addition, the molybdenum penetrator body thickness was held to 5 mm in this region to minimize the temperature drop resulting from heat conduction to the molten rock layer. Approximately half of the total heater power is developed in the thin constant area section embedded in the leading edge. Heater power is steadily reduced away from the leading edge where the melting power requirements of the penetrator are much less. This tailoring of the heater output is based on detailed computer calculations which are discussed in the analysis section of this report. Polycrystalline-graphite radiation receptors are used to improve the surface absorption characteristics of the heater cavity which is also filled with helium gas to provide additional conduction transfer across the narrow gap. Debris removal techniques in this penetrator system are completely analogous to those employed in the extended surface penetrator.

With an 89-mm-diam melting body, a HARE penetrator was operated in the laboratory at power levels of up to 24 kW and corresponding penetration rates in basalt rock up to 0.28 mm/s (3.31 ft/h) with debris-handling and glass-forming systems functioning properly. The calculated and experimentally measured advance rate vs power relationships are in excellent agreement. In addition to hard rock, HARE has been tested in compacted Hanford alluvium (packed density of 2.1 Mg/m^3) and produced a uniform glass wall approximately 12 mm thick using a longer temperature-controlled glass former. Earlier problems in producing a smooth glass borehole lining were largely attributed to the gases released from the rock during melting. A modification consisting of a long extrudate tube-nozzle system has been employed to alleviate this problem by controlling the back-

pressure at the glass-forming section thereby increasing the pressure in the melt layer and suppressing gas bubble production. Figure II-7 shows a HARE penetrator after testing in basalt.

4. Melt Flow Augmented Extruder. An attempt has been made to arrange the geometry of a penetrator in such a manner that hot molten rock is forced to flow past the leading edge and thereby prevent this region from cooling at higher penetration rates. A conceptual design is shown in Fig. II-8 to illustrate this technique. A melt reservoir is formed on the outside of the conical section and maintained under pressure by the applied thrust load. The pressure differential resulting from the debris removal causes the melt to flow forward past the leading edge. The hottest (and least viscous) rock flows most easily and carries a significant amount of energy forward to prevent cooling of the leading edge and vanishing of the melt layer thickness.

A new penetrator design that augments leading edge conduction heat transfer with forced melt flow has been developed and initially tested in an 86-mm-diam version. Heater configuration and debris removal system operation are based on the HARE design which has demonstrated successful performance in extensive laboratory testing. The penetrator assembly for this melt flow augmented extruder is illustrated in Fig. II-9 prior to testing. The melt flow passage is on the axis so that material melted near the perimeter of the hole must flow along the cone and over the leading edge in order to reach the exit

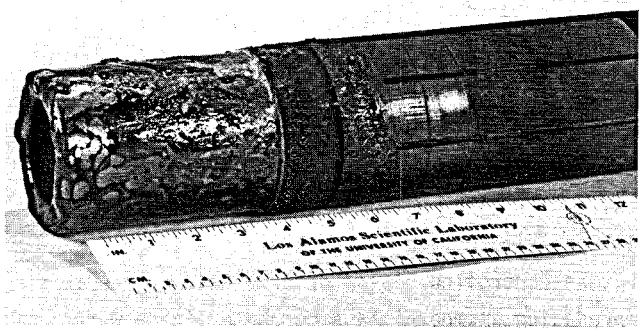

Fig. II-7. HARE extruder after several tests in basalt showing the molybdenum melting body with residual rock melt and the graphite glass former.

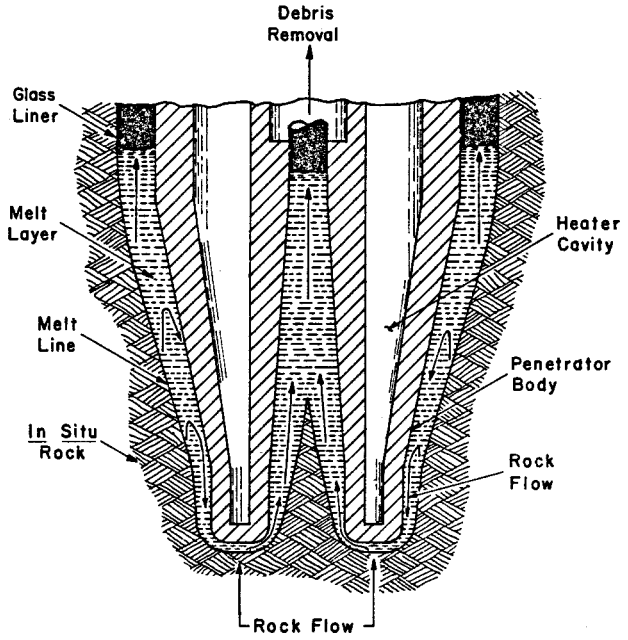

Fig. II-8. Conceptual design of a melt flow augmented penetrator.

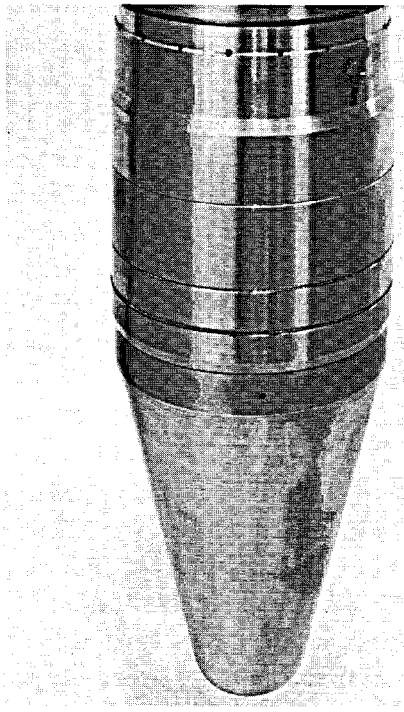

Fig. II-9. Melt flow augmented extruding penetrator with segmented molybdenum glass former.

passage. A segmented molybdenum glass former is employed. Tests showed that this penetrator can accept higher power levels at higher thrust loads with an increase in penetration rate without an increase in melting body temperature. In the initial testing, rates as high as 0.232 mm/s (2.74 ft/h) were attained.

The maximum velocity of the rock melt as it crosses the leading edge is approximately 200 times the penetration rate velocity. Despite this very appreciable velocity enhancement, absolute velocities are still quite low, and higher thrusts are required to provide this hydrodynamic pumping. Preliminary laboratory test data indicate that significantly higher melt velocities are required before any appreciable penetration rate increase can be realized as a result of melt flow augmentation. Further tests to better define the role of higher velocity rock melt flow in the leading edge region are planned.

5. Significant Achievements.

- All three new extruding penetrator systems have achieved penetration rates in excess of 0.2 mm/s. The HARE design was operated in the laboratory at power inputs of up to 24 kW with corresponding advance rates in basalt rock up to 0.28 mm/s (3.3 ft/h). Maximum penetration rates attained exceed those of the earlier 66-mm-diam design by a factor of 3 to 4.
- Efforts to develop advanced penetration systems capable of significantly higher advance rates have reached the laboratory experiment stage. Experiments relating to direct melt heating and plasma arc heating are in progress (see Sec. II. F. and II. H).
- Production of a 30-m-deep field hole in basalt has been completed with the 84-mm-diam extended surface penetrator operated from the experimental field unit (see Sec. IV. C. 3).
- As a proof-of-concept experiment for a geothermal energy prototype bit, an extruding penetrator system was used to melt a hole in a block of Dresser basalt preheated to 650 K. The results of this test were compared to another set of tests conducted at the same operating conditions with the exception of the basalt block temperature, which was at a normal ambient value of 290 K. The large specimen of Dresser basalt was surrounded with multiple electrical resistance heaters and brought to temperature over a 4-1/2-day heating period. Experimental data confirmed that the analytically estimated 25% increase in penetration rate in the hot basalt could be easily achieved. Results from this "hot rock" test have established that operation in very hot rock is feasible, and that enhanced penetration rate is an additional benefit.
- Data from a large number of laboratory and field tests have confirmed the operating performance maps and repeatability of the newer extruding penetrator systems. Typical of these data is the rate vs power relation implied by laboratory test data for the extended surface penetrator melting in basalt as indicated in Fig. II-10.
- Extruding penetrators have been used successfully to melt samples of basalt, granite, porous volcanic tuff, and compacted alluvium. Typical laboratory samples of basalt that have been penetrated in hardware development experiments are illustrated in Fig. II-11, which shows the resulting smooth-lined holes. A material particularly difficult to drill through by conventional techniques is high quartz-content granite gneiss. Samples of such a gneiss were supplied to the program from a quarry site in Virginia for melting experiments. Figure II-12 shows a hole melted in this granite gneiss by an extruding penetrator and some of the associated debris ejected in the form of short glass rods. Differences between typical basalt debris and the gneiss extrudate are attributed to the large difference in viscosity between the two glass melts and to the significant volume fraction of quartz crystals in the gneiss.
- Preliminary design of a larger diameter (150-mm) penetrator based upon the HARE configuration is in progress. The initial melting bodies will be made

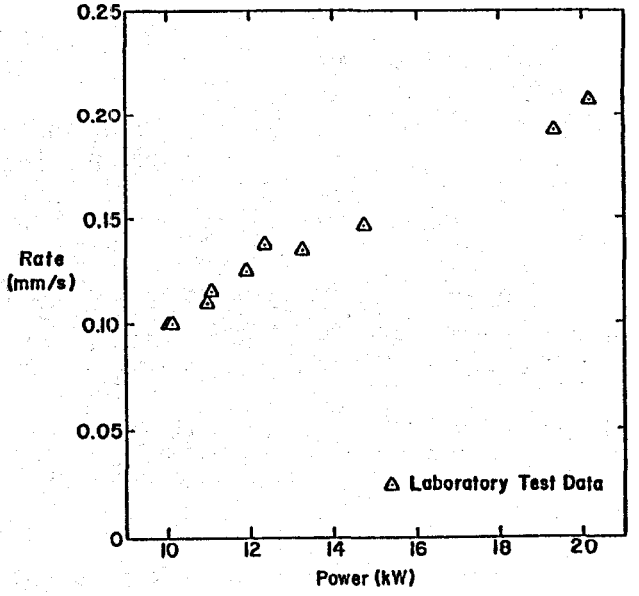

Fig. II-10. Rate vs power relationship for 84-mm-diam extended surface penetrator from laboratory tests in basalt.

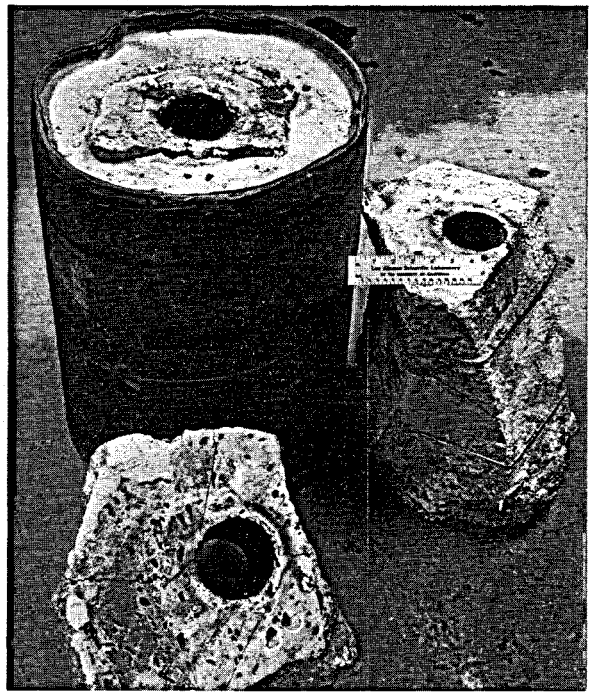

Fig. II-11. Extruding penetrator melted holes in typical laboratory samples of basalt.

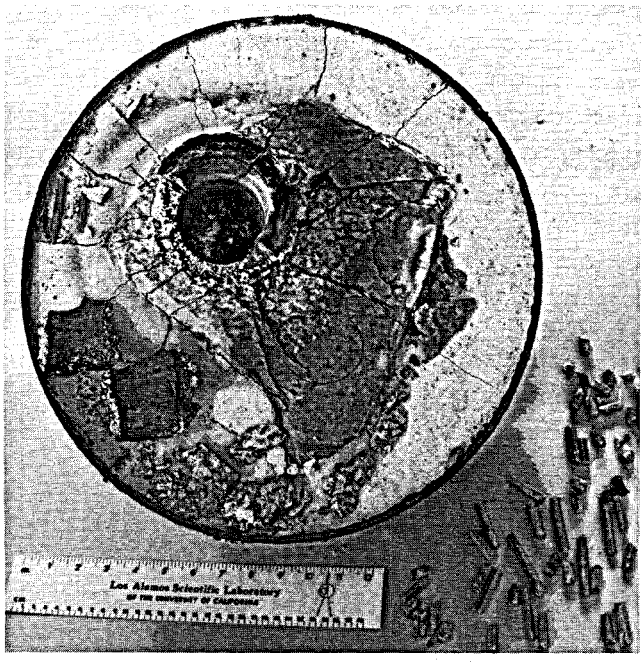

Fig. II-12. Hole melted in high quartz-content granite gneiss with extruding penetrator, including associated debris in the form of short glass rods.

from SiC-coated graphite which can be fabricated at a fraction of the cost of a refractory metal body. Laboratory tests indicate that this material will have a long enough lifetime for testing purposes, but it is not expected to be a practical material for production penetrators.

- Information from laboratory and field tests of extruding penetrator systems is being used to provide the basis for designs of larger diameter penetrator systems for high-pressure, deep-drilling geothermal energy applications.

6. Penetration Rate Paradox. Analytical calculations based on penetrator input power, calculated thermal fluxes, and available published transport properties of viscous rock melts have indicated the potential for appreciably higher penetration rates than could be attained in laboratory tests. While the basic agreement between the analytical calculations and the laboratory established penetrator performance data has been very good, two particular areas where this agreement breaks down have been noted. The first area of concern was that calculated penetrator thrust loads were considerably lower than those observed in actual tests. The second area of concern was the inability of penetrator systems to consistently achieve rates in excess of 0.25 mm/s with allowable body temperatures despite the fact that the analyses indicate higher rates should be possible with acceptable temperatures. Resolution of these discrepancies led to the investigation of molten rock thermal conductivities presented in detail in the analysis section of this report. The conclusion arrived at was that the thermal conductivity of molten rocks is appreciably lower than some data in the literature indicates. The source of the problem stems from correctly removing the thermal radiation contribution from the measured effective conductivity to arrive at the true thermal conductivity based only upon molecular conduction.

Using a value of 0.25 W/m·K for the thermal conductivity of molten basalt in the computer simulation program (this value is appreciably lower than the ones used in previous calculations), it becomes evident that the penetration rate of an extruding penetrator is limited by the heat flux that can be provided at the leading edge or flow stagnation point. Based on allowable temperatures in the molybdenum body, the new calculations indicate that the leading edge heat flux will restrict penetration rates in basalt to approximately 0.25 mm/s. This lower value of thermal conductivity also results in a thinner melt layer at the leading edge for the

same heat flux. A thinner melt layer necessitates higher thrust loads for penetration, and hence this also explains why the calculations with a higher thermal conductivity always underestimated the applied thrust load. Away from the leading edge, however, the conical shape of the melting body provides a significant geometrical enhancement and much higher penetration rates are possible. This concept was demonstrated in a laboratory test using a conical shaped penetrator melting into a basalt sample that was predrilled to remove the rock that would normally be melted by the leading edge region of the penetrator. With the penetrator body temperature below the operating maximum, sustained rates of just under 1 mm/s were attained. This represents a factor of 4 to 5 times the rate that would have been expected if the leading edge heat flux were controlling the rate. This conical penetrator and a section of the glass-lined hole in basalt that it produced are illustrated in Fig. II-13. Experimental confirmation of this analytically predicted result led to an intensive research program to introduce techniques for increasing the available leading edge heat flux.

Fig. II-13. Conical penetrator and hole melted at high rate in predrilled basalt sample.

C. Coring Penetrator Development

For applications such as geophysical prospecting, it is desirable to extract a relatively undisturbed core sample to identify the rock layers and fault structures at various depths. The Subterrene concept of rock penetration by progressive melting has been expanded to include a technique for obtaining geologically interesting core samples from the material being penetrated. The coring concept utilizes an annular melting penetrator which leaves a rock-glass encased core in the interior. Although the concept is applicable to either the extrusion or density consolidation mode of melt-handling, initial emphasis was placed on a consolidating-coring penetrator. A 114-mm-diam consolidating corer intended for use in porous alluvial soils has been designed, constructed, and laboratory tested. The core diameter is 64 mm and the melting body, which is vacuum-arc-cast molybdenum, is fabricated as a single structural component. The penetrator has a water cooling system which represents a departure from the conventional gas systems. Design power level is 13 kW, and initial testing was accomplished at 9 kW in tuff and alluvium with low thrust loads and penetrtion rates in the range from 0.05 to 0.15 mm/s.

During an initial test the penetrator assembly was allowed to cool in place after making a penetration into a volcanic tuff sample in the laboratory. After breaking away the rock sample and glass hole liner, the melting assembly is shown in place in Fig. II-14. The end of the core sample is visible leaving the core removal tube and a portion of the structural-glass hole lining can be seen behind the melting assembly. A typical segment of this external glass lining and a glass-encased core sample can be seen in more detail in Fig. II-15. The approximately 18-mm-thick glass hole lining results from debris disposal by the combined mechanisms of core removal and density consolidation.

Although the periphery of the core sample will be melted and an additional region will be thermally altered, the interior region can be preserved when the penetrator is operating at the correct design conditions. This is illustrated in Fig. II-16, which is a cross section of a Subterrene-produced core in Green River shale. The dark melted peripheral region can be clearly distinguished from the soft shale remaining in the interior. This unique ability

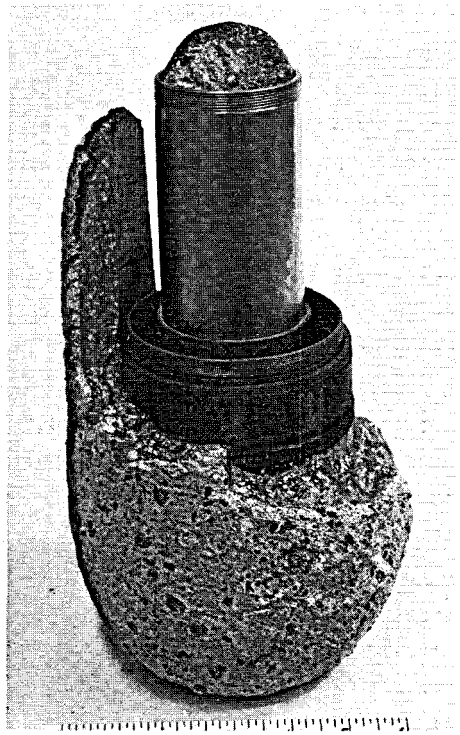

Fig. II-14. Melting assembly of coring penetrator at completion of test showing formation of glass hole lining and emerging core sample.

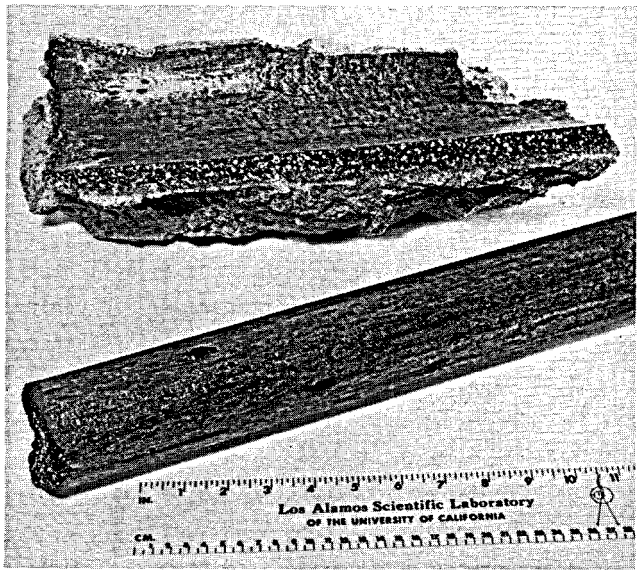

Fig. II-15. External glass lining and glass-encased core sample produced by Subterrene coring penetrator in volcanic tuff.

to "package" a core sample in a rigid glass casing leads to the potential for obtaining oriented geologically interesting samples in faulted or broken ground masses. Detailed analytical analyses of this initial coring penetrator design have been developed

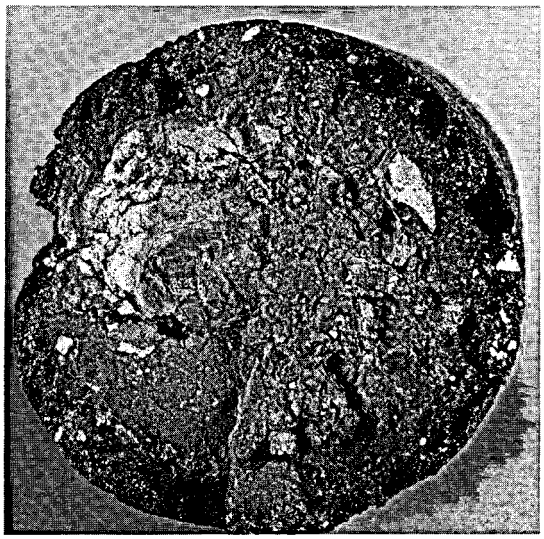

Fig. II-16. Cross section of a Subterrene-produced core in Green River shale showing glass lining and soft interior region.

and directions for significant performance improvements have been indicated. During the research period covered by this report, technical efforts were redirected at the request of the program-sponsoring organization and further development of the coring concept has not been pursued.

D. Thermal Stress Rock Fracturing Tool

Fracturing by developing thermal gradients in a rock mass by rapid heating or cooling of its surface is a well-known technique that has been employed in primitive forms of mining and tunneling since ancient times. The modern excavation industry does not typically employ thermal stress fracturing, but research being conducted at the University of Missouri indicates that the technique can be effectively utilized in tunneling of hard rock. Their experiments involve drilling an array of holes in rock face to a predetermined depth and inserting high-intensity heat sources at the hole bottoms. The resulting thermal stresses produce cracks normal to the rock face and also parallel to the rock face in a plane containing the heat sources. Thus the heading is advanced by breaking an incremental depth of the rock into fairly regular blocks which are subsequently removed by mechanical means. Requirements for the commercial application of this technique demand the availability of rugged, reusable, economical heat sources. Devices developed for rock melting as a part of the Subterrene program have these desired characteristics. They are capable of sustained operation at high

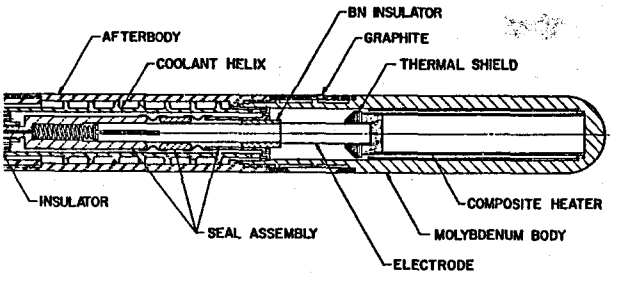

Fig. II-17. Cross section of thermal stress rock fracturing tool.

temperature in contact with molten rock; they are rugged and reusable, and in production could be manufactured economically. The development of a special tool for rock fracturing based on rock-melting technology was therefore undertaken.

The rock fracturing tool, shown in Fig. II-17, is 48 mm diam and 2 m long. The molybdenum heater body operates at ~ 1700 K and is hermetically sealed with helium for protection of the electrically powered graphite composite heating element which operates at ~ 2100 K. Peripheral equipment required for operation of the fracturing tool consists of a power supply (40 V, 250 A) and an air compressor for cooling gas (35 SCFM). A typical power level of 5 kW is required to produce fracturing.

Rock fracturing tools have been successfully operated in basalt, granite, limestone, and sandstone with 3 to 5 major fractures per hole occurring within 475 to 725 s after reaching operating temperature. The rock fragments typically range in size from 25 to 140 kg. Figure II-18 shows the initial fractures in a granite block produced by a single rock fracturing tool and the fragmentation of this block after fracturing from both predrilled holes. Spacing of the predrilled holes in the rock face has typically been 0.3 m. It is necessary to develop fractures to one or more free, unrestrained surfaces to facilitate breaking out the rock fragments and to provide a surface to which cracks can propagate.

E. Glass-Forming Technology

Early experiments with density consolidation penetrators melting in Bandelier tuff and alluvium demonstrated the basic features of forming the molten rock into a competent glass hole lining. Using

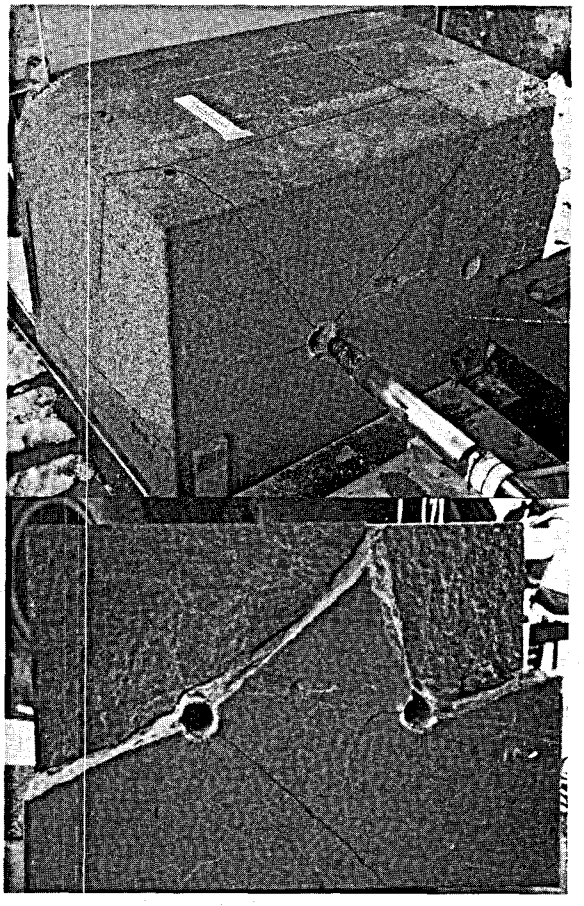

Fig. II-18. Thermal stress fragmentation of a granite block produced by electrically heated molybdenum fracturing tool.

a gas-cooled graphite glass-forming section directly behind the melting penetrator, smooth-walled linings were formed in a wide variety of soft ground and porous rock mediums which permitted extraction of the penetrator assembly with relative ease. Graphite was selected as the forming material because it minimized the tendency for the cooling glass to stick or adhere to its surface during the solidification process. The thick glass liners necessitated by density consolidation penetrators readily accommodated the presence of even large volumes of unmelted quartz crystals without seriously affecting the integrity of the liner. When experiments were performed with higher thrust loads, the glass walls of the resulting holes were of much better visual quality than noted previously. It appears logical that the higher thrust loads and associated higher pressures in the rock melt minimize gas-bubble evolution which can cause voids in the glass walls.

The use of extruding penetrators in hard competent rock presents a different set of conditions for

liner optimization. The melting penetrator is now continuously extruding molten debris for removal and transport to the surface,and the glass liner requirements for a stabilized hole in competent rock are very minimal. Penetrator development effort has been directed toward improving the ability of the system to control conditions in the molten rock to influence the character and properties of the bore lining and the extruded debris. After completing the 30-m-deep field hole in basalt, photographs of the hole wall were taken to determine its surface characteristics. The photographs indicated that two distinctly different wall conditions were evident. These conditons were characterized by either (1) a relatively smooth glass liner of fused basalt with a thickness estimated to be of the order of 1 mm or (2) a surface largely stripped of fused material leaving behind only slightly glazed virgin basalt. Wall surfaces alternate between these two types throughout the depth of the hole due to changes in penetrator glass-former design and operating characteristics during penetration. Both of these conditions had previously been observed in laboratory tests.

Initial experiments with extruding penetrators employed a segmented graphite glass-forming section based on consolidating penetrator experience. While capable of producing dense glass linings in hard rock, the early systems possessed two major shortcomings. The relatively soft graphite was easily scored by irregularities in the liner during extraction, leading to frequent replacement of the forming sections. This limitation was considered to be particularly important in view of the present program direction toward the development of deep hole systems for geothermal energy production. The second problem area concerns the dynamics of the molten rock layer when melting through basalts which contain both carbonate inclusions and bound water, resulting in appreciable gas generation during melting. Rapid gas evolution in the melt can result in voids in the glass lining and also surges of molten rock being forced into the debris removal nozzle of the penetrator. Extreme surging can overload the debris removal system resulting in blockage of the debris carry-off tube with chilled rock debris.

This latter problem area resulted in an extruding system modification employing a longer extrudate tube to significantly increase the pressure drop of the entering rock melt. Operating with this flow restriction, melt pressure levels at the glass-forming section are increased sufficiently to suppress gas bubble production while simultaneously minimizing the effects of surging at the debris-forming nozzle. Tests with an 84-mm-diam extruder incorporating a restricted extrudate passage, or surge suppressor, that increased the pressure in the melt have produced remarkably improved smooth glass borehole linings as illustrated in Fig. II-19.

The problem of graphite glass-former wear was addressed by designing more rugged, abrasion-resistant assemblies employing refractory metal segments in place of the all-graphite segments. An initial design used a molybdenum forming ring followed by a graphite release ring to minimize rock glass sticking during the critical cooling temperature range. In the cold condition, the graphite diameter is smaller than the molybdenum so that the abrasion from the hole wall is born by the metal parts. In laboratory tests the new glass former produced a cleanly stripped hole in basalt; i.e., the glass is wiped from the wall by the piston effect of the forming section and the aspiration effect of the extrudate nozzle. The seal between the forming section and

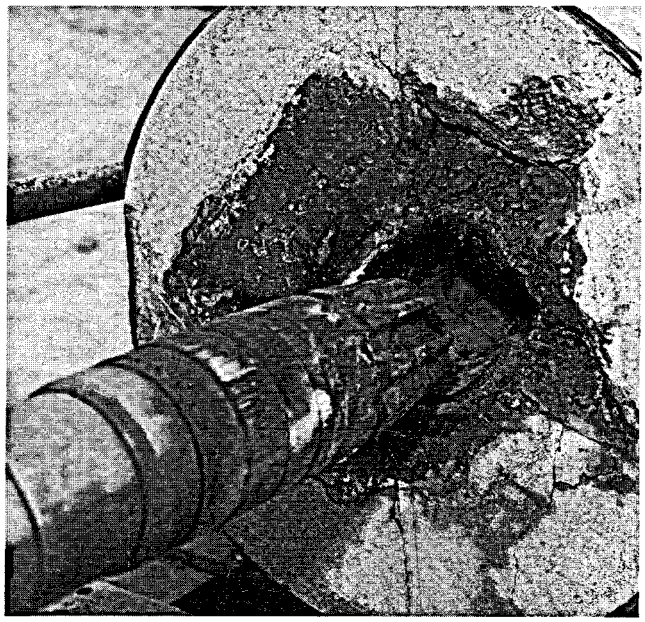

Fig. II-19. Horizontal hole in basalt. Note smooth glass lining produced by the penetrator with extrudate tube restrictions.

the rock wall is enhanced by an annular ring of solidified rock that has been observed to form in this region. This mode of operation is considered desirable in competent rock which requires no lining because it minimizes the power requirement and reduces the probability of difficulty with extraction and insertion. A glass stripping section currently being tested has entirely eliminated the use of graphite rings, employing only molybdenum segments for greater abrasion resistance.

F. Direct Melt Heating

1. Introduction. The electrical resistivity of most minerals decreases with increasing temperature in both the solid and liquid phases. In the liquid phase the resistivity is typically in the range of 1 to 10 Ω·cm which is comparable to the resistivity of materials currently used for penetrator heaters. The electrical resistivities of molten rocks are many orders of magnitude lower than those for the parent solids as illustrated in Table II-1. These factors make it possible to consider using direct electrical resistance heating in the liquid melt layer. Successful development of a rock-melting penetrator system which could utilize this heating concept would have significant advantages over the present penetrator designs. The current penetrator designs will ultimately be limited by the conduction of heat from the internal electrical heaters, through the penetrator structure and the melt layer to the melt-to-rock interface. The possibility of arranging the electric circuit of a rock-melting penetrator so that current passes through a molten region and deposits most of the melting power directly in the melt layer just adjacent to the melting interface has been recognized for a long time. This mode of rock melting has been investigated in recent preliminary laboratory experiments.

TABLE II-1

COMPARISON OF ELECTRICAL RESISTIVITIES OF ROCK, ROCK MELTS, AND GLASSES

Rock Type	Temperature (K)	Specific Resistivity (Ω·cm)
Granite		
Solid*	300	10^8
Molten	1800	6 to 15
Basalt		
Solid*	300	10^{10}
Molten	1800	2 to 4
Sandstone		
Solid*	300	10^{10}
Molten	2300	10^2
Glass	300	10^{10} to 10^{12}
Molten Na_2O-33% SiO_2	2020	0.5
Molten MgO-33% SiO_2	2020	5.0

* Typical of dry conditions.

2. Melt-Heating Experiments. Initial experiments were conducted with the "desk top" rock-melting demonstrator equipped with a substantially larger capacity power supply. The penetrator assembly of this device consists of a pair of tungsten electrodes (a 12-mm-diam rod slit axially) connected at one end by a thin wafer of pyrolytic graphite which serves as the heating element in the normal penetration mode. The electrodes are separated at the upper end by a thin insulating layer and clamped in massive brass electrode heat sinks. To operate the penetrator in the melt-heating mode, the power supplied to the unprotected pyrographite wafer heater is first brought to a level sufficient to start formation of a melt pool on the surface of the rock specimen. After the molten pool has been formed the heater power is increased substantially, which results in high pyrographite heater temperatures, rapid deterioration of the wafer, and increasing heater resistance. At the same time the resistance of the electrical path through the molten pool is decreasing so that a transfer of power deposition from the heater wafer to the rock melt occurs. Normal mode operation of the demonstrator would protect the pyrographite wafer from oxidation and it would remain as the resistance heating element as the tungsten rod heated up and the unit acted as a rock punch; i.e., no melt removal passages are included, and the hot melt flows back in the small annulus between the hole wall and the tungsten rod. This start-up and transition phase is illustrated in Fig. II-20(a) and II-20(b) for the melt-heating concept. The experiments revealed that once the current path through the melt was established as shown in Fig. II-20(c), the power supplied to the tungsten rod could be increased significantly, resulting in a greatly enhanced penetration rate. In several experiments the power was increased to > 5 kW. Five kilowatts of melting power is sufficient to melt a 12-mm hole in basalt at a

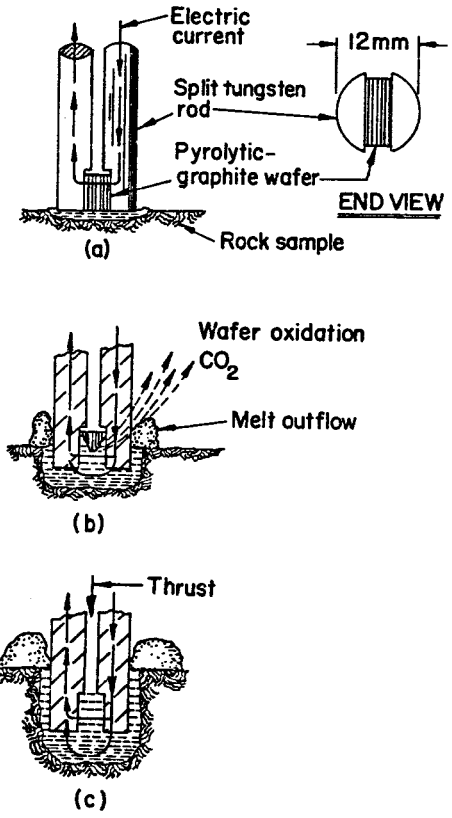

Fig. II-20(a). Initial heating in pyrographite wafer, with start of surface melting.
(b). Electrical current path and heating transfer to melt with oxidation of pyrographite wafer.
(c). Heating entirely in melt, increased power and rapid penetration rate.

rate of about 11 mm/s (130 ft/h)! The highest penetrator velocity actually observed was of the order of 1 mm/s, but the simple laboratory setup allowed large losses by conduction and radiation from the electrodes and by the escape of very hot gases. These initial experiments never achieved thermal equilibrium, and the penetrator was not designed to remove melt.

The melt-heating mode has been demonstrated in a series of experiments with basalt, granite, and tuff. Although in principle the melt-heating mechanism only requires a conducting liquid phase, there is reason to believe that the actual mechanism also involves the partial electrical breakdown of vapors evolved from trace elements in rock. The success of these preliminary experiments has initiated further experimental and analytical research to define the details of the heating mechanisms involved and the influence of the typical melt resistivity vs temperature behavior on the process. Molten rock resistivity data of the type depicted in Fig. II-21 are being incorporated into one- and two-dimensional calculational techniques to determine the electrical energy deposition profiles in rock melts subjected to both conduction and radiation energy transfer. Laboratory experiments using 60-Hz currents of 50 to 150 amps have achieved very hot, yet remarkably stable melt pools. No tendency to arc was observed at applied voltages below approximately 30 V. High-temperature experiments in molten Jemez basalt showed a stable ohmic behavior of the melt pool with no change in resistivity noted for variable current density or frequency in the 50- to 5000-Hz range. Laboratory tests are currently being conducted with an annular melt-heating penetrator consisting of two concentric cylinder power conducting electrodes separated by a high-temperature insulator. After establishing a rock melt pool, power is conducted from the outer cylindrical electrode to the inner one through the rock melt in a manner analogous to that shown in Fig. II-20 but now in an axially symmetric toroidal geometry. This configuration permits a melt removal path through the center of the inner electrode and has the potential to be incorporated into more conventional melting penetrator designs as a technique for overcoming the limitations of the leading edge stagnation point heat transfer rates. Melting augmentation of this type could improve advance rates severalfold, and preliminary experiments

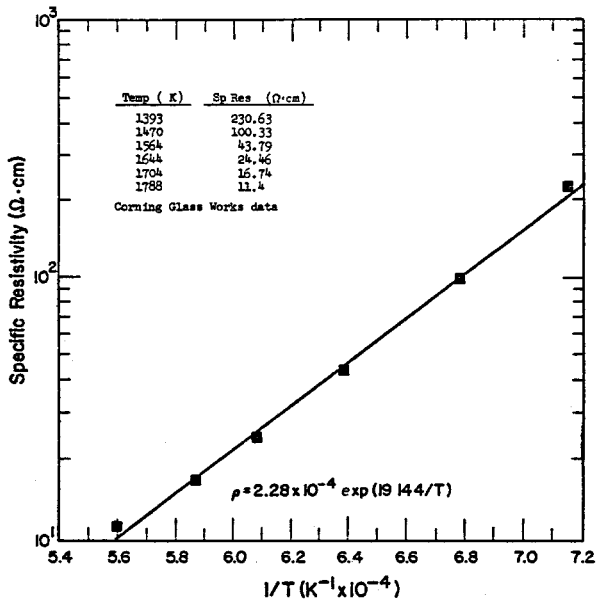

Fig. II-21. Temperature dependence of electrical resistivity for molten Dresser basalt.

indicate that electric current distributions are encouragingly stable and uniform. Research activities and laboratory experiments in this intriguing concept currently have a high priority in the current program.

G. Salt Borehole Plugging by Melting

The disposal of radioactive wastes in underground salt deposits depends on the long-term physical integrity of the selected salt formations. Preexisting boreholes, those formed for site evaluation, vault construction, and instrumentation monitors, must be sealed to restore the integrity of the salt formations proposed for radioactive waste storage. The plugs used to seal these holes must not represent a threat to the integrity of the salt formation during the hazardous lifetime of the wastes. A study of the feasibility of forming borehole plugs by melting and resolidifying salt similar to that found in the formation was initiated on the basis that a plug with physical and chemical properties close to those of the formation could be formed by this technique. Since melting and resolidification of rock salt causes practically no change in the chemical properties, emphasis was directed toward the resulting physical properties of the plugs prepared in this manner. The properties considered to be most important include the physical structure, fluid permeability, crush strength, and material bonding ability of the fused salt plug. Experimentally formed plugs were evaluated on these terms relative to the rock salt into which they were formed.

The resistance heating element used in these preliminary experiments was a metallic strip made of Haynes 25, selected for its corrosion resistance in the molten salt environment. Power was supplied to the heater through a water-cooled copper electrode, and the melting assembly was mounted on a piece of drill stem activated by a hydraulic cylinder in the rock laboratory test frame. Direct electrical current was passed through the heater strip to provide the energy necessary to melt the rock salt, and during the experiments the heater temperature was maintained close to the melting temperature of the salt (1077 K) because there was little thermal resistance between the heater element and the melt pool. Each experiment was initiated by inserting the melting assembly into a 77-mm-diam predrilled hole in a salt block sample and then filling the residual hole volume with granulated salt of similar origin. When the heating element approached operating temperature a molten pool formed at the bottom of the hole. This molten pool was maintained while the melting assembly was continuously withdrawn from the hole, additional granulated salt being added to the hole as required. Mechanical agitation of the molten salt was found to improve the quality of the resulting borehole plug. A cross section of a borehole plug formed by this technique in a block of livestock salt is illustrated in Fig. II-22.

Quantitative measurements of the physical properties of six borehole plugs formed in salt samples originating from a mine located near Lyons, KS, were performed and compared with the properties of the virgin salt block. The virgin samples had an average density of 2.1 Mg/m^3, average permeability of 0.5 darcys, and average crush strength of 28 MPa. The six laboratory-produced plugs yielded values of 1.6 Mg/m^3, 0.4 darcys, and 12 MPa, respectively for density, permeability, and crush strength, with both virgin and laboratory-produced samples showing considerable individual variations. Although the melted borehole plugs contained significant porosity, the permeability data indicate this porosity is unconnected, and potentially effective plugging can be achieved by this method. The plugs appear to be well

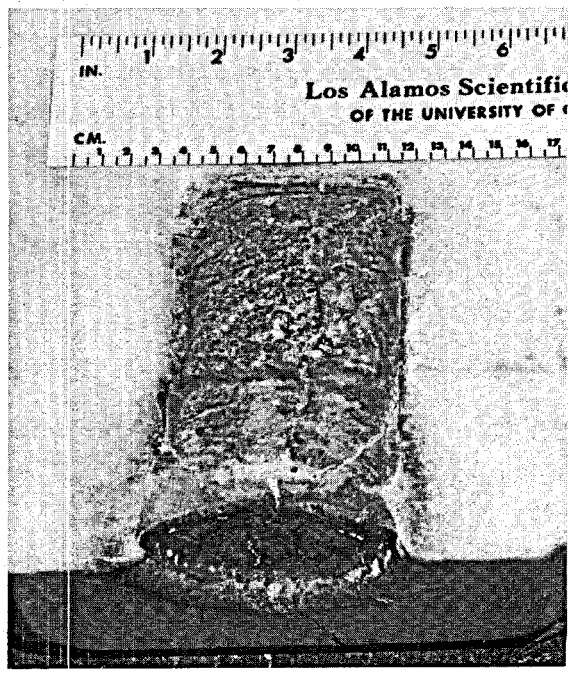

Fig. II-22. Cross section of a borehole plug formed in a salt block by melting and resolidification of granulated salt.

bonded to the hole wall as depicted in Fig. II-23, which is a magnified view of a typical plug - parent rock salt bond. The reduced plug density can be attributed to the large volume reduction during the liquid-solid phase transition and the large amount of thermal shrinkage which occurs when the plug cools to room temperature. Available data indicate that modest pressurization of the melt and the cooling plug would be extremely beneficial. Pressurization would tend to heal or prevent gross defects in the plug and in the bond between the plug and the surrounding formation.

Although the equipment used to prepare the borehole plugs in this study was quite rudimentary, it was useful in providing base-line operating experience from which design improvements can be made. Desirable features in a prototype field device would include provisions for melt pressurizing, agitation of the molten pool for better distribution of the melted rock salt, and a system to control the rate of addition of rock salt to the heated region.

H. Plasma Arc Experiments

A technical approach being investigated for Subterrene penetrators is the application of plasma arc heating to increase penetration rate and handle the highest melting-point rocks. Conduction designs now employed are limited by the temperature of the refractory metal through which energy is transferred to the rock. External application of energy permits some cooling of the penetrator body and the potential for applying much higher temperatures to the rock face. Plasma centerline temperatures in excess of 20 000 K are a reasonable expectation as these values are routinely attained with commercial equipment. Plasma arc thrusters have demonstrated continuous run durations of a month using radiation-cooled anodes operating at 1800 K. References in the literature also mention operations at pressures above 10 MPa (1500 psi). While the observation has been noted that a plasma torch readily melts a rock sample, apparently no one has faced up to the formidable task of providing a debris removal system for such a penetration device.

Fig. II-23. Microstructure of bond between melted plug and Lyons, KS, rock salt.

The Subterrene program has provided excellent experience in handling molten rock debris. Over 500 kg of molten basalt were fluidized and transported to the surface by a cooling gas from a single hole produced in the field by an extruding Subterrene penetrator. The technology being investigated is the combination of plasma arc heating with a molten debris removal system to produce a plasma-assisted Subterrene penetrator. Initial experiments were conducted with the simple plasma arc device shown in Fig. II-24. A tungsten anode and cathode are employed with a high-temperature insulator fabricated from boron nitride. The arc discharge nozzle in the cathode is visible in Fig. II-24. This unit has been operated at power levels up to 15 kW using nitrogen for the plasma gas. Maximum arc temperatures, estimated from an energy balance, were in excess of 20 000 K. Brief application of the arc discharge to a basalt sample produced the results shown in Fig. II-25. Conceptual designs have been prepared for an integrated unit which combines this high-temperature arc source with a molten debris removal system. Successful application of plasma heating in a Subterrene penetrator has the potential for providing a significantly higher penetration rate device through even the most refractory rocks.

I. Rock Laboratory Test Facility

The rock laboratory test facility has been moved from its previous location to a three-story high bay area providing 150 m^2 of floor space. The facility consists of two test frames, a control room, an assembly and work area, and an equipment pad outside of the building. One of the test frames was acquired from a previous laboratory project; the other was moved from the old location. The small frame has a stroke of 1 m and a load capacity of

Fig. II-24. Initial plasma arc heating device showing tungsten cathode and arc discharge nozzle.

40 kN, with a hydraulic cylinder mounted vertically and thrusting downward. Penetrator assemblies are mounted on the hydraulic ram and are thrusted into the stationary rock samples. The larger frame has a hydraulic cylinder mounted in the floor, with a 1-m-diam specimen platform that moves up from the floor with a 2-m stroke. Penetrator assemblies are mounted on the top of the test frame; rock specimens are clamped to the platform and move up into the stationary penetrator assembly. Figure II-26 shows

Fig. II-25. Basalt rock sample after brief exposure to plasma arc discharge.

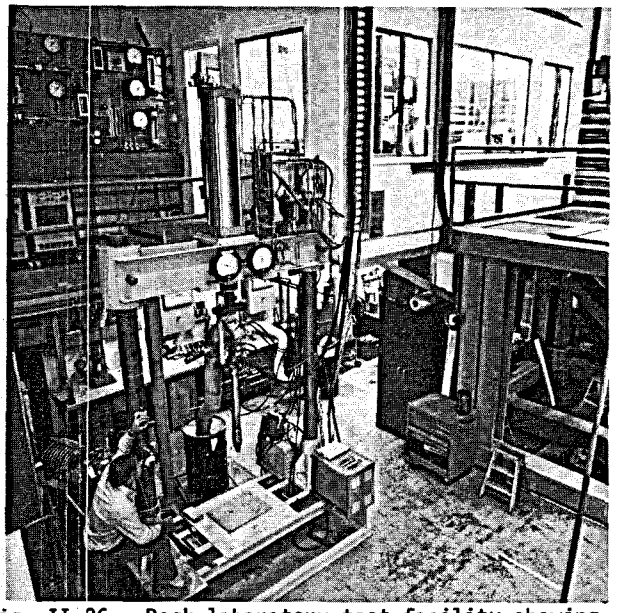

Fig. II-26. Rock laboratory test facility showing control room and two hydraulically thrusted test frames.

the laboratory test facility with an extruding penetrator in place in the 1-m test frame. The larger test frame is shown on the right side of Fig. II-26 and was only partially completed at the time the photograph was taken. The control room is visible on the balcony above the test frames and to the left of the room is the cooling gas and water control panel.

Figure II-27 shows the inside of the control room. In the foreground is the calculator-based data acquisition system with the hydraulic and power control rack visible in the far corner. During an experiment, closed loop servo-systems provide options for maintaining constant power, current, voltage, applied load, or penetration rate. Data acquisition is independent of these control activities, but provides processed data both during the experiment and in storage for future use. Sensor inputs to the system include voltages, currents, thermocouple outputs, pressure and flow transducer outputs, as well as load, rate, and position transducer outputs. These inputs are transformed into desired engineering units and printed and plotted in real time as well as stored on cassette tapes for further processing at a later time. Most of the posttest data processing, manipulation, and plotting can be performed with the calculator system, using its high-level BASIC language and 7904 word memory. A series of programs has been

developed for rapid routine data handling and stored in the form of cassette tapes which are easily loaded into the calculator memory.

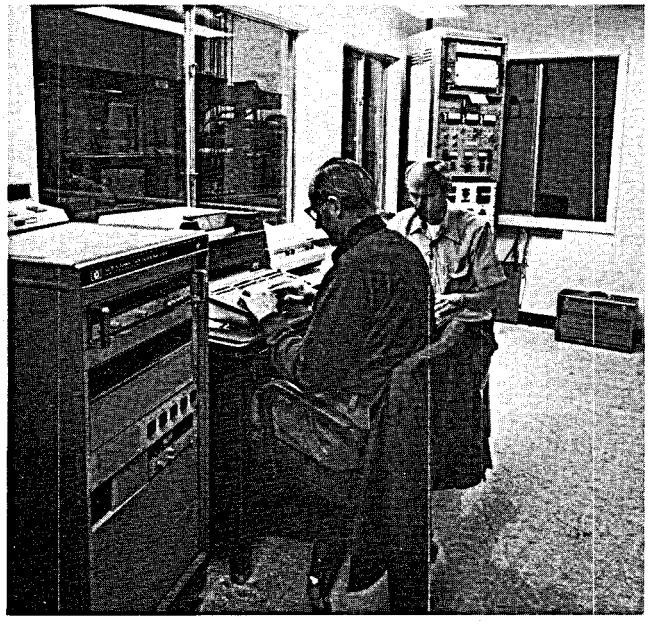

Fig. II-27. Laboratory control room with calculator-based data acquisition system.

III. POWER SOURCE DESIGN AND DIRECTED RESEARCH

A. Electric Power Sources

1. Introduction. Electrical power has been used to provide the rock-melting energy for all of the prototype Subterrene penetrators. Previous work has indicated that production systems would be most effective with electrical heating, at least in the range of diameters being considered for geothermal well applications. The heating technologies that have been studied fall into two general categories, one consisting of internal heat generation with heat conduction through the metal penetrator wall to the rock-melting interface, and the other consisting of energy deposition outside the penetrator surface. The latter category includes ohmic heating of the molten rock, dielectric heating of the heated solid rock, and radiant heat transfer from a plasma arc source.

2. Heater Development for Penetrator Research.

a. Introduction. While many different heater types have been tried, graphitic radiation elements in helium-filled cavities were selected for all the penetrators constructed since the early stages of the program. The successful use of pyrolytic graphite as a radiant heating element and the low thermal resistance of a polycrystalline-graphite radiation receptor were combined to produce a very stable heater assembly. Heaters typically consist of a stack of oriented pyrolytic-graphite disks or annular rings held in a graphite-lined cavity by a spring-loaded electrode as illustrated in Fig. III-1 for a density consolidation penetrator. The advantages of this system are based on the unique characteristics of graphitic materials and the wide range of mechanical, electrical and thermal properties obtainable in commercially available products.

Features of this design which contribute to efficiency and durability can be summarized as follows:

- A heater cavity containing only graphite in the high-temperature region.
- The use of a specialty graphite for the receptor whose thermal expansion characteristics match those of molybdenum and whose absorptivity for radiation energy is near unity.
- A nonisotropic pyrolytic-graphite heater stack oriented so that the high electrical resistivity is parallel to the penetrator axis, and the high thermal conductivity is normal to the penetrator axis and in the direction of principal heat transfer.
- A hollow heater cavity to allow control of the relative heat generation along the penetrator length.
- Utilization of the exceptional combination of high compressive strength and low thermal conductivity of pyrolytic graphite for the insulator between the heated penetrator body and the cooled afterbody.

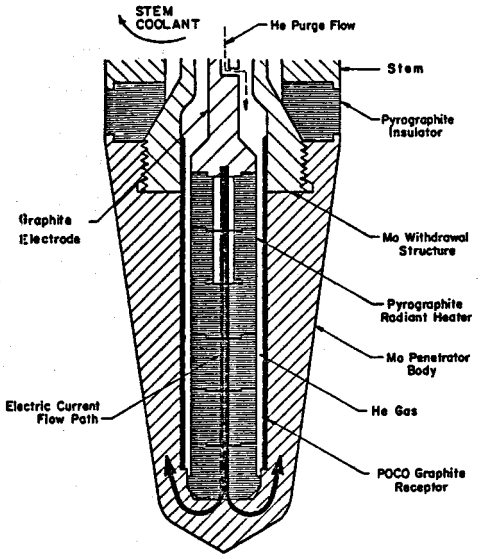

Fig. III-1. Cross section of a consolidating penetrator with stacked pyrographite radiant heater and graphite radiation receptor.

b. Tailored Heaters. A series of heaters in the form of either solid cylinders consisting of stacked disks or pellets (for the extended surface extruders and density consolidation penetrators) or hollow cylinders consisting of stacked annular rings (for the high advance rate extruder and melt flow augmented extruder) was designed, tested, and incorporated in operational penetrator systems. In each case, the desired power generation along the length of the heater was nonuniform and was tailored to meet the melting demands of the penetrator at a given axial location. The energy requirements along the penetrator length were calculated using the analytical methods described in Sec. V. C of this report. The validity of these calculations was confirmed in numerous laboratory experiments and by tailoring the output of the heater, localized over-

heating of the penetrator body can be avoided. A system of alternating segments of pyrolytic graphite and polycrystalline graphite was originated to approximate the required power distribution. Polycrystalline graphite has a relatively low resistivity and was used where essentially no power generation was needed. Pyrolytic graphite has a high resistivity across the grain and was used in areas requiring a high thermal flux. A specialty graphite made from highly oriented pyrolytic-graphite flour was used when an intermediate resistivity was required. An example of a tailored heater for the HARE extruder is illustrated in Fig. III-2.

c. Annular Heaters. Heaters in the form of thin-walled hollow cylinders were particularly effective in that both inside and outside surfaces could radiate, thus increasing the heat transfer area per unit heater length. Again, alternating rings of pyrolytic graphite and polycrystalline graphite were used. A stepped joint between the two graphites proved adequate for electrical continuity provided the entire heater assembly was maintained under spring-loaded compression, and that the joint was machined to close tolerances. The polycrystalline-graphite member had to be free to expand radially away from the pyrolytic graphite, with its much lower thermal expansion in that direction. The highest power demand from an operating heater is not radial but axial in the region of the leading edge of the penetrator. An ideal heater would consist of a very short disk or annular ring functioning as a heating element in contact with the leading edge of the penetrator followed by an extended heater assembly with much lower power generation per unit length. This configuration was evaluated and used in a 51-mm-diam density consolidation penetrator, and the HARE extruder and was capable of producing substantially higher heat fluxes through the penetrator leading edge. An exploded view of this heater system for the HARE extruder is illustrated in Fig. III-3.

d. Hermetically Sealed Heater Assembly. Practical penetrator assemblies for field hole production would benefit from a hermetic sealing of the heater cavity. The design, fabrication, and field-testing of an improved electric heater for consolidation-mode penetrators (in which the penetrator body, withdrawal structure, heater elements, and graphite electrode are a hermetically sealed unit) was completed. This design provided a small sealed reservoir of helium. Laboratory and field tests of the system showed that this technique was successful in maintaining a clean helium atmosphere in the heater cavity throughout the expected lifetime of the penetrator assembly. This penetrator system with the sealed heater assembly is shown in Fig. III-4 after testing. Included in this development program was the fabrication of a special heater-processing apparatus for filling the penetrator with helium and testing the hermetic seal at operating temperatures.

e. Power Supplies. Previous work indicated the desirability of operating the radiant heater system with direct current power and with the heating element positive with respect to the cooler

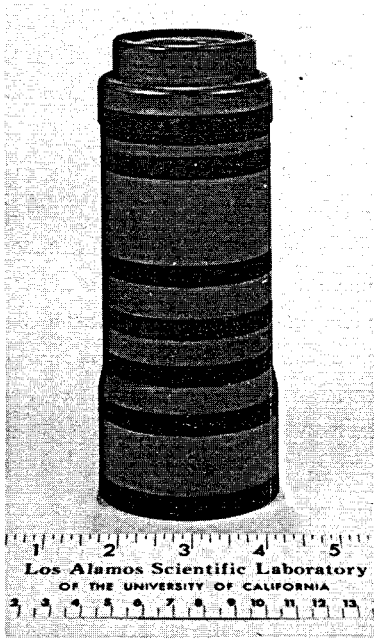

Fig. III-2. HARE extruder tailored heater assembly. Dark sections are pyrolytic graphite; lighter sections are polycrystalline graphite.

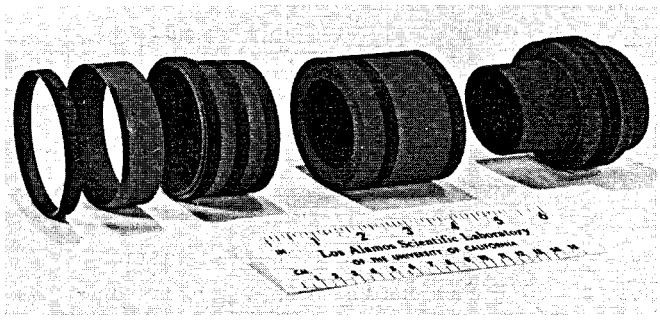

Fig. III-3. Exploded view of HARE extruder heater assembly. Note thin leading pyrolytic graphite heater ring for maximum energy generation near penetrator leading edge.

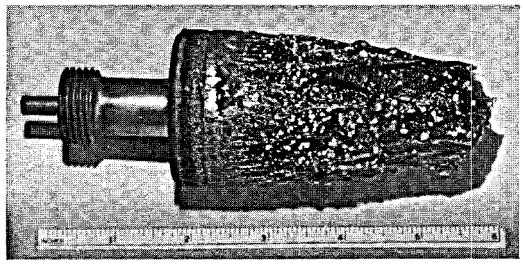

Fig. III-4. Consolidating penetrator with hermetically sealed heater assembly.

cavity walls. Power supplies were developed that provided a very stable regulated output. For experiments both in the laboratory and in the field, operation in a regulated constant power mode was used, with current and voltage limiting to protect both the supplies and penetrator hardware from circuit failures. An additional benefit from the high stability of these supplies was the ability to measure accurately the resistance of the heater system. The relationship between heater resistance and temperature then permitted an estimation of average heater temperature during operation. Overall heater voltages as high as 100 V were employed successfully in the consolidator penetrator assemblies.

3. Alternatives to Graphite Resistance Heating.

a. Introduction. While the graphite radiation heater configurations were adequate for the prototype penetrators, future requirements necessitate the investigation of different heat sources. Operation at the high lithostatic pressures encountered at depths of 5 to 10 km in geothermal well production preclude the internal penetrator cavities of radiation heater designs on the basis of required collapse strength. High-strength penetrator bodies devoid of extended internal cavities must therefore be developed. Penetration rates of penetrators relying only on heat conduction through a stagnant rock-melt film are a function of penetrator surface temperature. A practical limit seems to be between 0.2 and 0.3 $mm \cdot s^{-1}$ at reasonable metal wall temperatures. Research directed at higher penetration velocities must therefore address the technical problems associated with providing high-energy deposition rates in the solid and molten rock ahead of the penetrator leading edge.

b. Solid Heaters. The chemical systems C-BN-Mo and Re-BeO-Mo appeared to possess the necessary stability to be used for solid conduction heater systems devoid of extended internal cavities. A heater was designed for evaluation in the heater test facility consisting of a BN mandrel, a polycrystalline-graphite tubular heater, a BN insulator, and a Mo outer cylinder simulating a penetrator body. Small amounts of B_4C formed in a 1-h test at 2473 K in an argon atmosphere. Heater regions that did not exceed 2325 K did not appear to react. Extended operation at temperatures below 2300 K would appear to be feasible. This combination would be considerably less expensive to fabricate than oxide insulator-metal wire or ribbon heater assemblies. A similar test using BeO insulators and a Re heater composed of a spiral wrap of four 0.5-mm-diam wires was also successful. Figure III-5 shows this assembly after testing with parts of the outer Mo tube and BeO insulating sleeve broken away to reveal construction details. This configuration should provide adequate flux for all but leading edge applications, at wire temperatures low enough to insure a long service life.

c. Melt Heating. Power generation directly in the melt film at the leading surface of a penetrator can create higher film temperatures than in the metal wall, thus enhancing the penetration rate. The electrical resistivity of most minerals decreases with increasing temperature in both the solid and liquid phases. In the liquid phase the resistivity is typically in the range of 0.01 to 0.1 $\Omega \cdot m$, which is comparable to the resistivity of materials currently used for penetrator heaters. In addition, the electrical resistivities of molten rocks and soils are many orders of magnitude lower than those for the parent solids. Initial experiments were designed to demonstrate this principle in a simple

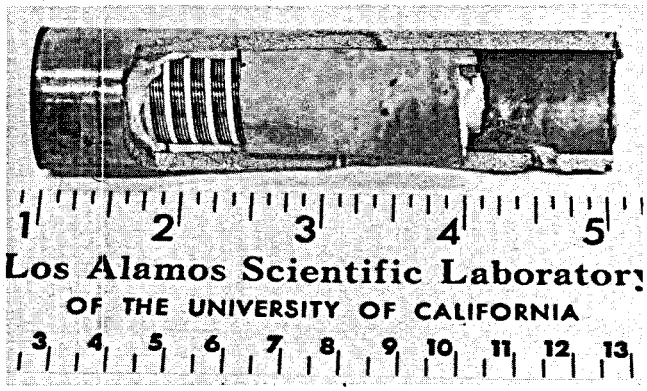

Fig. III-5. BeO-Re heater test assembly broken open after test to reveal internal details.

geometry, and later experiments concentrated on exploring the power generation and electrical stability in thin molten basalt films. Electrical resistivities of representative molten rock types were also determined under conditions approximating the freshly melted rock to be expected at the leading edge of an operating penetrator. Significant technical achievements in this area include:

- Demonstration of high penetration rates with a simple two-electrode system. Operation of this device is described in detail in Sec. II. F of this report, and the desk-top demonstration unit and power supply used in the initial melt heating experiments is shown in Fig. III-6.

- Demonstration of ohmic melt heating in a penetrator configuration. Hardware from the 58-mm-diam extruder experiments was modified to produce a penetrator with an annular melt flow passage. Alternating current was passed through this gap and produced sufficient power to penetrate a basalt sample. Two separate operational modes were identified. Initially, current flows of up to 10 A at impressed voltages of about 50 V could be sustained. The glass melt layer apparently was behaving as an ohmic heater in the vitreous state. Increasing the voltage beyond this point caused a spontaneous reverting to another stable condition with currents up to 200 A at sustaining voltages of about 18 V. This condition was apparently one of controlled submerged arcing. This unit produced about 75-mm total penetration depth in basalt rock.

- Direct electrical heating of thin molten basalt films. A series of experiments was conducted to evaluate the behavior of thin films of flowing basalt. A small amplitude perterbation analysis (details in Sec. V. C of this report) showed the possible buildup of electrical instabilities in a melt heating penetrator geometry in which the leading edge contained an annular electrical insulator between concentric electrodes. While the most direct way of determining the existence of these instabilities would have been to construct and test a series of prototype penetrators, time and funding restrictions led to another approach. Figure III-7 shows the last in a series of furnace experiments where preheated molten basalt was forced to flow under pressure in confined passages. The object of these experiments was to detect electrical current instabilities and temperature instabilities under conditions simulating those at the leading edge of a melt heating penetrator. The arrangement in Fig. III-7 provided for a melt film thickness of 1 mm and melt flow rates in the range of 1 $g \cdot s^{-1}$, at temperatures up to 2000 K, simulating penetrator conditions, but did not provide comparable heat sources and sinks or allow the formation of variable path cross sections. The results of these experiments were the production of stable currents up to 3.8 A at sustaining voltages of 220 V at 60 Hz through passage lengths of 20 mm. No serious electrical or thermal instabilities were detected.

- Determination of electrical resistivity of freshly melted basalt and granite. Resistivity data reported in the literature for rock melts generally appear to be obtained on material in equilibrium with atmospheric oxygen. Since the molten film

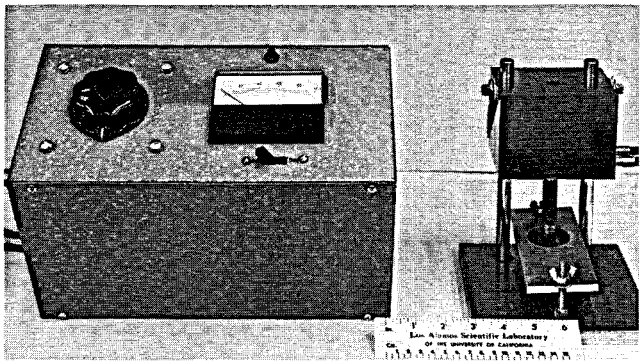

Fig. III-6. Desk-top demonstration unit used in initial melt heating experiments.

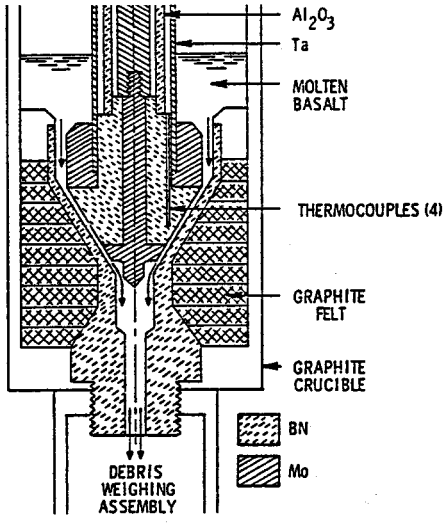

Fig. III-7. Furnace experiment for direct electrical heating of thin molten basalt films.

at the leading edge of a penetrator is in a confined freshly melted condition, resitivities could be substantially different. The resistance of freshly melted basalt and granite were determined by melting under an atmosphere of argon in a molybdenum-lined crucible. Data for Jemez basalt were similar to those obtained by Corning Glass Company on a sample that had been held at 1760 K for 4 h, except that the present results showed a less steep temperature dependence and could be represented by a linear relation between the log of resistivity and $1/T$, while the Corning data showed a definite nonlinear characteristic.

d. Dielectric Heating. The resistivity of rock generally decreases with temperature and also with increasing frequency of the applied voltage. One way to obtain higher advance rates is to deposit energy in the solid rock ahead of the penetrator. Success of this approach depends on the absolute value as well as the temperature dependence of the rock resistivity at temperatures within a few hundred degrees of the lowest melting point constituent of the rock. The low thermal conductivity of rock results in a very steep temperature gradient in front of the advancing penetrator and a correspondingly low cross sectional area of heat-affected material. An ideal combination of solid rock dielectric properties (alternating current resistive losses) and molten rock resistivities would enable the successful operation of a simple penetrator configuration. One such configuration might consist of an internally conduction-heated extended conical surface as used in the consolidation penetrators. The leading edge, however, would consist of a central debris-removal passage joined to the conical surface through an electrically nonconducting ring. Alternating voltage impressed between the conical surface and debris passage would cause a current to flow through the melt film between the rock and advancing penetrator. As the frequency of the impressed voltage is increased, more current would flow in the rock ahead of the film until the desired balance of power deposition was achieved. A continuing supply of freshly melted rock would flow into this region from the conical surface, and a constant stream of melt would flow away from the region out the debris-removal passage.

Dielectric properties of local Jemez basalt were determined as functions of frequency and temperature. These results, illustrated in Fig. III-8, were combined with the direct current resistivity data to estimate the conditions needed for proper operation. It appeared that the frequency would need to be above 1 MHz and that the melt film thickness would have to be very small for this configuration to produce high advance rates. One other aspect of this geometry has to do with the nature of the melting interface. Studies were made in which an advancing melting rock interface was "quenched" and examined microscopically. A region of partially melted crystals in a molten matrix was present between the solid rock and advancing molten pool. The effect of the velocity of melt flowing past such an interface, and the electrical paths within such a region, have not been adequately evaluated.

e. Plasma Arc. Utilization of plasma arc technology for rock-melting penetrators requires a stable arc source and adequate coupling to the rock-melting interface. Several design studies explored ways in which the melted rock could be removed from the melting interface, thus maintaining high rates of heat transfer through the molten film. A test fixture using a tungsten radiation-cooled anode and cathode structure and BN electrical insulators was

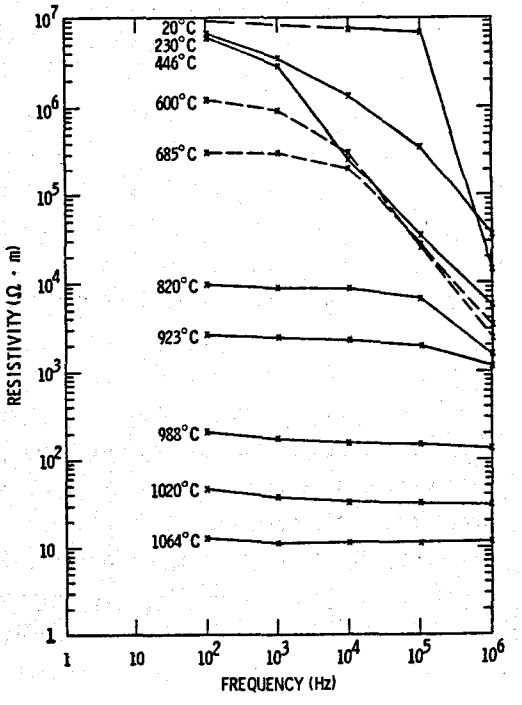

Fig. III-8. Alternating current resistivity of Jemez basalt.

tested in the laboratory. The desirability of higher power operation led to construction of a water-cooled copper anode assembly. The first unit accepted powers up to 18.5 kW (66 V and 281 A) using a flow of 9×10^{-4} kg·s^{-1} nitrogen gas and a calculated plasma temperature of over 10 000 K. Another operating mode was explored in which the arc was transferred from the integral anode structure to an external water-cooled plate. It is possible that a rock-melting penetrator could be designed in which the molten rock pool ahead of the penetrator would be a good enough electrical conductor to permit it to function as the external electrode. Some data are available that indicate that a plasma arc may be made to operate at pressures encountered in geothermal hole completion tasks.

B. Materials Science and Technology

1. Introduction. A major and continuous effort has been expended on the materials science aspects of the Subterrene program. The very high temperatures originating within the penetrator and ultimately transmitted to the ambient rock environment have required the use of refractory materials for penetrator construction. In turn, a wide spectrum of corrosion studies has been generated including: (a) external refractory alloy - molten silicate (rock) interactions; (b) internal power source material interactions; and (c) miscellaneous corrosion effects on pipe stems and support systems. In addition, qualitative compatibility and screening tests were performed as part of a general search for materials with improved corrosion profiles in various geochemical media. The rock-glass liners produced during the melting operations were subjected to an intensive program of physical and mechanical strength measurements. Fabrication technologies for the refractory metals molybdenum (Mo) and tungsten (W) were investigated, resulting in significant improvements. Advances in the preparation and use of new high-temperature brazes were also accomplished. As might be anticipated, the basic knowledge of the geosciences was used extensively throughout the program.

2. Refractory Alloy - Rock Melt Interactions. Corrosion studies were performed in the laboratory, and when possible, during and after field tests. Most laboratory investigations were done in static test systems in order to derive base-line data with the understanding that dynamic test systems would evolve as the program progressed. Both Mo and W and the alloy Mo-30W were studied in various rock media including: tuff, basalt, andesite, granodiorite, amphibolite, and granite. In addition, the corrosion effects within a series of basalts, e.g., Jemez, Dresser, Hawaiian tholeiitic, and East Pacific Suboceanic Ridge, were determined. In this manner, the degree of corrosion was correlated against a wide range of rock chemical compositions. Significant technical results obtained from the laboratory studies included the following:

- Molybdenum and possibly some of its alloys have corrosion resistance superior to that of W in all tested rock types. The measurements of Mo and W solubility show that Mo is less soluble, on the average, by factors ranging from 4 to 20.
- A significant correlation was obtained at constant temperature, time, and similar viscosity between metal solubility and the ferric-ferrous ratio, Fe^{+3}/Fe^{+2}, of the various basaltic compositions. Corrosion was found to vary with the basalt type, i.e., increasing with an increase in Fe^{+3}/Fe^{+2}. Thus, high Fe^{+3} content basalts such as Dresser will be more corrosive.
- The more siliceous rock melts exhibited lower degrees of corrosion. This is due, in part, to the higher viscosity and lower metal diffusion rates.
- Corrosion proceeds via at least three general mechanisms as observed experimentally. These include oxidation and solution, alloying, and gas bubble oxidation. The details of these corrosion mechanisms have never been determined completely. Gross variability in chemical composition, viscosity, density, and flow rate differences with their effects upon diffusion rates, solution thermodynamics, and variable rock oxygen potentials makes such determinations formidable tasks. The gross difference in corrosion between Mo and W can be explained in part thermodynamically and kinetically on the basis that W has the potential for faster reaction rates, for example, in high-temperature steam and other oxidizing media.
- Based on geometric considerations and the static test data, a model for the surface recession rate of the outer surface of a cylindrical penetrator was derived. Combined with engineering design data, it was thus possible to make estimates of penetrator lifetime based on chemical action alone.

Mechanical erosion effects were not considered although these add to the surface wear, particularly at the penetrator tip. The surface recession rate, $\Delta r'$, is given as

$$\Delta r'(\text{mm/s}) = 10^{-3} \frac{D_p}{2} V \cdot \left\{1-\left[1-4f(1+f)K'\right]^{1/2}\right\} ,$$

where
- D_p = penetrator diameter, mm
- V = penetration velocity, mm/s
- $f = \delta/D_p$
- δ = thickness of dissolved metal boundary layer in the glass lining, mm
- $K' = \frac{1}{H_p} \cdot \left(d_g/d_p\right) \alpha_p$
- H_p = penetrator length, mm
- d = density of glass (d_g) or penetrator (d_p)
- α_p = solubility by weight of metal in glass.

Assigning certain engineering parameters and average 1900-K solubility values, the curves shown in Fig. III-9 were constructed. The value of δ, 0.1 mm, was representative of observations in the static experiments. Modifications could be made to the model as additional data from dynamic tests become available. These lifetime estimates indicate lower chemical corrosion wear rates for molybdenum as compared to tungsten. Exceptionally long lifetimes can be expected from molybdenum penetrators operating in either Bandelier tuff or granitic rocks. As a practical example, consider a cumulative surface recession of 0.1 mm observed for a molybdenum penetrator in Jemez basalt operating under the assumed parameters of Fig. III-9. This value is indicative of an operating time of $\sim 2.8 \times 10^3$ ks (778 h). Typical penetrator designs would permit considerably larger surface recessions before a failure occurs, and hence the potential for long operating lifetimes under these conditions is excellent.

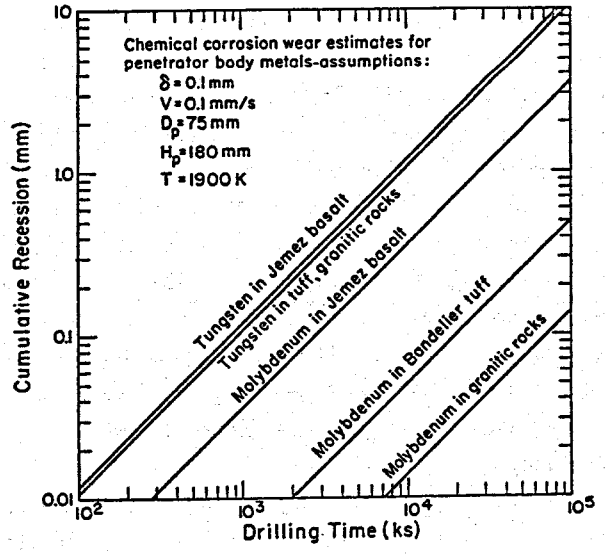

Fig. III-9. Estimated lifetimes of Mo and W penetrators in basalt and granitic rocks.

- A number of qualitative compatibility tests were made to identify useful penetrator materials other than Mo and W. Materials considered worthy of further study included: Mo alloys containing rhenium (Re), rhenium (pure Re provided reasonable fabrication techniques), certain high-melting-temperature noble metal alloys containing rhodium and iridium for highly oxidizing environments such as exist in carbonate sedimentary rocks, and certain ceramics such as HfC and ZrB_2. Although these ceramics all react to some degree, they still may be useful provided the reaction follows parabolic-type kinetics. Molybdenum disilicide, $MoSi_2$, was found partially satisfactory, particularly at temperatures below 1700 K. Both silicon carbide, SiC, and SiC-conversion coated graphite resist attack (in basalt) to some degree, generally below 1800 K. Quantitative corrosion data for the materials mentioned above were not obtained with the exception of some very limited data for Re. The solubility of Re was a factor of 5 to 10 less than that of Mo, which was encouraging. It may also be possible to use the ductile alloy Mo-34 at.% Re (Mo-50 wt% Re).

- In view of the deep geothermal drilling application, it was deemed prudent to test the penetrator materials Mo and W in types of basement rock likely to be encountered. Granodiorite and amphibolite samples, obtained from the LASL Geothermal Energy Project at a depth of approximately 750 m, were used for these tests. Solubility of the metals in this particular grade of granodiorite was similar to that in surface tuff and granites. Amphibolite, however, proved to have corrosion potential equal to or worse than surface basalts.

To assist in the clarification of details of the corrosion mechanisms, a subcontract was awarded to Professor A. Muan of Pennsylvania State University. The objective of the work was to determine the degree of importance of the various corrosion mechanisms. The studies feature control of oxygen potential (P_{O_2}) and the thermodynamic solution relationships in the Mo-Fe and W-Fe systems. This work was specifically directed at the activity-composition relations in Mo-Fe and W-Fe alloys, and the characteristics of the oxide chemistry of tetravalent molybdenum, including the stability relations of phases formed between MoO_2 and important rock-forming oxide components.

Activity-composition relations in Mo-Fe and W-Fe alloys were determined in the temperature range 1370-1770 K by equilibrating alloys within this system with Fe-Cu alloys of known activity-composition relations. The method is based on the assumption that the solubility of Cu in Mo-Fe alloys of low Fe contents, and the solubility of Mo in Cu-Fe alloys, are small enough to have an insignificant effect on the activity-composition relations of the main constituents of the two alloys concerned. The compositions of the alloys, following equilibration, were determined by electron microprobe analysis. Both alloys, Mo-Fe and W-Fe, were found to display large positive deviations from ideality. In the reaction between Mo- or W-metal and iron oxide of various rock melts, a suspected mechanism of corrosion of the metal probe is the reduction of some of the iron oxide to form iron which in turn may form a dilute alloy of iron in the Mo or W. Hence, for an evaluation of the problem of corrosion of Subterrene probes, the Mo-rich and W-rich regions of the Mo-Fe or W-Fe alloys are of primary interest. In order to make intelligent inferences regarding the behavior of MoO_2 dissolved in silicate melts, and hence regarding the interactions between Mo penetrators and silicate phases, it is necessary to expand knowledge of the crystal-chemical and thermodynamic behavior of Mo^{4+} in oxide and silicate phases.

In the application of Mo- or W-probes as hot penetrators in basaltic rocks, the main oxidation-reduction reaction likely to take place and have a close bearing on the rate of corrosion of the probe is

$$2(FeO)_{\text{silicate melt}} + Mo = 2(Fe)_{\text{alloy}} + (MoO_2)_{\text{silicate melt}}$$

for which the equilibrium constant may be written

$$K = \frac{a_{MoO_2} \cdot a_{Fe}}{a_{FeO}} ,$$

where as an approximation a_{Mo} has been set equal to unity. (Identical equations may be written for the W-Fe-O system.) Clearly, the strong positive deviation from ideality in the alloy system would mean that the iron concentration in the alloy phase in equilibrium with an iron-oxide-containing liquid would be very small unless the iron and iron oxide activities are very high. It is concluded that severe corrosion of Mo (or W) penetrators should not take place as a result of reactions between the refractory metal and FeO of the rock at oxygen potentials determined by the equilibrium expressed in the above equations. However, it is likely that these relations may be changed drastically if the penetrators are operated in an atmosphere of higher oxygen potentials, such as to promote the formation of Mo- or W-oxides of higher valence status (MoO_3 or WO_3).

In addition to laboratory data, corrosion data were also obtained from field test operations such as the 30-m hole in Jemez basalt using 84-mm fluted extrusion penetrators fabricated from Mo and Mo-30 W. The observed corrosion in that operation, as expressed by surface recession rates and compared with the laboratory predictive model, was estimated to be greater by a factor of 15-20. A detailed analysis revealed the following:

- An oxidizing environment beyond that expected in normal Jemez basalt existed during major portions of the basalt operation. This was attributed to excess water and possibly some hydrated or carbonated minerals. The predictive model had been generated from data obtained from "dry" basalt.
- Significant gas phase corrosion was observed.
- The complex geometry of the fluted penetrator would result in a spectrum of surface velocities during the downward penetration. Forced convection of a fluid is known to increase corrosion rates on refractory materials.

• Determination of a gross change in Fe^{+3}/Fe^{+2} after penetration corroborated laboratory work and lent credence to corrosion mechanisms involving the iron components of the basaltic melts.

• Alloying was also identified as a corrosion mechanism, again corroborating laboratory experiments.

Qualitative visual and metallurgical observations were made on several field-tested 50-mm consolidation penetrators used in tuff and alluvial soils. These penetrators were fabricated from Mo and, in one case, thoriated W. Both solution and gas phase modes of corrosion were observed. Grain growth stabilization was observed both for the thoriated W unit as well as areas of the Mo units where carbon diffusion (from the internal heater) had occurred. Intergranular cracking, internal cavity blisters, and voids were also observed in varying degrees of severity.

3. Power Source Materials. The radiant heater design with an internal inert gas-filled cavity has been used successfully in all penetrator development models. Only for the advanced application of deep geothermal drilling and the associated high lithostatic pressures has it been necessary to consider other designs, e.g., solid conduction heaters.

The basic chemical reactions for the radiant heater system concern those in the Mo- or W-carbon systems. These have been studied extensively both from thermodynamic and kinetic viewpoints. Their characteristics are reasonably well known and the lifetime of some of the internal components can now be estimated. For example, using available Mo-C and W-C reaction rate data, the cylindrical receptor thickness required for a 1000-h (3.6-Ms) lifetime was calculated at selected internal operating temperatures. Eventually, the metal carbiding that slowly progresses provides a means for receptor failure. To reduce the scope of the carbiding reaction, a diffusion barrier was introduced and successfully tested. Preliminary calculations and testing in the materials laboratory identified stoichiometric tantalum carbide, $TaC_{1.0}$, as an excellent barrier against carbon diffusion. Graphite receptors of the size used in 50-mm consolidation penetrators were coated with TaC ($\sim$ 0.03 mm thickness) by means of a chemical vapor deposition process (see Fig. III-10) and subjected to two lifetime tests of duration 200 h (720 ks) and 278 h ($\sim$ 1 Ms), respectively. Other test parameters included: internal heater temperatures of

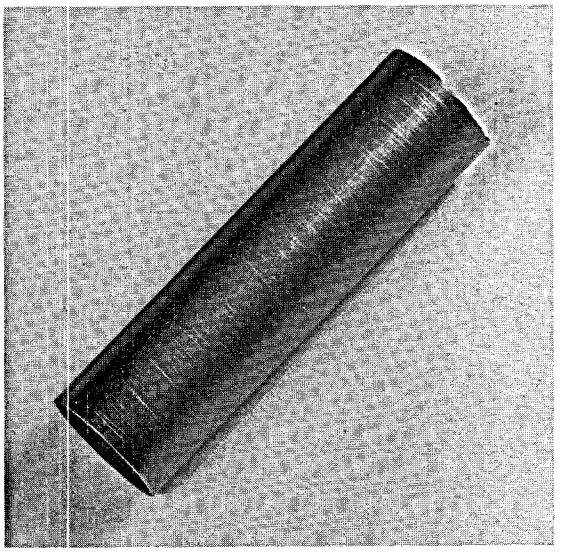

Fig. III-10. Tantalum carbide coated graphite receptor used in penetrator radiant heater system.

$\sim$ 2300 and 2450 K; Mo body temperature of $\sim$ 1800 K; input power, 4-4.6 KW; heat flux at the heater surface of 1.2-1.4 MW/m^2; and several thermal cycles down to 300 K. The test units appeared operable after shutdown. Analysis has demonstrated that a coating as thin as 0.03 mm reduced the carbiding reaction by at least an order of magnitude. A number of small thermal stress cracks and some coating separation were observed.

The very high lithostatic pressures associated with depth preclude the use of the radiant heater design for deep drilling. Solid contact or conduction heaters appear as a suitable alternative. Several high-strength systems were investigated thermodynamically and experimentally. An early conceptual design using Mo and boron nitride (BN) is shown in Fig. III-11. A cylindrically symmetric Mo electrode is embedded in pyrolytic BN, which is encased in the Mo body. At 300 K, BN is an electrical insulator with a resistivity of $\sim 10^{16}$ $\Omega \cdot cm$. However, by $\sim$ 1900 K, the resistivity has dropped to $\sim 10^{5}$ $\Omega \cdot cm$ across the grain ("c" direction) and to $\sim 5 \times 10^{3}$ $\Omega \cdot cm$ with the grain ("a" direction). However the Mo-BN system was shown to be thermodynamically unstable (except perhaps under very high nitrogen gas pressure) at operating temperatures of $\sim$ 2300 K.

The use of systems such as Mo-ZrN or W-HfN was investigated, but again the decomposition probability was high. Further, the nitrides become excellent electrical conductors at high temperatures. Consideration of other solid-state resistive heating

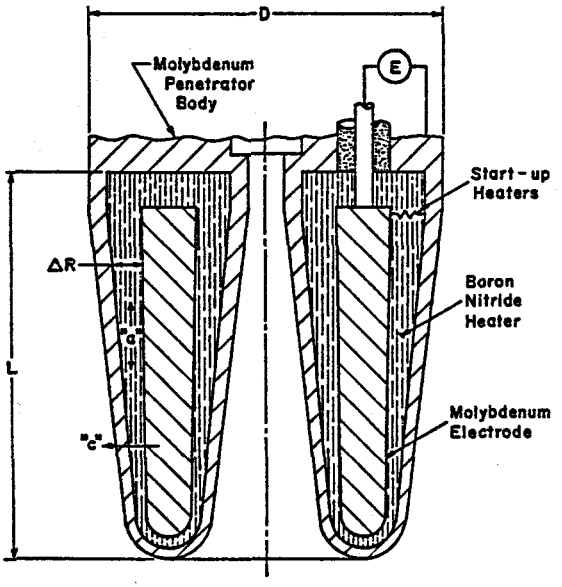

Fig. III-11. Conceptual design of a contact heater melting body utilizing a pyrolytic boron nitride heating element.

systems suggested the use of stable oxides for the electrical insulator part of the system. The severe thermal and electrical requirements eliminate the majority of the known binary oxides and a considerable number of ternary oxides as well. Of those remaining, beryllia, (BeO), and thoria, (ThO_2), were considered the best. Magnesia, (MgO), might be used provided its volatility can be reduced substantially and compatibility with Mo and W established. Alumina, (Al_2O_3), would also be useful provided operating temperatures are lowered.

The compatibility of BeO with the metals Mo, W, Re, and graphite was investigated. Both BeO-Re and BeO-C appear to be acceptable combinations. Although the thermodynamic stability of BeO-Mo and BeO-W is also good, experimental studies have shown that electrical shorting eventually occurs on wire-wound heaters due to conductive material deposition over the oxide surface. In the case of Mo, the metal itself has an appreciable vaporization rate at operating temperature. A small test unit comprised of wire-wound Re about a BeO core encased in Mo was run for short periods and yielded some heat flux, power and temperature data. Maximum Re wire temperature recorded was 2376 K at a flux of $\sim$ 1.23 MW/m^2. Based on the results of this test, this configuration should provide adequate flux at wire temperatures low enough to insure long service life.

4. Structural Glass Liner Results. Density consolidation Subterrenes are used to form glass-lined stabilized bores in porous or unconsolidated formation without any debris removal. As the hole is being melted, the rock melt is consolidated into a glass lining forming a strong, relatively impermeable boundary. To provide quantitative data on these formed-in-place rock glass linings, a contract was initiated with Terra Tek to characterize the lining formed in Bandelier tuff and compare its properties to those of the parent material. With knowledge of the material properties, the engineering potential can be better evaluated. Since the formation of rock-glass linings by a Subterrene penetrator is a relatively new process, little is known of the properties of the solidified melt material forming the lining.

To better characterize the lining material, Terra Tek performed physical and mechanical tests in all three principal directions whenever possible. Figure III-12 shows the orientation of test samples with respect to the original liner as supplied by LASL. Bandelier tuff samples containing the glass linings used in this study were supplied by LASL in the form of hollow cylinders. The inner diameters were either 51 mm with a lining of the order of 20 mm thick or 76 mm with a 25-mm lining, typically being 500 mm long. The lining material was observed to be generally competent except for the presence of radial fractures. Tuff samples not containing the fused lining were also supplied for tests on the parent tuff.

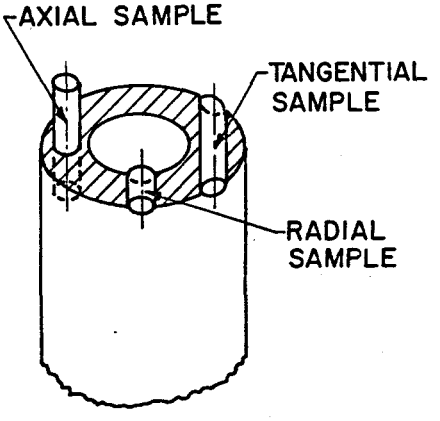

Fig. III-12. Cross section of glass lining showing orientation of test samples.

The dry and grain densities and porosity were measured for both the parent tuff and glass liner; the results are presented in Table III-1. The debris disposal mechanism of density consolidation is evidenced by the 50% increase in dry density and greatly reduced porosity of the liner material compared to the original tuff. Even lower liner porosities are probably achievable through the use of higher penetrator thrusts resulting in greater melt pressures. The density and porosity values obtained for the tuff are typical of other tuffs. Permeability as a function of effective stress (confining pressure) was measured on several radial lining samples. The results of one of these tests are shown in Fig. III-13. As the confining stress was increased, the permeability decreased from about 8 millidarcys at very low confining pressure (~1 MPa) to 200 microdarcys at a confining pressure of 50 MPa. On unloading, the permeability did not completely recover. Changes of the order shown in Fig. III-13 are not common for typical rocks with about the same initial permeability, suggesting the cause for the decrease is probably associated with minor imperfections in the glass liner which are closed at higher pressures. These values compare to a permeabilitity of approximately 300 millidarcys for the parent tuff, indicating the sealing properties of the liner.

Compression and tension tests were performed on both parent tuff and the glass linings at confining pressures ranging from 0 to 50 MPa. For the lining the axial and tangential samples were significantly stiffer than the radial samples, and in general, all samples were considerably stiffer at higher confining pressures. Axial and tangential samples showed the same strength within the experimental scatter; the radial samples, however, were weaker because they

TABLE III-1

COMPARISON OF DENSITIES AND POROSITY FOR PARENT TUFF AND FUSED GLASS LINER

Material	Dry Density (Mg/m^3)	Grain Density (Mg/m^3)	Porosity (%)
Parent Tuff	1.50	2.54	41
Glass Lining	2.23	2.40	7

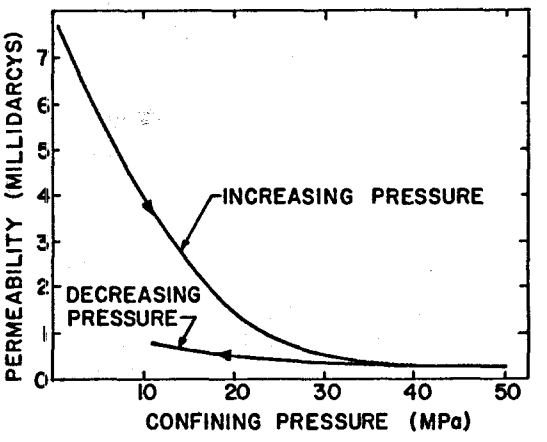

Fig. III-13. Effect of confining pressure on the permeability of a typical radial glass liner sample.

contained the transition zone between the lining material and the parent tuff. The radial samples always failed at the "soft" end (outside end) suggesting that the strength of the lining is a function of the distance from the inside radius. This anisotropy does not appear to be associated with a thin transition layer alone, but rather is inherent throughout the material as a function of the radial coordinate. The linings have a low tensile strength (0.8 to 1.6 MPa) that does not increase with confining pressure and is independent of orientation. Such low tensile strength is probably due to local inhomogeneities and flaws caused by the thermal stresses in the cooling melt. Neither mechanism would detract from the ability of the glass lining to carry compressive stresses but would influence its ability to support tensile or bending loads.

The Terra Tek study represents a significant initial step by characterizing one particular material (Bandelier tuff) and the rock-glass linings formed from it. From the information obtained during this study, the following conclusions can be drawn.

- The lining materials can be modeled as a cylindrical, transversely isotropic media with the radial direction weaker and less stiff than the axial and tangential directions.
- The lining has higher compressive strength (~ 50 MPa) than the parent Bandolier tuff (~ 4 MPa). Strength increases with confining pressure for both the glass lining and the parent tuff.

- Both the glass lining and the parent tuff material possess tensile strengths of the order of 1 MPa.
- The lining material has a permeability of the order of 10 millidarcys at low confining pressure (compared to approximately 300 millidarcys for the parent tuff) but decreases rapidly as the confining pressure increases.
- The results are very encouraging in that the enhanced material properties of the lining are far superior to the parent material and present the possibility for many engineering applications.

C. Refractory Alloy Fabrication

1. Introduction-General Fabrication Problems. The high temperatures at which rocks melt and the requisite higher internal operating temperatures of Subterrene penetrators mandated the utilization of refractory alloys or materials for construction. A large effort was made to locate and use commercial fabrication sources and to develop appropriate fabrication techniques to accommodate large stock size requirements and design complexity. In addition, requirements of high mechanical strength and molten rock corrosion resistance at various design joints necessitated expenditure of effort on a high-temperature braze program. Development of several useful braze formulations was accomplished.

The objectives relative to refractory metal fabrication were: to identify the state of the art, locate facilities and associated skills, expand upon the state of the art where required, and aid in the development of the industrial sources for the penetrator hardware. An extensive nationwide survey was made in support of these objectives. A list of those organizations handling molybdenum (Mo) and tungsten (W) is given in Table III-2.

TABLE III-2

FABRICATORS FOR TUNGSTEN AND MOLYBDENUM PARTS

Work Has Been Performed As Follows. Sources Indentified, But Not Yet Used, Are Marked With An Asterisk.

1. Vacuum-arc-cast, extruded molybdenum bar:
   Climax Molybdenum (Amax Specialty Metals) Cleveland, OH.
2. Powder-metallurgy, extruded molybdenum bar:
   Climax Molybdenum
   General Electric, Cleveland, OH.
   Sylvania, Towanda, PA.
3. Powder-metallurgy tungsten blanks:
   General Electric, Cleveland, OH
   *Sylvania, Towanda, PA.
4. Extruded tungsten bar:
   Canton Drop Forging and Mfg, Co., Canton, OH.
   Nuclear Metals, W. Concord, MA.
5. Upset forging -- molybdenum and tungsten:
   Oak Ridge National Laboratory, Oak Ridge, TN.
   *Ladish Co., Cudahy, WI.
   *Northwest Industries, Albany, OR.
6. Molybdenum sheet spinning:
   Laeger Metal Spinning, East Linden, NJ.
7. Chemical vapor deposition:
   Ultramet, Pacoima, CA.
8. Ring rolling:
   *Ladish Co., Cudahy, WI.
   *Airco Viking, Verdi, NV.
9. Silicide coating:
   Vac-Hyd Processing, Torrance, CA.
10. Machining:
    Los Alamos Scientific Laboratory, Los Alamos, NM.
    Northwest Industries, Albany, OR.
    Thermo Electron, Woburn, MA.
11. Medium-temperature brazing:
    Los Alamos Scientific Laboratory, Los Alamos, NM.
    Air Vac, Carrollton, TX.
    *Thermo Electron, Woburn, MA.
12. High-temperature brazing:
    Oak Ridge National Laboratory, Oak Ridge, TN.
    Thermo Electron, Woburn, MA.
    Advanced Technology, Pasadena, CA.
13. Electron-beam welding:
    Los Alamos Scientific Laboratory, Los Alamos, NM.
    Electrofusion, Menlo Park, CA.
    Electron Beam Welding, Inc., Los Angeles, CA.
    *Thermo Electron, Woburn, MA.
14. Alloy development (in conjunction with LASL):
    *Climax Molybdenum, Cleveland, OH.
    *Wah Chang, Albany, OR.

Vacuum-arc-cast low-carbon Mo has been the prime test material for penetrator development. Although W and some alloys such as thoriated W have certain high-temperature metallurgical advantages (small-scale tests have been performed), the state of the art suggests that a large fabrication development program would be necessary to bring W technology up to a level comparable to the sophisticated quality standards and fabrication know-how of present-day Mo. An additional deterrent to large-scale use of W has been the greater degree of corrosion observed in molten rock experiments.

The various penetrator designs including density consolidators, fluted extruders, conventional extruders, and single-piece melting body corers resulted in the need for both current and advanced fabrication techniques to produce appropriately sized stock billets of material. Close cooperation was achieved with the commercial organizations in this respect. In particular, the development of large-diameter Mo penetrator blanks was a significant achievement. Excellent billets of fully wrought Mo (150 mm diam) have been produced by forging and diffusion-bonding three shorter sintered stock billets together for a total length of 450 mm.

2. High-Temperature Braze Development. This program was conducted under a two-phase effort. The preliminary phase was largely on a screening level with results as follows:

- The specific braze compositions Ti-10Cr, Ti-30V, Ti-65V, V, Cr, and Ni (for diffusion bonding) were laboratory tested in sample cups. The cups were used to hold Jemez basalt for the molten rock compatibility test portion of the program. Of these compositions, only V and Ti-65V were considered as good vacuum furnace brazes. General applications for the Ti-65V alloy would be limited to <1670 K and to <1960 K for V. Neither material could be expected to survive for any significant length of time in contact with molten basalt, and oxygen-contaminated atmospheres are to be avoided.
- Activated diffusion bonding of Mo with Ni holds great promise.
- Pore formation from the Kirkendall effect became a problem when braze joints were overheated.
- Mo-Mo, W-W, and Mo-W brazing were interchangeable.

The major phase addressed the problem of the development of other brazes for use to ∿1900 K, elimination of pore formation within the braze joints, shear strengths of the braze joints, as well as conducting further compatibility tests. Conclusions are best discussed in terms of the individual braze formulation.

- Ti-65V. Kirkendall void formation was eliminated by heating the joint ∿40 K above the alloy flow temperature. The upper limit of compatibility with basalt was confirmed at ∿1670 K. The high-temperature strength was better than recrystallized vacuum-arc-cast Mo. Data for all brazes are shown in Table III-3. A typical shear test specimen is shown in Fig. III-14.

TABLE III-3

SHEAR STRENGTH OF BRAZE JOINTS IN Mo AT 1670 K

Braze Material	0.2% Yield Strength (ksi)	(MPa)	Ultimate Shear Strength (ksi)	(MPa)
Ti-65V	2.6		5.1	
	2.0		3.4	
	2.9		6.8	
	2.2		3.6	
	2.5		5.8	
Average	2.4 ± 0.3[a]	16 ± 2	4.9 ± 1.5	34 ± 10
Pure V	1.6		4.7	
	2.6		6.0	
	1.4		4.7	
	2.5		4.6	
	---		---	
Average	2.0 ± 0.6	14 ± 4	5.0 ± 0.7	34 ± 5
50V-50Mo	1.8		[b]	
	1.8			
	1.4			
Average	1.7 ± 0.2	12 ± 1		
50MoB-50MoC	1.8		[b]	
	2.3			
	3.2			
Average	2.5 ± 0.7	17 ± 5		

[a] ± values are standard deviation of the means.

[b] Joint was substantially stronger than the base metal.

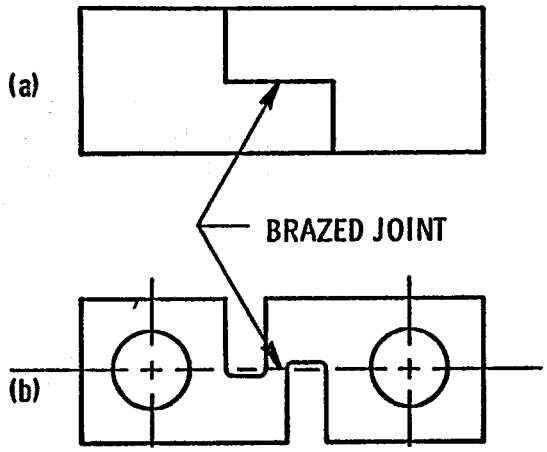

Fig. III-14. Braze shear test specimen, (a) as brazed blank, (b) finished specimen.

• 50Mo-50V. Kirkendall voids were not observed, probably due to prealloying. Corrosion resistance was improved over that of pure V. Joints were substantially stronger than the base metal.

• 50MoB-50MoC. Although not an optimum mixture, it was clear that the basic formulation was good since the joints exhibited exceptional high-temperature strength, good corrosion resistance to at least 1670 K, and no void formation. This system shows excellent potential for joining Mo.

3. Silicon Carbide Conversion Coatings. Parts fabricated from the refractory alloys for routine laboratory testing are reasonably expensive. To reduce development costs, a preliminary evaluation has been made of silicon carbide (SiC)-coated graphite for both glass-forming elements and developmental penetrator bodies of various sizes. The coating is produced by a surface conversion on premachined graphite parts. The finished unit is relatively inexpensive and offers the potential of improved mechanical wear and oxidation resistance. Compatibility tests in basalt have demonstrated resistance to corrosion to ∿1800 K for periods of ∿4 h (14.4 ks). Coating thickness should be of the order of 0.5 mm. Careful dimensional design is necessary to avoid undue thermal stress cracking. While refractory metal penetrator bodies would be required for field tests and lifetime studies, the SiC-coated graphite parts offer a new dimension in flexibility for low-cost laboratory preliminary evaluation tests.

D. Geosciences

1. Introduction. Engineering of Subterrene systems for many applications has been materially assisted by the various disciplines composing the geosciences. Many illustrations of Subterrene system - geoscience interaction have been encountered. Familiarization with basic physical and chemical property data of many rock types has been required for logical and orderly Subterrene development. A large amount of literature data for solid and molten rocks as well as rock glasses was accumulated during the course of the program. Included were: chemical and mineralogical composition, thermodynamic functions, density, viscosity, melting ranges, thermal diffusivity and conductivity, specific heat, coefficient of thermal expansion, permeability, electrical resistivity, and dielectric constants. A number of these values were obtained as a function of temperature and pressure, and selected experimental measurements were also made, adding to the data base. For example, a precision gas comparison pycnometer was obtained which was capable of measuring rock volumes to 0.1 cm^3 (out of a total of 50 cm^3). Coupled with appropriate sample preparations and a direct weight measurement, bulk density, grain density, and porosity could be determined.

2. Melting Range Experiments. Melting range measurements were accomplished routinely using either an induction heater optical or hot-stage microscope technique (Leitz 1750 model). Although much data was available in the literature, the large variability in rock composition justified acquisition of accurate information relative to the specific rocks used in the test program. These measurements were very important since the melting range encountered would affect a decision on (1) whether or not a conventional Subterrene penetrator could be used for that particular type of rock and (2) if it could, which specific engineering design would be appropriate. It is known that a number of rock formations do not melt at ambient pressure but rather decompose (for example, pure limestones).

In addition to measurements made on the local rock formations, a number of rock types from other localities were checked. These included: sandstone from Pecos National Monument, NM; basement granite from the Fenton Lake region, NM; caliche soil from Sandia Corporation's test grounds, NM; granite gneiss from Ft. Belvoir, VA; various soils from the Hanford radiochemical tank storage farms, WA;

Columbia river basalt from Bend, OR; and alluvial soils from the Nevada Test Site, NV.

The National Park Service had also expressed an interest in using a Subterrene penetrator to melt holes for purposes of wall strengthening and water drainage in a number of archeological sites. As part of an independent program, melt tests were conducted on various rock formations from such Southwest areas as Tuzigoot, Tumacacori, Casa Grande, and Montezuma Castle, all national monuments in Arizona, as well as Ft. Bowie Historic Site, AZ. These tests showed that although many of the rocks, soils, and adobe structural materials could be melted at conventional Subterrene operating temperatures, certain others could not.

Another use for the hot-stage microscope was the visual study of the melting kinetics of multicomponent systems as well as individual minerals and crystals. For example, Bandelier tuff, when initially melted, yields a highly fluid liquid which contains large crystals of quartz and cristobalite. This high fluidity permits easy penetration. As melting progresses, the liquid begins to dissolve the crystals with an attendant increase in viscosity.

3. Molten Rock Property Studies. The Subterrene system is capable of melting many types of rock, but penetration rates can be reduced because of high viscosities exhibited by, for example, granites. In general, the melt should be no more viscous than a commercial glass, which is normally worked below a viscosity of 10^3 Pa.s. A typical operating envelope based upon this criterion and the practical temperature limitations of a Mo penetrator is defined in Fig. III-15. Corning Glass Works assisted the program by obtaining molten rock viscosity data. A typical viscosity curve (for Dresser basalt) is shown in Fig. III-16.

To alleviate the penetration rate problem, the concept of pressurized flux injection was considered. The addition of a fluxing or mineralizing agent under pressure just preceding the advancing penetrator should have beneficial results. A two-fold effect occurs in that both the viscosity and the absolute values of the melting range are reduced. These are well-documented phenomena and typical fluxing agents include water, boric oxide, borates, or alkali halide salts. Fig. III-17 illustrates the reduction in melting temperature with a pressurized water system.

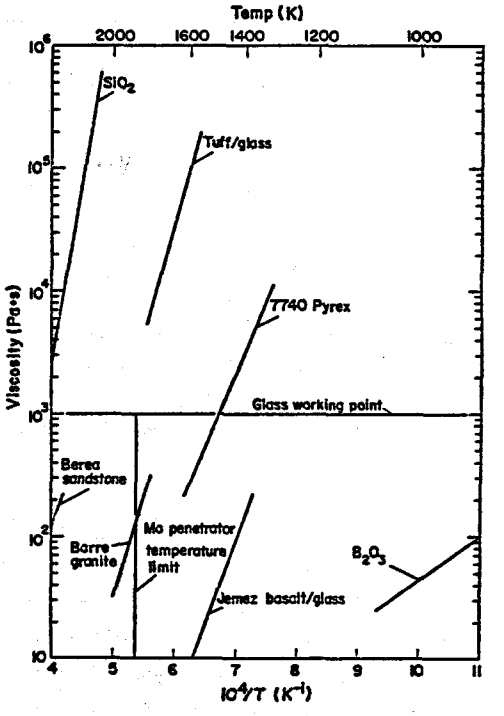

Fig. III-15. Temperature dependence of viscosity for molten glasses and rock glasses.

4. Directed Research. Various rock types have been used in experiments to determine the response of geological materials to Subterrene penetrators during the melting process. Careful analysis of the rock before and after passage of the penetrator is a prerequisite to an understanding of the chemical and mechanical interactions between the metallic

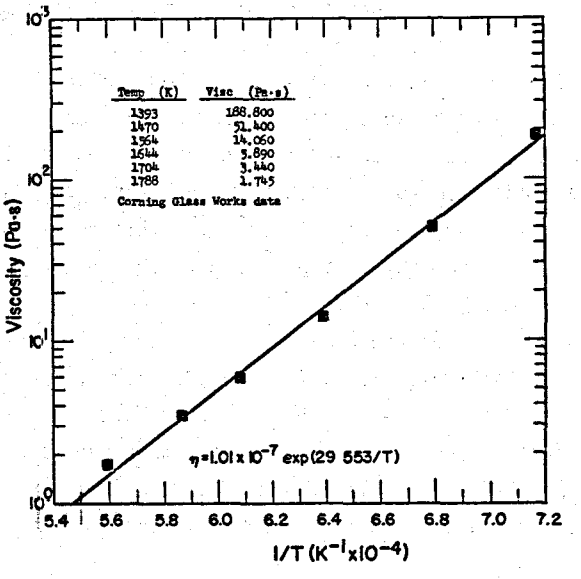

Fig. III-16. Viscosity of molten Dresser basalt.

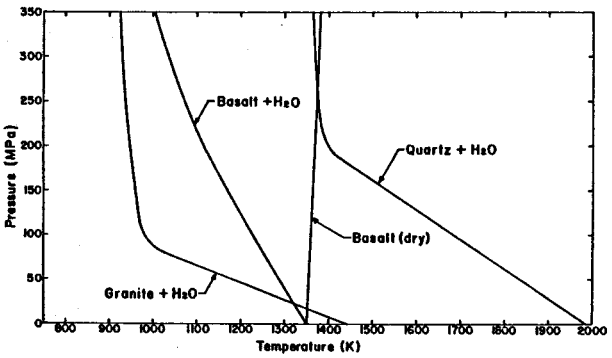

Fig. III-17. The effect of pressure on the melting curve (solidus) of several rock-water systems.

penetrator and the molten rock. Many rock types must be studied if a capability is to be developed for predicting the behavior of the Subterrene in various geologic environments. A preliminary study was performed to illustrate the type of information that can be obtained by petrographic and microchemical analysis of rock-melt samples. Further work on determining the degree of chemical inhomogeneity in the glasses, the proportions of crystals to glass as a function of distance from the penetrator, and the identification of quench products will contribute greatly to the understanding of the interactions between the metallic penetrators and the complex rock-glass mixtures.

Petrographic modal analyses of numerous rock-glass samples were made with a Swift automatic point counter. Corresponding chemical analyses were made with an Applied Research Laboratories Electron Microprobe. Subterrene samples show analogous textures to rocks which have undergone partial fusion in geological processes. Petrographic descriptions were prepared for samples from the glass linings formed in various rock types. The thin sections examined were cut perpendicular to the hole wall. Each sample has three regions: (1) unaltered rock, unaffected because of its distance from the penetrator face; (2) a transition zone, closer to the penetrator face, in which the rock shows alteration effects (such as darkening of the matrix or certain minerals) or a small amount of partial melting, but does not appear to have been converted to a dominantly glassy state; and (3) a fused zone, closest to the penetrator face, consisting of glass with gas bubbles and <50% unmelted inclusions. In most cases, the boundaries between these zones are much narrower than the zones themselves.

Partially fused rock samples exhibit an increase in the amount and degree of homogeneity of glass toward the penetrator face. This observation is consistent with the fact that highest temperatures are maintained for the longest times nearest the penetrator face. Thus, textures of incipient fusion are preserved at the outer edge of the fused zone, whereas the most advanced stage of fusion is present at the inner edge. The mineral and glass mixtures in the samples are the product of a complex interplay of temperature gradients with time of penetration. The rapidity of the Subterrene fusion and quenching process precludes attainment of chemical equilibrium in the molten zone.

Interpretation of the sequence of the fusion process is hindered by uncertainties in (1) the effects of flow of the molten rock during penetration, (2) the geometry of migration of the rock-melt interface during heating, and (3) the nature and duration of thermal gradients in the rock during penetration. The rocks record only the maximum thermal profiles effective over varying time intervals. Molten rock flow during Subterrene penetration is indicated by the finely laminated texture of glass near the penetrator face and the presence of streaks of melted mineral grains parallel to the hole wall. The laminations are defined by variations in color, refractive index, and major element content (and probably oxidation), and they generally parallel the penetrator face, suggesting laminar flow during fusion. In several specimens, laminae show complex swirling patterns suggesting that the entire fused zone underwent mixing during penetration. Such action could mix crystals and liquid in the fused zone and could transport partially molten crystals from the penetrator face throughout the fused zone, thereby hindering the interpretation of the sequence of alteration and fusion.

Petrographic information derived from samples exposed to Subterrene penetration may be used in the Subterrene development program in the following ways:

- Petrographic analysis can provide data on the identity, volume percentage, and size distribution of relict unmelted crystals and quench products in the fused zone of Subterrene samples. Estimates of

the degree of abrasion (mechanical and chemical) by such crystals in various rock types can then be made. The metallic penetrator tip may be abraded by the mixing action which brings angular relict crystals, such as quartz and olivine, into contact with the tip. Such abrasion might be lessened if mixing were suppressed and if a narrow zone of completely fused material could be formed along the penetrator face, as is present in the Bandelier tuff samples.

- Penetration rate is inhibited by high viscosity, particularly in highly siliceous melts. Effective viscosity measurements, coupled with determination of temperature gradients in the samples, can be correlated with petrographic data to investigate possible ways to reduce the viscosity of liquid-crystal mixtures in the fused zone.
- Fluid flow patterns, traced by the dark streaks of graphite and fused iron oxides in the glass walls of the holes, can be examined in detail by cutting series of oriented thin sections. Calculations of the geometry of the glass flow can then be verified by careful observation of these patterns.
- Petrographic techniques can be used to determine the sequence in which the minerals in rocks melt under the nonequilibrium conditions of the Subterrene system. The early-melting fraction produces the liquid composition into which additional minerals will react and through which the Subterrene will penetrate at a given temperature. The degree of chemical corrosion of the penetrator may be dependent upon the chemical composition of the partially melted rock which, in turn, is dependent upon the temperature gradients in the sample.

Deep geothermal drilling requires knowledge of the effects of both the lithostatic pressure and high temperatures, alone and in combination, upon the penetrator materials. Although experimental high-pressure studies were not completed, a laboratory drilling experiment with preheated (650 K) basalt was accomplished. The feasibility of Subterrene-type drilling in hot rock was thus successfully demonstrated.

IV. FIELD TEST AND DEMONSTRATIONS

A. Field-Demonstration Units

1. Introduction. The principal objectives of field-testing complete penetrator systems are the performance evaluation of the system under actual field conditions and the acquisition of realistic data on system reliability and expected service life. Data and experience from field tests form an important input in the penetrator-system design-optimization process. The field-test program was established with the design, construction, and utilization of a portable, modularized field-demonstration unit (FDU). This initial FDU provided a self-contained unit for demonstrating small-diameter rock-melting penetration system capabilities at locations away from the immediate Los Alamos area. The major components of the FDU and their basic functions include dual hydraulic cylinders for thrusting the penetrator assembly, a hydraulic power supply and control console for operating the thruster, an electric power supply and control console for providing the penetrator melting power, an air compressor to supply cooling air to the melting assembly, and the associated Subterrene penetrator and required stem sections.

Field-demonstration units were initially used with density consolidation penetrators to form both vertical and horizontal glass-lined holes in porous and unconsolidated rocks. A sequence of exposures taken as a light source was moved along the bore of one of these 15-m-long holes is shown in Fig. IV-1, depicting its smooth surface and straightness. Eight water drainage holes were melted with an FDU at the Rainbow House and Tyuonyi archeological ruins at Bandelier National Monument, NM, in cooperation with the National Park Service (NPS). A program to melt additional water drainage holes at Tumacacori, Tuzigoot, and Casa Grande Ruins National Monuments and Fort Bowie Historical Site in Arizona has been under development with the NPS. Rock and soil samples from these areas have been received, and preliminary melting-penetration experiments are in progress.

The versatility of the original FDUs has been expanded by adapting them for operation with hard rock extruding penetrator systems through the addition of a debris removal stem configuration. Figure IV-2 shows a field-demonstration unit being

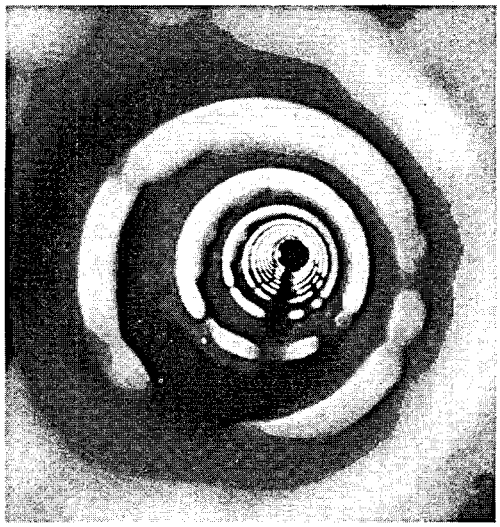

Fig. IV-1. Multiple-exposure photograph taken in glass-lined bore produced by consolidating Subterrene penetrator.

used for a hard rock extrusion experiment in a packaged rock sample. This test was incompatible with the indoor rock laboratory test facility. Service facilities for the FDU are being provided by the mobile experimental field unit which is described in detail in Sec. IV. C of this report.

2. Tunnel Lining Experiment. A significant advantage of a Subterrene-derived system for tunneling or excavating in loosely compacted formations is the glass lining produced in place around the periphery of the melting penetrator. The structural

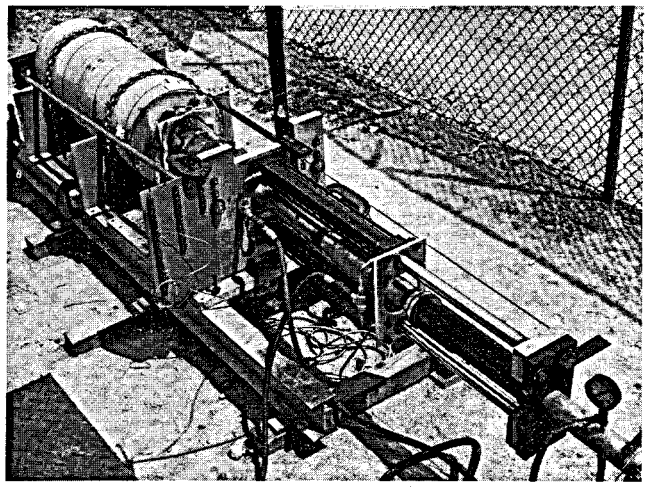

Fig. IV-2. Field-demonstration unit in position for horizontal hard rock extrusion experiment.

integrity of this lining could be utilized to support the roof of a tunnel until a permanent lining can be installed. Use of the Subterrene system could potentially increase the safety and efficiency of tunneling in formations which are not self-supporting and might make possible the use of tunneling, instead of the disruptive cut and cover method, for the construction of underground facilities. The basic feasibility of this tunneling concept has been demonstrated by an excavation experiment conducted in a loose alluvial dirt fill behind a wooden retaining wall which was formerly used as a blast shield bunker. The existing wooden wall made an ideal portal for the prototype tunnel opening (2 m high, 2 m deep, and 1 m wide) which is shown in Fig. IV-3.

The roof and side walls of the tunnel were formed by melting a series of 50-mm-diam horizontal holes approximately 2 m deep in the loose soil fill material using electrically heated density consolidation Subterrene penetrators that are ordinarily used for laboratory and field development tests. The holes were placed sufficiently close together for the glass linings to fuse and thus produce a double-walled lining reinforced by webs between the individual holes. Four vertical holes were melted from the surface at the closed end of the tunnel to stabilize the formation in that region. After the holes were melted to form the roof and walls of the tunnel, the interior volume was excavated by hand to expose the glass lining. An FDU was easily adapted for the task by mounting the hydraulic thruster unit on an adjustable scaffolding as illustrated in Fig. IV-4. Holes were predrilled in the wooden retaining wall of the bunker at the proper locations for insertion of the Subterrene penetrator to produce the continuous glass lining. The penetrator assemblies employed a new design replaceable graphite glass former which produced smooth glass linings and showed radial wear of less than 0.005 mm per meter of lining produced. Gaseous nitrogen was used to chill the melt and solidify the glass, and the maximum penetrator power consumption was 4.5 kW. The excavated tunnel volume was 4 m^3 and the volume of the glass lining which forms the wall was approximately 0.2 m^3. This small test tunnel demonstrates the concept of supporting the overburden of a tunnel with a glass lining formed in situ by a kerf-melting penetration system. The production of tunnel linings by multiple Subterrene penetrators operating simultaneously is a logical extension of this test.

B. Public Demonstrations

1. Washington, DC. The LASL Subterrene staff staged a series of field demonstrations of consolidating and extruding rock-melting penetrator systems at the U.S. Army's Engineering Proving Grounds quarry

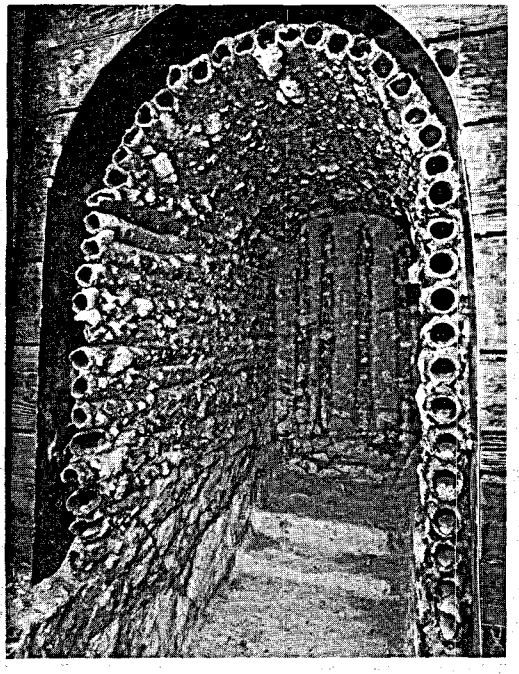

Fig. IV-3. Subterrene-produced prototype tunnel opening showing detail of left wall.

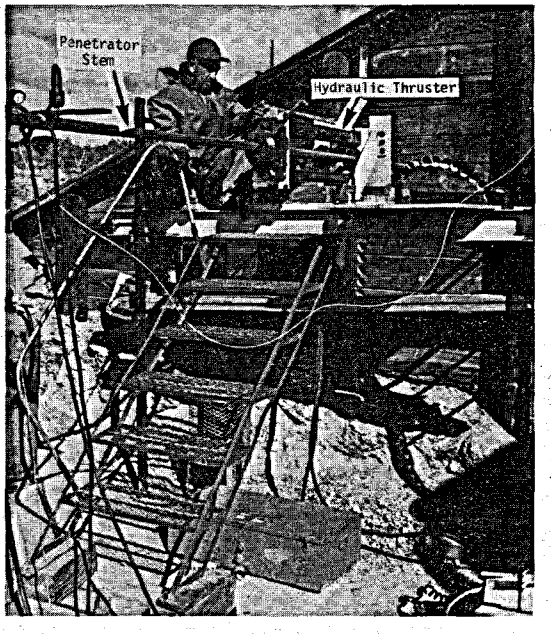

Fig. IV-4. Field-demonstration unit melting holes for tunnel roof.

area at Fort Belvoir near Springfield, VA. Attendance averaged above 80 for the first three demonstrations and approximately 45 for the final presentation. Attendees at the sessions were primarily from the following groups:

First Morning - Atomic Energy Commission, Congressional Representatives, Military Personnel.

First Afternoon - National Science Foundation, Congressional Representatives, Military Personnel.

Second Morning - Industrial sector including representatives from tunneling, horizontal hole boring, major oil companies, and manufacturers of support equipment.

Second Afternoon - Representatives from all areas.

Each demonstration was initiated with a welcoming address and introduction by a representative of either the AEC or NSF. A LASL scientist then presented a brief historical and technical account of the Subterrene program, the ways it differs from conventional drilling methods, potential practical applications, and the characteristics of the melting penetrators which the audience would observe during the actual demonstrations. Part of the Subterrene field demonstration equipment is shown in Fig. IV-5 during one of the Fort Belvoir demonstrations.

Each of the two portable Subterrene field units was then demonstrated, beginning with a horizontal consolidator penetrating a section of alluvium encased in a steel shell. The consolidator was allowed to break through the end of the sample which enabled the audience to watch as the molten earth was displaced from the end of the shell and the hot, glowing penetrator was visible. After each demonstration the shell was removed and the observers were allowed to examine the glass casing formed by the penetrator. This was followed by an extruder, operated in a vertical position, penetrating a hard rock sample and demonstrating the concept of molten debris removal by the cooling gas stream.

Subterrene staff members were available during the rock-melting demonstrations to explain the sequence of operations and answer questions on rock and soil melt handling, potential applications, and the simplicity of the field-test equipment and operations. In addition to examining the penetrators, associated equipment, and the melted holes at close range, the observers were invited to visit the display trailer to obtain copies of Subterrene reports. Additional background information was provided by the 20 specially prepared display posters located in the trailer, as depicted in Fig. IV-6. This demonstration series was sponsored by the Atomic Energy Commission and the National Science Foundation - RANN Program with additional inspiration provided by the Interagency Committee on Excavation Technology (ICET).

2. Denver, CO. As guests of the Bureau of Reclamation, the LASL Subterrene staff staged a series of field demonstrations of consolidating and extruding rock-melting penetrator systems at the Denver Federal Center. Two demonstrations were given in the

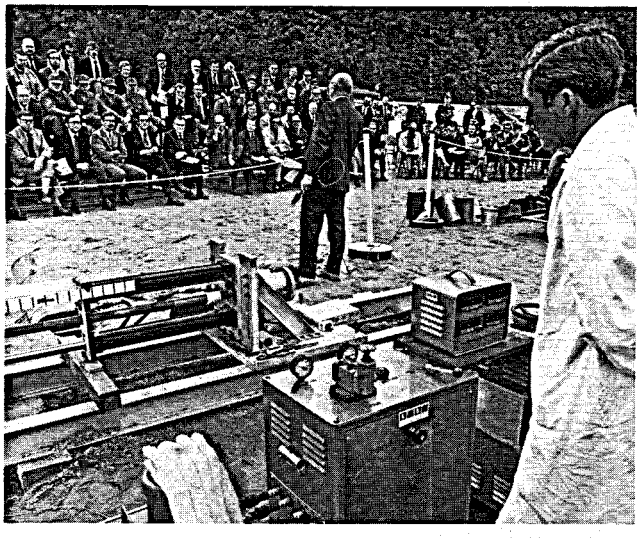

Fig. IV-5. Subterrene rock-melting demonstration and briefing before audience in Fort Belvoir, VA.

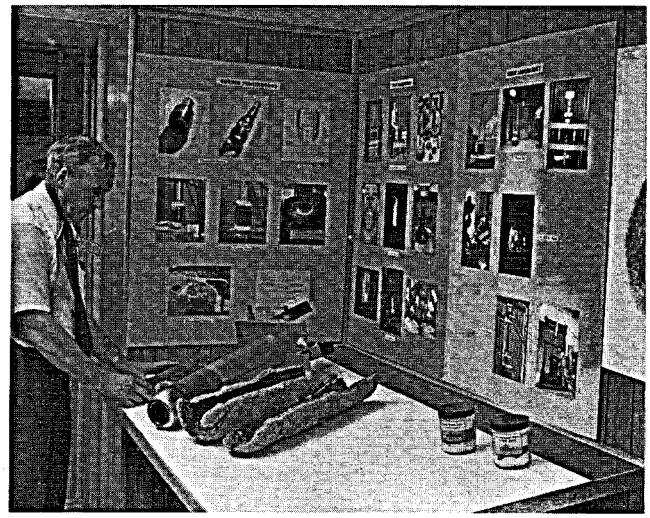

Fig. IV-6. Subterrene demonstration display trailer.

morning, with an average attendance of 85, and one in the afternoon with a phenomenal attendance of over 400 visitors. The program for the demonstrations was similar to that used at Fort Belvoir, VA, with a representative from the Bureau of Reclamation welcoming the group and introducing the LASL speaker. After a brief historical and technical account of the Subterrene program, the two portable field units were demonstrated. The observers then inspected the penetration systems, melted glass-lined holes, and visited the display trailer to collect technical reports and study the display posters on the Subterrene program.

3. Tacoma, WA. During the past three years, Tacoma has attempted to create an environment in city government for experimenting with innovative techniques and developing better procedures and hardware for improving city operations through the use of new technology. A Technology Transfer Center has been created to aid in the development and implementation of proposed solutions to departmental problems in the city and to establish an intercity center for technology applications. As a part of this program, Tacoma hosted a Technology Transfer Field Day Program to illustrate how it is attempting to mobilize its resources to aid productivity improvements throughout the city. The Field Days were held to communicate information about progress in the application of technology to municipal operations directly from the hardware developers and to provide observers with first-hand experience in handling several types of new hardware and to view operational improvements in service delivery systems. The Los Alamos Scientific Laboratory was invited to participate in this program by providing Subterrene rock-melting penetration system demonstrations aimed at the potential use of this technology for underground utilities emplacement.

The soil sample provided for the demonstrations was loosely consolidated local alluvium described as "pit-run gravel" which consisted of material varying from fine particles to 50-mm characteristic size conglomerates. The sample was visibly wet and packed in a 1.2-x 1.5-x 2-m plywood sample container. After melting a sample hole through the alluvium to test the equipment and provide a finished hole for the observers to inspect, two additional holes were melted and stabilized with glass linings during the actual demonstration. Visitors were briefed on the technology and equipment while they observed the actual melting operation at close range. The finished holes were smooth and stable and immediately available for inspection upon withdrawal of the penetrator system. After cooling, segments of the glass liners were provided to the spectators to conclude the demonstration. The demonstrations and equipment were viewed by a wide ranging audience of engineering, city management, and technology transfer oriented visitors.

C. Mobile Experimental Field Unit

1. Introduction. The extension of the field test program to larger diameter, deeper penetrations into hard rock formations has led to the design, fabrication, and field utilization of a specialized mobile Experimental Field Unit (EFU). This EFU is designed to operate with consolidating, coring, and extruding penetrator systems under field conditions and in areas remote from the laboratory. For hard rock penetrations with extruding systems, this means that an appreciable thrust load must be applied to the penetrator melting body in order to provide extrusion pressures in the rock melt sufficiently high to force the molten material to flow through the debris-removal passages in the melting body. In nonstable formations such as caving or squeezing soils or formations containing trapped ground waters, it may be necessary to produce melt pressures greater than the overburden stress to stabilize and support the hole and prevent blowout. Since the weight of the currently used gas-cooled stem is insufficient to produce the required pressures, a large pull-down capability has been provided. This hydraulic pull-down feature and the absence of a rotary table are the characteristics which distinguish the EFU from a conventional, lightweight, work-over rig. The Experimental Field Unit, as received from the commercial fabricator, is illustrated in Fig. IV-7.

Significant design features of the EFU are briefly summarized below:

- The mast will handle 300 m of 114-mm-(4.5-in.-) diam dual string pipe in 10-m lengths. It is raised and lowered hydraulically and is designed to work when vertical or near vertical. With modifications it can be operated at greater inclinations, even approaching horizontal penetrations.

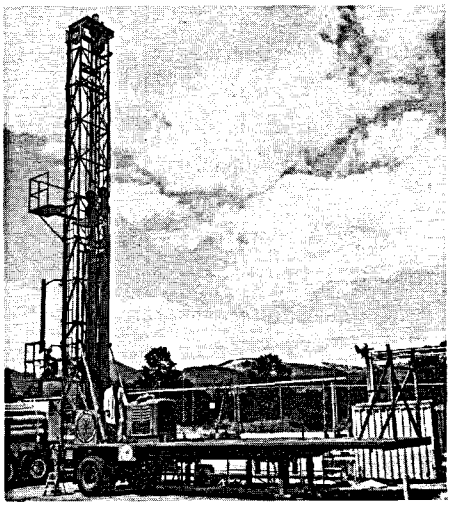

Fig. IV-7. Mobile Experimental Field Unit as received from fabricator.

• The unit is hydraulically powered and controlled. Dual two-way hydraulic cylinders attached to the fastline side of the mast, Fig. IV-8, provide the force to move the pipe in or out of the hole and to pull down on the string. Each cylinder's "drilling" line attaches to its individual hydraulically operated gripping elevator which can transmit a pull-down or extraction force of 89 kN (20 000 lb) to the drill stem. Both elevators can be used simultaneously to exert a force of 178 kN.

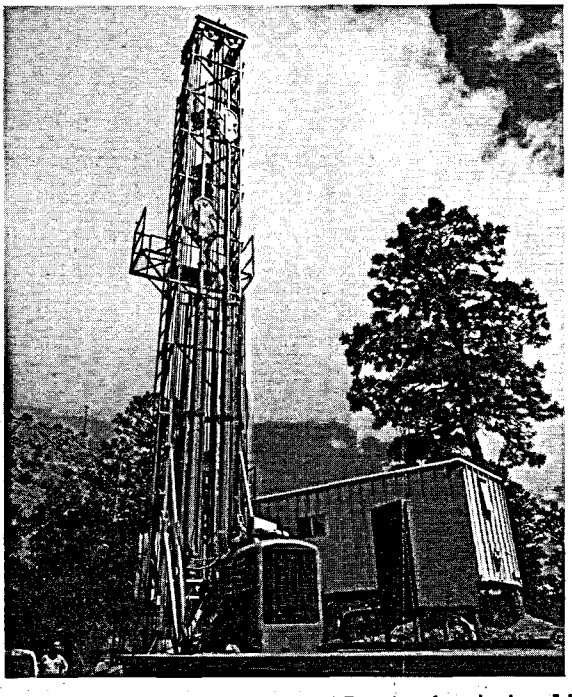

Fig. IV-8. Fastline side of EFU showing hydraulic cylinders, drilling lines, and diesel-hydraulic power unit.

• Penetrating and hoisting speeds are continuously variable, from 0 to 5 mm/s (1 ft/min), and can be remotely controlled with an electrically positioned spool valve in the hydraulic supply line. Manual controls produce higher speeds for tripping or other light-load operations.

The mast, pull-down and hoisting systems, hydraulic pump and prime mover, and a hydraulic powered sandline are mounted on a tandem float. With the mast stored in a horizontal position, the unit is legal to move with a commercial tractor without a special permit.

Operation of the system is straightforward and requires only an operator and helper for routine penetration and tool tripping. Automatic, closed-loop servomechanism control in several modes of penetration (constant load, constant rate, or position demand) is provided, and monitor and alarm circuits warn the operator of abnormal conditions. The present experimental nature of the operation dictates more complete instrumentation and recording of penetrator performance than would be required in routine hole forming.

2. Stem Design and Performance. A 78-mm-diam stem was designed, fabricated, and utilized for field operations with the EFU. This stem was designed for either consolidation or extruding Subterrene penetrators operating at increased depths at power levels up to 30 kW. The concentric tube design of the stem provides, in addition to structural support, electric power supply to the penetrator, coolant and debris removal gas, debris removal carry-off tube, inerting gas (helium) supply, and instrumentation capability. The outer shell is the main structural member and is fabricated from 6061 T-6 aluminum on the basis of its low resistivity, high strength, atmospheric corrosion resistance, and low weight. Designed to allow 100-kN (22 500-lb) loading in either direction, the shell is also the negative lead for dc power transmission to the penetrator. The inner stainless steel tube is for debris removal while the annulus provides the space for the coolant gas flow, three insulated parallel copper power leads, helium gas line, and instrumentation leads. An end view of a typical stem section is shown in Fig. IV-9 illustrating these functions, and some additional pertinent data on the stem design is presented in Table IV-1.

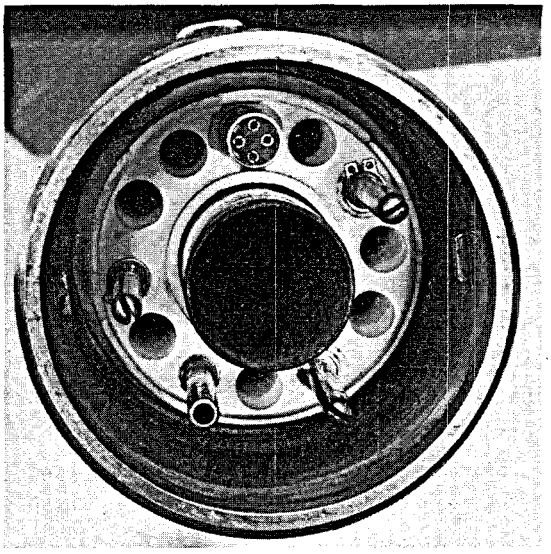

Fig. IV-9. End view of 78-mm-diam stem section.

TABLE IV-1
PERTINENT 78-MM-DIAMETER STEM DATA

Section lengths	4.05 m
Debris carry-off tube i.d.	24.0 mm
Weight per section	25.9 kg
Resistance of copper electrodes per section	4.65×10^{-4} Ω
Resistance of aluminum shell per section at 300 K	1.13×10^{-4} Ω
Measured dielectric strength	1200 V (minimum)

A structural coupling of Inconel 718 joins successive sections and transmits tensile loads while compressive loads are absorbed by a mating shoulder on adjacent sections. This mechanical design coupled with simple "slip in" power and flow connectors allows fast makeup of the drill string. Under field conditions the contact resistance between adjacent aluminum stem sections was less than 2×10^{-4} Ω at moderate penetrator thrusts, indicating excellent electrical performance. Field testing has confirmed the validity of the stem design in providing all necessary penetrator service functions and no difficulties were encountered in the continuous gas transport of the rock wool/scoria debris to the surface for collection.

3. Proof-of-Concept Field Experiment. As a proof-of-concept experiment, the EFU was utilized to produce a 30-m-deep hole in a thick flow of Jemez basalt in Ancho Canyon, southeast of Los Alamos. The depth goal of 30 m was selected as a compromise on the basis of demonstration of capability and field expense and does not represent any technological limitation of the penetrator or its support system. Deployment of equipment for the field operation with the EFU is shown in Fig. IV-10. In addition to the diesel-powered EFU, the following auxiliary equipment was required.

- Power conditioning and control equipment for the electrical power input to the penetrator.
- 220-V three-phase power supply to match the penetrator power conditioning requirements.
- Cooling gas supply for hole forming assembly cooling requirements and debris removal.
- Instrumentation for monitoring and controlling the penetrator system operation.

The instrumentation control, recording, and power conditioning equipment is housed in the trailer to the left of the EFU in Fig. IV-10.

The extruding penetrator selected for the experiment was the 84-mm-diam fluted molybdenum body design described in more detail in Sec. II. B of this report. This extruder was designed specifically to produce a deeper basalt penetration than had previously been made and to do so under field conditions. Preliminary laboratory testing, followed by tests employing rock specimens mounted on the EFU preceded actual production of the 30-m hole. Production of the 30-m-deep basalt hole was completed, and an aggregate of 505 kg of debris was processed

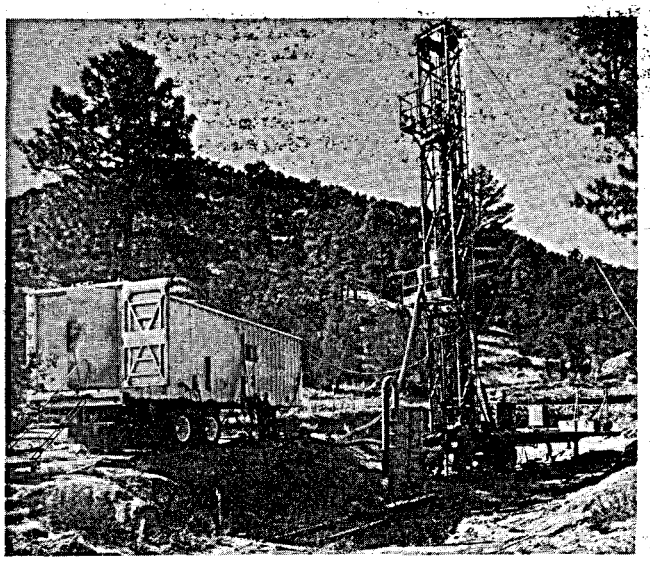

Fig. IV-10. Deployment of EFU in basalt hole melting field operation.

in the operation. The debris is characterized as approximately half rock wool and half scoria or solidified pellets. The cyclone separator and debris storage drums shown in Fig. IV-10 were added to collect the rock wool and scoria prior to exhausting the coolant gas to the atmosphere. The overall experiment effected a sizable gain in knowledge and experience in field operations of Subterrene penetrator systems in general and the 84-mm extruder in particular. All of the new field techniques required for this novel method of hole production were successfully developed over a relatively short time span. In this same interval the 84-mm system evolved by moderate changes from a 3/4-m-depth laboratory extruder to a field device capable of sustained continuous operation at modest depths. It is noteworthy that field testing brought out problem areas and solution approaches that passed essentially undetected in the preliminary laboratory tests.

Hard rock buildup in the lower portion of the debris carry-off tube was a primary cause of field operation stoppages at the beginning of the experiment. Surging is a phenomenon associated with this type of stoppage and occurs when very rapid penetration is made into a built-up melt pool. This causes a large mass of molten rock to be suddenly injected into the carry-off tube substantially "overloading" the transporting gas which allows the slow-moving molten rock to contact the side wall. When the tube wall temperature exceeds 600 K the molten rock debris can stick or adhere to the surface, and this buildup can continue until a complete blockage is present. The solution of this problem was an internal design modification which lowered the temperature of the carry-off tube, thus preventing sticking and blockage. Subsequent deep hole penetrators may find water more effective for cooling of this region coupled with distinct advantages for debris transport. Plans for the EFU include field testing of advanced penetrator assemblies in basalt and other formations at sites near Los Alamos. Other potential applications include utilization in forming test holes for heat flow measurements in several geothermal resource areas, formation of drainage holes in archeological ruins, and production of near horizontal holes for utility emplacement.

V. SYSTEMS ANALYSIS AND APPLICATIONS

A. Geothermal Well Technology

1. Introduction. At the request of the project-sponsoring agency, increased emphasis was devoted to the application of the Subterrene concept to the production of geothermal energy wells. Consistent with this task, the general status of the geothermal industry and the technical problems being experienced in producing geothermal wells were extensively reviewed and evaluated. An earlier LASL publication (LA-5689-MS) presented a summary status review of geothermal well technology, including drilling and operational problems. Another objective of this study was to begin the analysis and evaluation of producing wells by means of the Subterrene rock-melting process. In addition to the use of published literature and data, many personal discussions were held with people in various fields of the drilling and Geothermal Energy (GTE) industries in an effort to arrive at correct and objective conclusions. A list of these contacts is presented later in this section.

2. Current Technological and Cost Status.

a. Exploration. Geothermal resource areas of the vapor-dominated or hydrothermal types are scattered throughout the world. Steam fumaroles or hot-water springs are indicators of such areas and as a result of oil and gas drilling activities, other anomalous high heat flux areas have become known. Data from these sources provide only rough indications of geothermal energy resources because a significant geothermal reservoir is a complex system depending on location, nature of the heat source, recharging characteristics, interrelation of permeable and nonpermeable strata, and on the total volume of the system. Much more information is needed before the full extent and nature of the geothermal resource is well understood. With the exploratory methods available, the presence of a significant GTE reservoir must still be proven by drilling. Exploratory holes can be used for measurements of temperature and pressure profiles, permeability, porosity, lithology, stratigraphy, fluid compositions, and production flow tests. These uses of exploration holes are consistent with today's capabilities for drilling, downhole measurements, and logging except that in many cases the measurement equipment available is not designed to withstand the high geothermal temperatures.

An additional desirable capability is that of continuing drilling past the anticipated production zone towards the source of heat that drives the reservoir. This could mean penetrating into hard igneous and metamorphic rocks at very high temperatures. The objectives would be to gain a better understanding of the basic system and to determine whether reinjection fluid, or even additional fresh water, might be added at the lower hotter depths to percolate upward into the production zone. The latter could greatly augment and artificially stimulate both the production and useful life of the reservoir. At the Geothermal Resources Research Conference in Seattle, in September 1972, two recommendations* were that high priority be given to immediate improvement of exploration methods and to the development of cheaper drilling methods in high-temperature formations. These improvements would result in improved reservoir and economic models which, the conference attendees concluded, were sorely needed. The average costs for shallow oil and gas wells reported by the 1972 Joint Association Survey are presented in Table V-1.

TABLE V-1
AVERAGE DEPTH AND COST PER DEPTH
TOTAL UNITED STATES IN 1972[a]

Average Depth (km)	Type of Wells and Average Cost[b] per Meter ($/m)			
	Oil	Gas	Dry	Total Weighted Average
1.3	44.10	45.10	25.10	35.90
(4300)	(13.40)	(13.80)	(7.70)	(11.00)
1.9	52.95	53.80	34.80	45.20
(6200)	(16.10)	(16.40)	(10.60)	(13.80)
2.6	68.00	82.90	54.40	65.00
(8500)	(20.70)	(25.30)	(16.60)	(19.80)

[a] Numbers in parentheses are ft and $/foot.
[b] Includes drilling and casing.

*W. J. Hickel, "Geothermal Energy - A National Proposal for Geothermal Resources Research," University of Alaska Conference held in Seattle, WA (September 18-20, 1972).

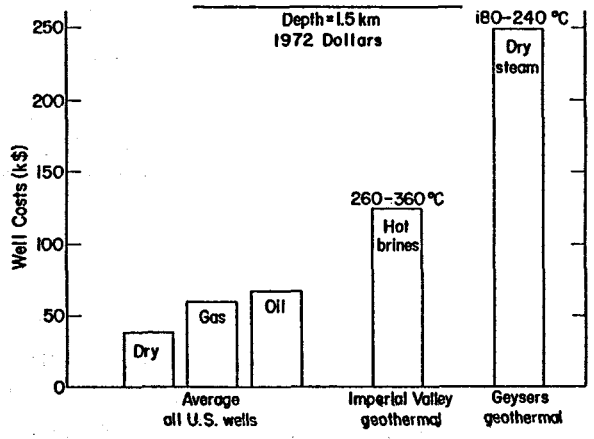

Fig. V-1. Typical well costs for 1.5-km-deep wells.

Cost data compiled at LASL showed that average geothermal wells are considerably more expensive than indicated in Table V-1 for oil and gas wells. These data are represented in Fig. V-1 where it can be seen that the Imperial Valley hot-water wells and The Geysers steam-dominated wells are two to five times more expensive than the average oil and gas wells.

Greider* of Chevron Oil compiled cost data on geothermal exploration wells. Wells to depths of 1.5 km (5000 ft) in most geothermal provinces in sedimentary basins in the U. S. average 65 to 100 $/m (20 to 30 $/ft). In remote areas or in those with interbedded volcanic rocks, costs run from 100 to 200 $/m (30 to 60$/ft). To run casing and to prepare for production in these 1.5-km wells costs 33 to 50 $/m (10 to 15 $/ft). Thus, costs of geothermal wells range from 100 to 250 $/m (30 to 75 $/ft) or approximately two to five times higher than the average costs of oil or gas wells given in Table V-1. Greider presented other cost data: Surface exploration costs run from $75 000 to $90 000 per typical area of interest. Only one out of four of these areas would probably justify an exploratory hole, resulting in $300 000 to $360 000 per drillable prospect. Only one of four of these prospect wells would be worth running pipe and completing for extensive testing. The three unsuccessful wells would cost ∿ $100 000 to $200 000 each and the completed wells ∿ $150 000 to $250 000. The net average cost for each prospect worth completing and testing extensively is then $650 000. Perhaps one of four of the completed prospect wells would result in the discovery well of a reservoir large enough to be commercially attractive. The ratio of total wells drilled to each discovery well is thus 16:1. Greider feels that this is a realistic ratio as the industry matures after the large easily located reservoirs are drilled. Greider's definition of a good discovery well is one defining a reservoir capable of 275 MW(e) power output. A summary of his cost model is shown in Table V-2. This simple calculation of exploratory drilling costs indicates that the costs are high enough to easily justify the cost of research leading to lower exploration drilling costs. The much higher costs associated with the production and reinjection wells will be discussed later.

b. Problems in Completing Geothermal Wells. The methods used in making geothermal wells are essentially the same as those for oil or gas wells. Indeed, this very fact somewhat impedes GTE development because geothermal well drillers are forced to use materials and equipment that are not necessarily best for geothermal wells with their higher temperatures and corrosive conditions. Problem examples are: (1) only oil-well tubular goods and bits are available, (2) muds and cements are not checked out for high-temperature use because

TABLE V-2
COST TO PRODUCE A DISCOVERY WELL
FOR A 275-MW(e) RESERVOIR

	Cost ($)	% of Total
Land acquisition (nontechnical leasing, bonus, rentals, etc.)	3 580 000[a]	45
Drilling (12 unsuccessful + 4 completed holes)	2 600 000	32
Surface exploration (geology, geochemistry, geophysics)	1 840 000	23
Total	8 020 000	100

[a] Considering the high bids made at the Jan. 22, 1974 KGRA competitions in California, these costs are probably low.

* R. Greider, "Economic Considerations for Geothermal Exploration in the Western United States," presented at the Symposium, Colorado Department of Natural Resources, Denver, CO (December 6, 1973).

suitable high-temperature laboratory equipment is not available, and (3) bit-bearing lubrication systems are not designed to withstand GTE temperatures. This dependence is designated as an important consideration in the NSF-sponsored study of impediments to geothermal development by Bechtel Corp. for The Futures Group, Inc. In current geothermal wells, drilling is easy in some sedimentary basins and is very difficult in hard, fractured rocks found, e.g., at The Geysers. The latter results in high bit wear and often in failures of bit bearings due to a combination of temperature, stress, corrosion, and fatigue effects.

To better understand the factors affecting geothermal well drilling, the activity logs for 125 geothermal wells drilled in California were studied.* The majority of the data were either from the general Geysers area or from Imperial Valley, California, and are here designated Steam, Hard Rock (SHR); and Hot Water, Sedimentary (HWS); respectively. The data include 92 SHR and 33 HWS type wells. Their depths are indicated in a frequency of occurrence-versus-depth plot in Fig. V-2. Selected depth intervals are 300 m. About 40% of the Imperial Valley wells ranged in depth from 1300 to 1900 m (4300 to 6200 ft). In The Geysers 50% of the wells are in the 1900- to 2500-m (6200- to 8200-ft) range. A similar plot is shown in Fig. V-3 for overall average penetration rates where the average includes total time for spudding-in to total depth. In the Imperial Valley the penetration rates were 1.5 to 2.5 m/h (4.9 to 8.2 ft/h) for 42% of the wells analyzed. In The Geysers, 52% of the wells were drilled at 1 to 2 m/h (3.3 to 6.6 ft/h), somewhat lower than the rates in the Imperial Valley.

The above discussions of cost centered primarily on wells in conventional GTE areas where maximum depths may not exceed 3 km. For hot dry rock and geopressurized developments, the depths and drilling costs could be considerably higher. Costs increase very rapidly with depth, as illustrated in Fig. V-4. The average oil-and gas-well costs are shown shaded; typical Geysers and Imperial

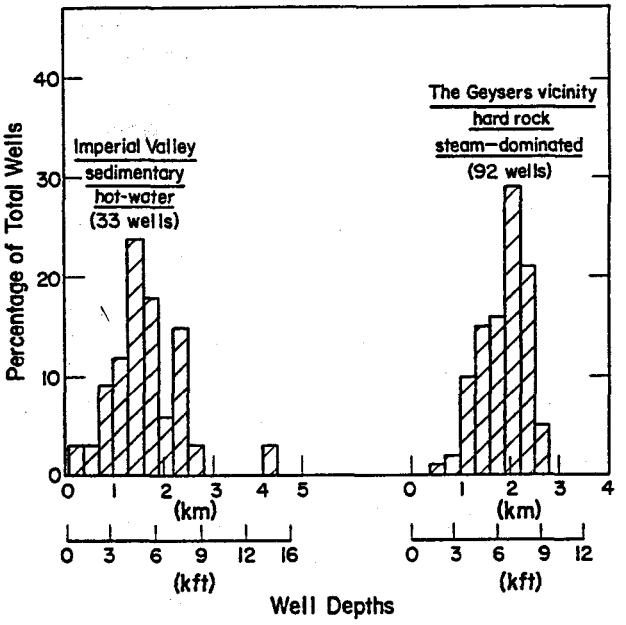

Fig. V-2. Depths of geothermal wells drilled in two geothermal regions.

Valley geothermal costs are shown as 160 $/m (50 $/ft) and 80 $/m (25 $/ft), respectively. For depths of 15 km, costs could be ∿ $20 000 000 to $26 000 000 per well. Clearly, GTE drilling with current techniques could be very costly (e.g., running into tens of billions of dollars) making it worthwhile and cost-effective to develop new, cheaper techniques and equipment.

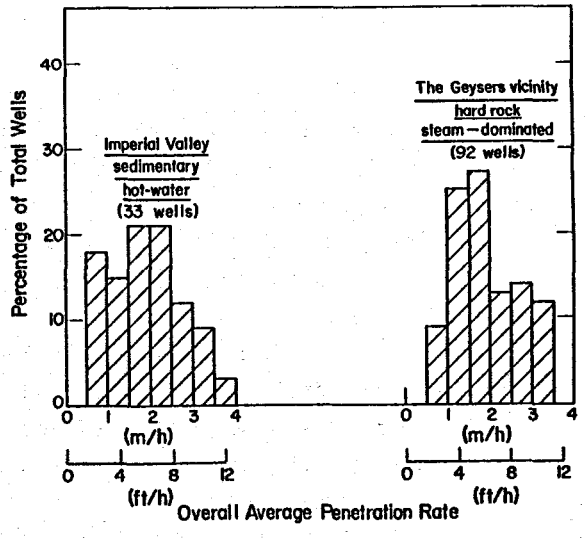

Fig. V-3. Overall average penetration rates in typical geothermal wells.

*Petroleum Information Corporation, Denver, CO, "Drilling Data File for Approximately 300 Geothermal Wells," supplied to Los Alamos Scientific Laboratory for study purposes (March 1974).

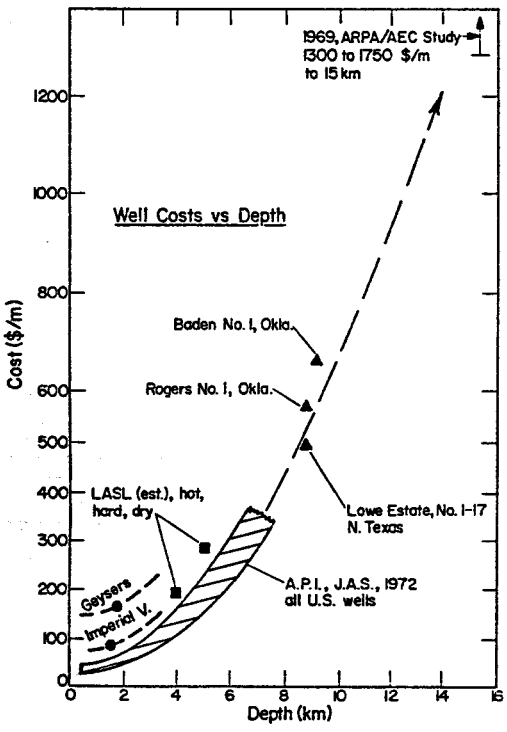

Fig. V-4. Cost of wells per meter vs total depth.

It has been amply demonstrated that naturally occurring hot-water or vapor-dominated geothermal reservoirs can be penetrated by rotary drilling methods that have been developed for oil and gas wells. However, there are factors in geothermal fields such as high temperature, corrosive fluids and gases, unfavorable siting conditions, and, in many cases, hard abrasive rocks, which combine to make the average rotary-drilled geothermal wells more expensive than the average oil or gas wells of comparable depth. High well costs could significantly impede the expansion of geothermal energy sources. There are many applications for geothermal temperatures less than 660 K, which is about the upper limit measured at well bottom to date. To attain the higher temperatures desirable or required for many heretofore unexploited GTE applications, one has to consider penetration into deep hot zones. Current drilling methods (especially the use of muds and cemented casings for hole control and support) will thus be severely strained technically and will probably make the wells excessively expensive. An evaluative summary of the various current drilling problems in geothermal wells is presented in Table V-3.

3. Conceptual Applications of Subterrene Devices to Geothermal Wells. New Subterrene technology would open up options for obtaining the most economically and technically suitable methods for any particular set of conditions and requirements. For example, it could be most economical to use rotary drills for making holes rapidly in known, easily penetrated formations. Then, in hot, hard zones, the tools and methods might change to Subterrene technology to complete the job. Listed below are current rotary drilling problems in geothermal wells followed in each case by a discussion of how the use of Subterrene devices could either help solve or eliminate the problem.

- Problem: Hole stabilization in unstable formations.

Subterrene: The optimum well hole production process minimizes excavation damage to the inherent structural integrity of the ground or rock and is then followed by the continuous installation of a structural support and seal to prevent the inflow of ground fluids. This process may well be accomplished by a Subterrene system which makes the hole by melting and simultaneously forms a structural rock-glass liner.

- Problem: Rock bit wear and temperature-induced failures.

Subterrene: A Subterrene depends upon melting, not on cutting or mechanical fragmentation, and therefore eliminates this problem. Also, high rock temperatures would enhance the performance of the Subterrene bit because the bit has to supply less thermal energy to melt the rock.

- Problem: Cements at high temperature.

Subterrene: Steel casings may not be necessary if good structural rock-glass hole linings can be made. If steel casings are used, the relatively smooth surface inside the glass lining should facilitate the flow of the cement. Also, the requirements that the cement be both strong and impermeable should be lessened because of the presence of the glass lining.

- Problem: Production-zone hole completion.

Subterrene: The Subterrene could penetrate the production zone with a glass-lined hole. This penetration would not kill or impair the zone's production capability because drilling fluid, cuttings, and lost-circulation material would not be

TABLE V-3

SUMMARY OF CURRENT GEOTHERMAL DRILLING PROBLEMS

Item	Type GTE Field: Sedimentary Hot-Water	Type GTE Field: Hard, Igneous Vapor-Dominated	Symbols and Problem Descriptions
Surface locations	--	G	G: Difficult geological conditions typical of many GTE fields, including sites, hard rocks, caving formations, etc.
Drilling-rig design	R,X	R,G,X	R: Rigs of high mobility are needed, adequately equipped to handle rapid changes in hole conditions.
Other surface equipment	T,C,X	T,C,E,X	X: Dependence on oil- and gas-industry materials and equipment, competition for supplies.
Bits and drillability	T,C,D,X	G,T,C,D,X	T: Temperatures up to ∿ 660 K cause rubber, elastomer, metallurgical, mud, cement, and electronic problems.
Mud-circulation systems	T,G,F,X	T,G,F,X	C: Corrosion problems caused by ground fluids and gases.
Hole support and control	G,T,F	G,T,F	E: High stem, casing, and surface-equipment erosion by air + steam + rock cuttings.
Cements	T,X	T,X	D: Directional drilling equipment not available for hard rock at high temperatures.
Downhole measurements	T,X	T,X	F: Hot saline waters contaminate drilling muds. Also, muds can reduce or kill well productivity or may hydrate clays.
Tubular goods	T,C,X	T,C,X	O: Lack of organized GTE wells drilling-data bank and ways to use such data to optimize drilling programs.
Optimized drilling	O	O	H: Costs are typically high because of interrelating effects of items listed above.
Costs of geothermal wells	H	H	

pumped into the zone. Also, the sealing action of the lining would facilitate stem and bit changes, if necessary. Several ways to ultimately complete the well and to allow the hot water or steam to flow into the well are conceivable. One might be to shatter the glass liner with a linear explosive; another, to conventionally perforate the liner with shaped charges.

- Problem: High torque on long drill stems in deep wells.

Subterrene: Subterrene bits are not rotated and therefore the torque requirements are eliminated.

- Problem: Corrosive environment.

Subterrene: The corrosion problem will change because different materials will be used. Any drilling system must live with the corrosive materials encountered in the earth. However, Subterrene-produced holes should be more effectively sealed from the corrosive materials. Also, stem and bit need not rotate so that protective coatings should be easier to maintain.

- Problem: Formation evaluation and sampling.

Subterrene: The Subterrene offers the possibility of extracting a continuous, oriented glass-encased core. The glass hole lining eliminates the problem of making logging measurements through a heavy steel casing or through variable depths of mud invasion. Because the glass-lined hole interior is better protected than the unlined hole, the possibility of developing continuous downhole logging may be enhanced.

- Problem: Directional drilling in hot, hard rock.

Subterrene: Hot, hard rock does not bother the Subterrene bit. Directional change is possible by either mechanical means or by controlling the temperatures circumferentially around the bit.

In exploration and resource assessments, Subterrene devices might make small-diameter, shallow (e.g., 50-mm-diam by 150-m-deep), self-cased holes for thermal-gradient measurements. Many such holes will be needed in the near future. For production wells and systems, there are two specialized back-up or auxiliary devices that could be used in conjunction with conventional rotary drilling systems. First, a hole-stabilization tool for use in caving formations, hydrating or swelling clays, or lost-circulation zones. This tool would be a thermal device producing either a rock-glass lining or injecting structually stabilizing materials into the borehole walls. Second, the tool would be used for completing holes into production zones where high static temperatures and hot fluids are encountered and where reservoir contamination is not desirable.

In certain water or steam reservoirs, or in magmas and lavas that are difficult to penetrate with rotary drills, Subterrene systems could be used to produce entire production wells. Production fields would probably include waste-water reinjection wells and injection wells for production-augmentation purposes. These latter type wells, of smaller diameter than the production wells, could have the same diameter as the exploration wells. Note that one of the desirable requirements for small exploration boreholes is that the holes be readily enlargeable, if desired, to the size of a production well. With conventionally cased holes, such an enlargement is very difficult and costly because the casing is very securely cemented into place. In a glass-lined hole the lining might be either reamed out with a rotary bit or it could be melted and the hole enlarged with a Subterrene bit.

4. Contacts Made to Discuss Geothermal Well Drilling Problems. The following people were willing to discuss drilling problems and contribute data that were useful in preparing report LA-5689-MS, "Geothermal Well Technology and Potential Applications of Subterrene Devices - A Status Review."

1. A. L. Austin, Lawrence Livermore Lab., Univ. of California, Livermore, CA.

2. L. O. Beaulaurier, Drilling Problems, Geothermal Technology Assessment Study for The Futures Group, Inc., Bechtel Corp., San Francisco, CA.

3. W. E. Boyd, Industrial and Business Training Bureau, Petroleum, Univ. of Texas, Austin, TX.

4. M. Carasso, Project Mgr., Geothermal Technology Assessment Study for The Futures Group, Inc., Bechtel Corp., San Francisco, CA.

5. Tony Chasteen, Engineer, Union Oil of Calif., Santa Rosa, CA.

6. Joe Cook, Rock Bit Production Mgr., Administration Div. Hughes Tool Co., Houston, TX.

7. Glenn Damewood, Tech. V.P., Southwest Research Institute, San Antonio, TX.

8. John P. Finney, Project Engineer, Geysers, Pacific Gas and Electric Co., San Francisco, CA.

9. Jim French, GTE Data Bank, U. S. Geological Survey, Garden Grove, CA.

10. Ed Gallo, Director of Research, Hughes Tool Co., Houston, TX.

11. T. C. Gipson, Calvert Western Exploration Co., Tulsa, OK.

12. Bill Glass, V. P. and Operations Mgr., Big Chief Drilling Co., Oklahoma City, OK.

13. John Goode, Cement Lab., Halliburton Services, Duncan, OK.

14. R. Greider, Senior Geological Consultant, Chevron Oil, Minerals Staff, San Francisco, CA.

15. J. L. Kennedy, Editor, Oil and Gas Journal, Houston, TX.

16. R. T. Littleton, Bureau of Reclamation, Boulder City, NV.

17. Jack Marsee, V. P. Engineering, Loffland Bros. Drilling Co., Tulsa, OK.

18. John McNanee, Bureau of the Census, Maryland.

19. R. W. McQueen, V. P., Dresser Security Bits, Houston, TX.

20. K. Mirk, P. Witherspoon, and H. Wollenberg, Lawrence Berkeley Lab., Univ. of Calif., Berkeley, CA.

21. Howard Morton, Technical Repr., Rocky Mts., Baroid Div., N. L. Industries, Inc., Tulsa, OK.

22. M. Newsom, R. Alvis and C. Morse, Sandia Corp., Albuquerque, NM.

23. Dexter Polk, V. P., Dresser Oil Field Products Div., Houston, TX.

24. Henry J. Ramey, Jr., Dept. of Petroleum Engineering, Stanford Univ., Stanford, CA.

25. W. Randall, Research, Amoco Production Co., Tulsa, OK.

26. R. W. Sartor, Dresser Industries, Dallas, TX.

27. Calvin Saunders, Gen. Mgr. Research, Halliburton Services, Duncan, OK.

28. H. Snow and V. E. Suter, District Operations Mgr., Union Oil Co. of Calif., Santa Rosa, CA.

29. Ken Tanner, Mgr. Tech. Services, Baroid Div., N. L. Industries, Inc., Houston, TX.

30. Ted Welp, Internal Revenue Service, U. S. Treasury Dept., Washington, DC.

31. Jim Youngblood, V. P., Dresser Magcobar, Houston, TX.

B. Geothermal Well Systems and Cost Analysis

1. Introduction. In light of the fact that a significant part of the cost of a geothermal energy extraction facility is associated with well costs, improvements in geothermal well drilling technology would be particularly beneficial. When the hot dry rock (HDR) and geopressurized extraction systems are developed, geothermal energy could become very important as a national energy source. According to estimates made by White and Williams,* the geothermal energy resource available to HDR and geopressurized systems in the regional conductive environments (depths down to 10 km, not including any methane contribution) is $\sim$ 33 500 000 x 10^{18} J (8 000 000 x 10^{18} cal = 31 800 x 10^{18} Btu). This is 2600 times the estimated value for conventional steam and hot water geothermal energy resources and 440 000 times the total U.S. energy consumption in 1972 of 75.9 x 10^{18} J.

Both HDR and geopressurized wells can be difficult to produce. Hot dry rock wells are intentionally made in solid and preferably very hot basement rock, hence their name, whereas geopressurized wells are in high pressurized (approaching lithostatic) and difficult-to-drill formations. A study was initiated on the application of the Subterrene concept to the production of these difficult-to-drill wells. The basic study objectives were to:

- Study the application of the Subterrene concept to the production of deep wells such as may be used for hot dry rock or geopressurized geothermal energy extraction systems.
- Make technical and economic comparisons with rotary drilling techniques and systems.

The results are published in LASL report LA-6555-MS, "Technical and Cost Analysis of Rock Melting Systems for Producing Geothermal Wells" by J. H. Altseimer (October 1976) and are summarized in the following sections of this report.

*White, D. E. and Williams, D. L., Ed. "Assessment of Geothermal Resources of the U.S. - 1975," U.S.G.S. Circular 726 (1975).

2. System Model

a. GEOWELL. A computer program called GEOWELL was developed to analyze the critical technical and economic aspects of a Subterrene well-production system. System assumptions and the various technical and cost elements that make up the model are presented in the following discussions. Because both rotary and rock-melting systems are cost-optimized for producing different parts of a well, the program contains both rotary and rock-melting prediction capabilities for deep geothermal wells. For future studies and as more geothermal well data become available, the program's capabilities can be expanded to include a complete spectrum of geothermal well types.

b. Well Designs. Two exploratory gas wells of recent years, drilled under difficult conditions and to record depths, used some of the best rotary drilling technology available today: (1) E. R. Baden No. 1 drilled to 9158 m (30 050 ft) and (2) Bertha Rogers No. 1 drilled to 9583 m (31 441 ft) in the Anadarko Basin in Western Oklahoma by Lone Star Producing Co. of Oklahoma City. After reviewing well designs used in many other wells both in the U.S. and abroad, the designs of these two wells were selected as guidelines for GEOWELL. Figure V-5 shows the well design for a total depth of 10 km drilled completely by rotary bits. Moderate formation and fracture pressures, i.e., approximately hydrostatic, were assumed in the upper 4300 m. High pressures, i.e., approaching lithostatic, were assumed from 4300 to 7000 m. Thereafter, to total depth, it was assumed that pressures were moderate again. Figure V-6 shows the well design when rock-melting bits are used below the 660-mm (26-in.) hole section. It was assumed that the 914- and 660-mm holes would always be made by rotary drilling. Below the bottom of the 660-mm hole, rotary drills would continue to be used until it was desired to start rock melting. The size of the hole at total depth in this well is identical to that shown for the all-rotary case. However, note that intermediate hole and casing sizes are smaller due to the advantageous use of the rock-glass liner.

c. Surface Equipment. Surface equipment requirements for a combined rotary/rock-melting

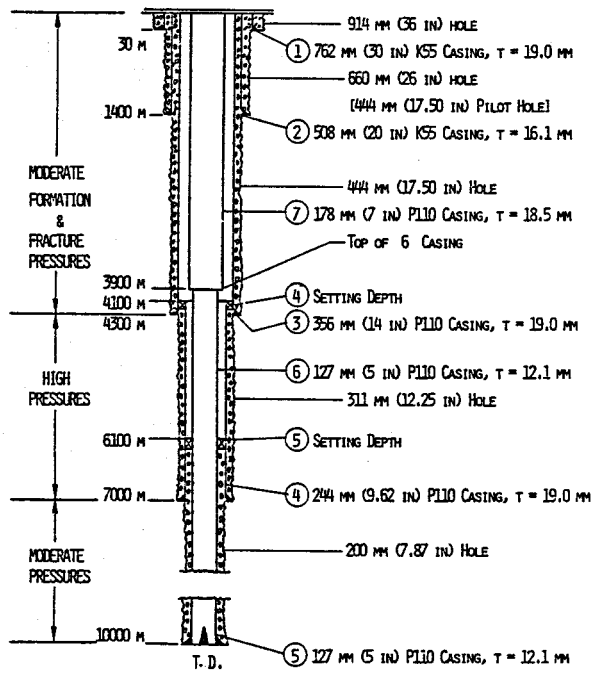

Fig. V-5. Well design for the all-rotary drilled well.

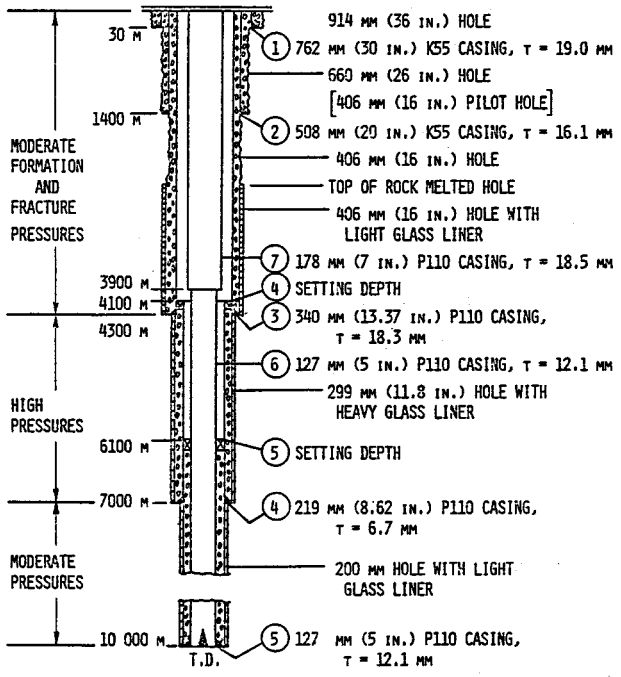

Fig. V-6. Well design for rotary/rock-melted well.

system are similar to those now used for all-rotary projects. Also, the power levels required for rock melting are compatible with those already required on rotary deep-well rigs, e.g., up to 3000 hp. In GEOWELL, the drilling contractor's cost is divided into rig (CRIG) and drill-pipe (CPIPE) costs. For these estimates 1973 oil and gas data were compiled from the open literature and then upgraded to 1975. Using EL as the total target depth in meters, the resultant curve-fit equations used in the program are:

$$CRIG = 1453 + 0.2022\ (EL) + 10.19 \times 10^{-6}\ (EL)^2,\ \$/d$$

$$CPIPE = 106.8 - 0.0419\ (EL) + 20.55 \times 10^{-6}(EL)^2,\ \$/d.$$

d. Drill Pipe. Design studies produced a Subterrene drill pipe capable of carrying both electric current and the downflow of drilling fluid. The pipe is shown in Fig. V-7 and consists of two concentric 7075 aluminum tubes separated by a 2-mm-thick layer of material that, structurally bonds the tubes together and acts as an electric insulator. A conventional tool joint on the outer tube serves as the structural connection with adjacent pipe. The current in the outer tube flows across the thread contact surfaces and the smooth metal contact and sealing surface at the joint leading edge. The inner tube has a tight sliding fit at the joint for electric contact, but no axial forces can be transmitted. Handling and operational characteristics of this pipe are very similar to those of conventional drill pipe. The initial cost is approximately three times higher but this disadvantage is reduced by an enhanced operating lifetime for the Subterrene pipe due to the fact that Subterrene pipe does not rotate and is not exposed to the usual rotary pipe fatigue stresses and frictional wear.

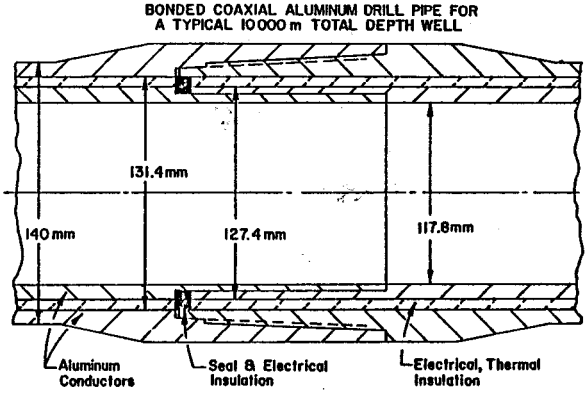

Fig. V-7. Subterrene coaxial aluminum drill-pipe concept.

A pipe with an o.d. of 140 mm (5.51 in.) was found to fit well in all sections of the borehole being studied and was therefore selected as a standard. Thus, in the GEOWELL analysis the o.d. is maintained at 140 mm, whereas the other dimensions are varied to meet current and load criteria. Costs are calculated on the basis of these dimensions to arrive at a basic material and fabrication cost. Other estimates are made as to delivered pipe cost, pipe lifetime, drilling contractors profit, etc., to finally arrive at a Subterrene drill-pipe cost in dollars per day.

e. Bits. The Subterrene bit required for producing deep wells is the melt-extruding type using either gas or liquid as the drilling fluid. The assumed design-point bit performances are a lifetime of 300 h and a rate of penetration (ROP) of 1 mm/s (11.8 ft/h) at a rock temperature of 283 K. Note that rock temperature is specified because ROP varies with rock temperature. Attaining and demonstrating longer lifetime and higher ROP remain development problems for melting bits. Another problem is obtaining sufficient clearance between the glass former (located immediately behind the melting face) and the hole so as to facilitate bit travel during trips. A clearance of several millimeters on the radius is desirable to prevent bit damage or high-pressure drops across the bit during fast trips. At least five approaches to solving this problem have been identified.

GEOWELL also includes rotary-bit performance estimates. Field performances vary widely depending on site and operating conditions. An attempt was made to simulate relatively easy rotary drilling in the sedimentary upper formations and harder drilling in the deeper, more crystalline formations. The equations defining performance vs depth used in the program are for rotary penetration rate, RROP, at any rotary depth, ROTEL, in meters:

$$RROP = 591.62 \times (ROTEL)^{-0.6739}, \text{ m/h}$$

and for bit meterage:

ROTEL < 1440 m: BITM = 884.0 - 0.553 (ROTEL), m/bit

ROTEL > 1440 m: BITM = 97.0 - 0.0033 (ROTEL), m/bit.

Some additional performance variations are included to account for multiple operations like pilot holes followed by hole-opener operations. The above equations give a range of ROP from 592 m/h at spudding-in to 1.2 m/h at 10 000-m depth. Meterage ranges from 884 m initially to 64 m at 10 000-m depth. For rotary bits catalog data was used for carbide bits. The rock-melting bit costs, PENC, are based on Subterrene program experience and are defined by the following equations, where DPEN is penetrator diameter in meters:

$$PENC = 1286 + 20556\ (DPEN) + 69053\ (DPEN)^2, \text{ 1975 \$}.$$

f. Electric Power Generation and Transmission. For power transmission alternating current is the better choice over direct current for several important reasons, the most important one being corrosion. The presence of dc electric power flowing in a conductor immersed in mud or drilling fluid would enhance production of corrosion cells due to the potential gradient along the conductor. Such corrosion would be particularly detrimental around any conductor anomaly such as a threaded joint. By its inability to establish and support such corrosion cells, ac has a distinct advantage. Direct-current equipment capable of a continuous voltage change over a wide range would be costly, bulky, and difficult to control. However, such voltage requirements could be met easily by the combination of an ac power source and transformer or saturable reactor. The use of ac also has some disadvantages such as inefficiencies due to hysteresis, dielectric losses, and changing power factors. However, with proper design, the small losses remaining in the transmission circuit and other related equipment are acceptable. For power-cost estimates, GEOWELL includes calculations for the costs of diesel electric generators amortized over 10 yr as well as diesel fuel costs.

g. Drilling Fluids. The drilling fluid for a rock-melting system has to perform the following functions: (a) form solid debris, (b) cool the glass-former section, (c) control formation pressures and prevent caving, (d) carry out debris, (e) hold solid additives in suspension under stagnant flow conditions, (f) reduce corrosion, and (g) lubricate moving pipe or casing. Based on rotary drilling experience, drilling fluids like water, water-based muds, oil-based muds, etc., could perform functions (c) through (g). It is estimated that functions (a) and (b) could also be

handled even though this capability has not yet been demonstrated experimentally. For the well models set up for this study in which high formation pressures are postulated, muds are deemed essential to carry out function (c).

Open-literature data for mud costs in oil and gas wells were used to estimate the mud costs for the rotary well model. For normal geothermal gradients, the total mud costs, CMUD, are:

$$\text{EL} > 1354 \text{ m: } \text{CMUD} = 21912 - 28.64\,(\text{EL}) + 0.0108\,(\text{EL})^2, \text{ 1975 \$.}$$

For Subterrene mud costs, the beneficial effects of the precise hole size control with rock melters compared to rotary and also glass-lining benefits i.e., isolation of mud from the formations, resulted in an estimate that Subterrene mud costs are $\sim$ 0.75 times rotary.

h. Hole Support. The following glass-liner characteristics were assumed: (1) the solidified melt seals the hole effectively; (2) the collapse strength of the rock-glass lined wall is high; (3) liner wall thicknesses are controllable; and (4) liner tensile strengths are negligible. For the steel casing used in the modeled wells, the conductor and surface casing are made of low-cost K-55 grade steel, whereas the remainder is made from a higher grade such as P-110. Casing costs were obtained from industrial catalogs. Cementing costs in dollars per unit volume are mainly based on LASL hot dry rock geothermal drilling experience. With the input dimensions, the program calculates the weight of the casing and the delivered-casing costs. For cement costs, the total volume of delivered cement is calculated for the well model being considered, and this volume is multiplied by the appropriate cost in dollars per cubic meter.

i. Thermal and Hydraulic Conditions. Equations for the thermal and hydraulic conditions in rock-melted boreholes were set up to facilitate the evaluation of rock melting. The following assumptions are incorporated into this part of the program.

- Geothermal temperatures increase linearly with depth.
- A typical drilling mud, based on water properties as a function of temperature and pressure, is assumed with multipliers of 1.5, 30.0, and 0.77 on density, viscosity, and heat capacity, respectively.
- The flow rate of the drilling fluid is based on upper annulus dimensions and is calculated to be sufficient to move the excavation debris (assumed as spherical particles) upward at a velocity equal to the terminal velocity of the particles multiplied by 1.5.
- Maximum particle diameter is 10 mm with a density of 2700 kg/m^3.
- Friction factors for the pipe and annulus are based on absolute roughnesses of 4.57×10^{-5} and 3.05×10^{-4}, respectively.
- Tool-joint pressure losses are zero inside the drill pipe because of flush design. Outer-joint losses are estimated.
- Heat transfer through the wall of the coaxial aluminum pipe is included.
- Heat transfer to or from the surrounding rock is included, based on transient heat conduction in a semi-infinite slab as a function of drilling time.
- Heat addition to the drilling fluid from the debris and cooling of the glass lining is included as a lump sum at the penetration location.
- Heat addition along the length of the stem due to power-transmission losses is included.

3. Study Results. The GEOWELL analytical results presented in this section are limited to the most severe technical conditions, i.e., a rock-melting bit advancing at 1.0 mm/s at the bottom of a 10 000-m deep well. Figure V-8 plots the mass flow rate required to lift the debris in the annulus as a function of debris diameter for the well design illustrated in Fig. V-6. For the maximum particle size of 10 mm, the required mud flow rate is 46.1 kg/s. If the maximum particle size (and hence flow rate) is reduced, then the corresponding increase in maximum mud temperature is as shown in Fig. V-9. Even if the flow rate is halved to 23 kg/s, corresponding to a particle size of 2.5 mm, the maximum mud temperature would still be a reasonable 336.5 K, even at the high geothermal gradient with a rock temperature of 1033 K at total depth. Thus, the mud flow rate is established by the particle-removal criterion and not by the mud temperature.

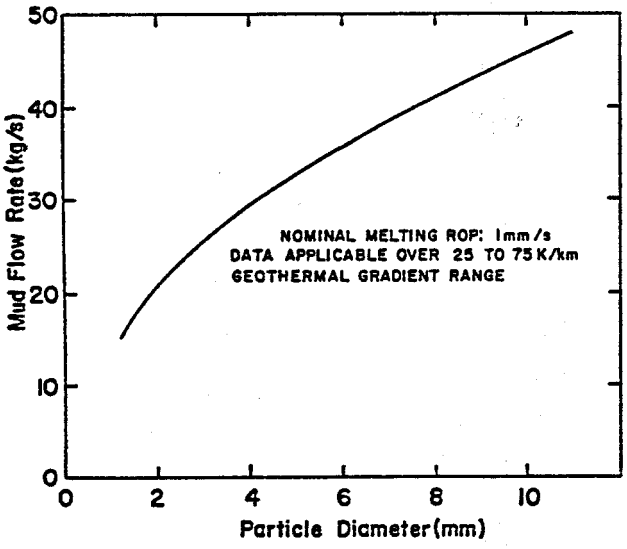

Fig. V-8. Typical mud flow rate vs debris particle diameter for rotary/rock-melted 10 000-m-deep well.

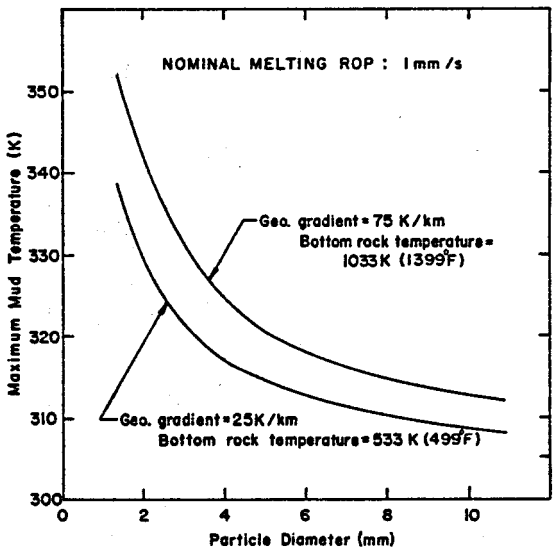

Fig. V-9. Maximum typical mud temperatures for rotary/rock-melted 10 000-m-deep well.

For a particle diameter of 10 mm the horsepower required from the well inlet to the outlet is ∿ 720 hp. Taking into account surface inlet pressure drops and motor inefficiencies, the actual pump power might have to be as high as 900 hp, well within the range of power levels on current drilling rigs. The total pressure drop between the drill pipe and the annulus flow channel is 18.04 MPa (2620 psi), of which 11.56 MPa (1680 psi) is in the drill pipe and 6.48 MPa (940 psi) is in the annulus. In contrast to the normally high drops across rotary bits, the drop across the rock-melting bit is negligible. Using the coaxial aluminum pipe for a 10-km well and including an allowance for a 650 000-N (146 000-lb) breakaway load, the maximum stress in the aluminum pipe is 364 000 kPa (52 700 psi) at a yield-to-load safety factor of 1.33. Under normal operating conditions at this depth the maximum stress is only 170 900 kPa (24 800 psi). Thus, no severe stress problems are indicated.

The GEOWELL program calculates the various downhole losses, total required power, and the transmission efficiency assuming that the coaxial aluminum drill pipe is used to transmit alternating current. Total power required ranges from 580 to 740 kW at depths of 5000 and 10 000 m, respectively. The 10 000-m efficiency tends to remain high compared to the 5000-m values because of the beneficial effects of higher rock temperatures on the melting process. These calculations do not indicate any particular power-transmission problems to depths as great as 10 000 m for any of the examples studied.

4. Cost Analyses

a. Normal Geothermal Gradient Wells.

Figure V-10 shows both rotary and Subterrene cost predictions vs total depth. The Subterrene wells use optimized ratios of rotary to Subterrene well depth intervals, and the geothermal gradient is 25 K/km. For these wells the state-of-the-art nominal melting rate of 0.2 mm/s is not cost-competitive with rotary. The rates required for the melted wells to equal the rotary-drilled well costs range from 0.24 to 0.42 mm/s for 10 000- and 5000-m deep wells, respectively. However, at 0.6 mm/s the cost savings of melted over rotary wells range from 18 to 8% for 10 000- and 5000-m deep wells, respectively, and at the rate of 1.0 mm/s the corresponding savings are 23 to 16%. These savings are for wells being made under relatively cool, normal-gradient conditions.

b. High Geothermal Gradient Wells. A hot well is defined as one that has a bottomhole temperature of 673 K (752°F). Very few statistics are available for this class of wells because (1) not

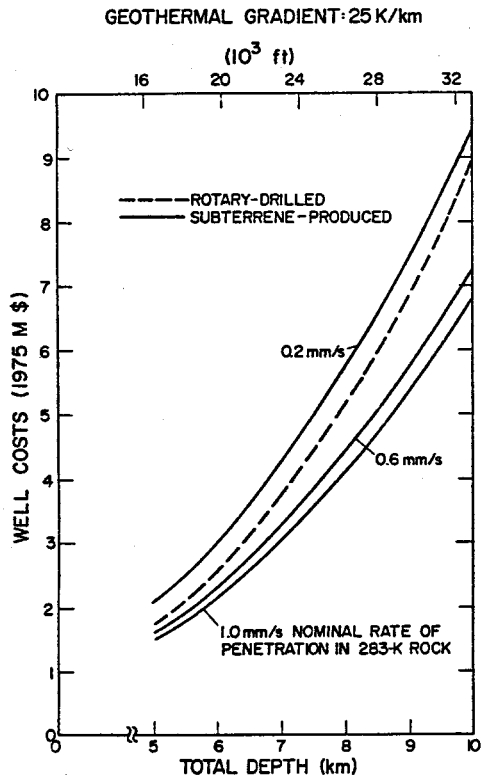

Fig. V-10. Well cost vs total depth in cool wells with a geothermal gradient of 25 K/km.

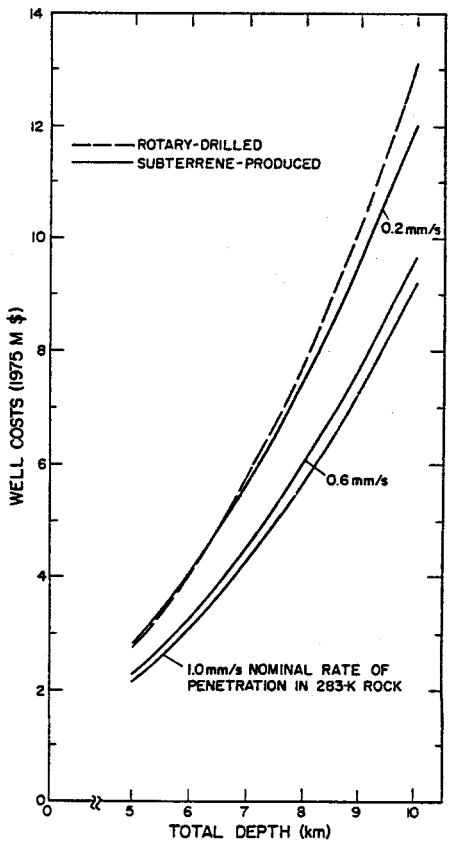

Fig. V-11. Well costs vs total depth in hot wells with various melting bit performance. Rock temperatures increase linearly to 673 K (752°F) at total depth for all wells.

many very hot geothermal wells have been drilled and (2) little detailed data have been released by the companies drilling the wells. Nevertheless, estimates can be made to allow a comparison of Subterrene and rotary systems. The procedure used is to apply correction factors to the appropriate cost equations in GEOWELL. The computed results for hot wells as defined above are shown in Fig. V-11. Because all bottomhole temperatures are assumed to be 673 K, the geothermal gradients vary with depth, but across the range of data plotted all gradients are above normal. It can be seen that with the state-of-the-art nominal melting rate of 0.2 mm/s, the Subterrene well cost is not much different from that for rotary drilling. At 0.6 mm/s, midway between current and program target rates, the cost savings are significant (20 and 17% for 10 000-and 5000-m depths, respectively), and are also greater than for comparable depth normal-gradient wells. At 1 mm/s the Subterrene cost is indicated as being 30 and 21% less than rotary for 10 000-and 5000-m depths, respectively.

c. Study Conclusions.

- The GEOWELL computer program is a good simulation of deep and difficult wells of the type defined, allowing the evaluation of major technical or cost items. Other well models could be specified and the program adjusted accordingly for further studies.
- The Subterrene concept can be combined with conventional drilling operations without major operational perturbations. However, for very hot boreholes, a change in system design and operation is indicated to develop the capability of maintaining continuous, or nearly continuous, circulation while working in the hot part of the borehole. This applies to both rotary and Subterrene systems.
- Subterrene performance of ∿ 0.2-mm/s penetration rate and 100-h bit life can, in some cases, provide marginal cost savings. However, if the

Subterrene system achieves the performance goal of 1 mm/s penetration rate and 300-h bit life, then Subterrene-produced wells would be significantly less expensive than rotary. In hot wells (673-K bottom temperature) savings of 30 and 21% are predicted for depths of 10 000 and 5000 m respectively. Even in cool, normal-gradient conditions, the savings are favorable, ranging from 23 to 16% for depths of 10 000 and 5000 m respectively.

- Penetration rates of 0.4 to 0.6 mm/s also result in significant savings for deep geothermal wells.
- All other Subterrene design or operational problems that were studied appear to have viable solutions.
- The most interesting feature of the drilling by melting concept is to form rock-glass liners on the borehole wall. These liners offer opportunities to solve well-production problems associated with hole control, lost circulation, casing design, cementing, and high-pressure packers.

C. Mathematical Modeling and Analysis

1. Introduction. The analysis effort has been directed at understanding and predicting Subterrene performance and in guiding new penetrator designs. The program has included the development and use of detailed computer programs adapted to the specific geometries, physical phenomena, and material properties germane to Subterrene performance. The development of analytical models has contributed to the basic understanding of specific relationships such as the leading edge flux limitations and the thrust-velocity dependence. Also of major importance was the theoretical calculation of material properties when the experimental values were not appropriate or available. The application of these models and techniques to specific designs and the interpretation of test results has received the largest portion of the analysis program time.

a. Computer Program Development. The finite element code AYER has been the single most important analysis tool and has seen the most applications to Subterrene problems because of the ease of operation and the versatility provided by the subroutine input. Any desired additional programming can be included in the five subroutines. The basic AYER code provides a time-dependent solution to the nonlinear two-dimensional heat conduction equation in plane or cylindrically symmetric coordinates with temperature- and time-dependent material properties. This basic code incorporating penetrator material properties, in situ rock properties, and various treatments of the radiation has been used extensively.

Two specific additions to the basic code have extended the usefulness of AYER. One is the inclusion of a hydrodynamics subroutine for the melt-layer flow. This treatment of the melt-layer hydrodynamics was developed for the VFQ code. Its incorporation in AYER eliminates the necessity of separate set-ups and the transferring of data from one code to the other. Since this routine calculates the velocity flow field in the melt and the hydrodynamic forces on the penetrator, it gives the immediate interaction of the melt velocities and temperatures with the internal temperature distribution. The calculated forces on the penetrator, which are extremely sensitive to the surface temperature distribution, are automatically available for each change of penetrator configuration. A second addition was an energy deposition routine for heating the melt layer at the leading edge with an electrical current. The present form of this calculation has proved useful where the electric field could be assumed to have a simple distribution. It gives the effect of the temperature-dependent electrical resistivity of the melt on the power distribution and provides the interaction between the power deposition, heat flow, and hydrodynamics. An extension of this routine could include a more complete solution of the Maxwell equations for the electric field configuration in the case of spatially dependent resistivity and dielectric constant.

Other special-purpose codes have been written to address the problems unique to the Subterrene penetrators. For instance, VFQ is a finite difference program for computing steady-state thermal and hydrodynamic characteristics of the melt flow to determine such things as required thrust loads and thickness profile of the melt layer. PLACID, a finite-element program for stress analysis, has been used for the thermal and loading stress analysis of the heated penetrator.

b. Analytical Models. A number of simplified analytical models have been used to examine specific physical phenomena that affect the performance of Subterrene penetrator systems. In many cases these models have supplemented the more comprehensive computer programs and contribute to the overall understanding by isolating specific effects. Some have been incorporated into the computer programs or have yielded specific results that were used in the computer analysis. These models have been used to calculate material properties, the leading edge flux, the thrust-velocity relationship, stem cooling, and melt-heating stability analyses. Some of these models will be briefly reviewed here and the effects on the penetrator performance calculations will be outlined in the next section.

Since the conditions at the penetrator leading edge are critical in the determination of velocity and thrust for a given penetrator surface temperature distribution, it is necessary to calculate the radiative and conductive fluxes accurately. The data available indicates that, above the melting temperature, rocks and glasses are transparent to radiation over distances of several millimeters. This implies that the thin melt layers ($\leq$0.5 mm) are optically thin. An optically thin approximation for radiation crossing the melt layer was developed and installed in AYER. A maximum in total flux is indicated when the optical thickness of the layer is one; that is, when the melt can reradiate and is still transparent. At this maximum the total flux is only $\sim$20% higher than the total flux occurring when the optically thin approximation is applied. Mainly because of the low emissivities of refractory metal penetrators, radiation can contribute only a small fraction of the required leading edge flux.

It is the molecular contribution to the thermal conductivity of the melt that controls the leading edge flux and the penetrator performance. The thermal conductivity of basalt and many other rocks has been measured to temperatures well above melting. However, the heat flux due to the radiation cannot be separated from that due to molecular motion without detailed knowledge of the temperature and frequency-dependent absorption coefficients of each rock sample, and thus it has been necessary to produce theoretical calculations of the thermal conductivity. An average molecule model was adopted, and the thermal conductivity of liquid basalt was calculated with three different theories. For basalt these three methods give results from 0.10 to 0.34 $W \cdot m^{-1} \cdot k^{-1}$. A value of 0.25 $W \cdot m^{-1} \cdot k^{-1}$ was chosen for the performance calculations. Thus far these methods have been applied only to basalt but could be used for any rock for which the sound speeds are known for the solid and liquid and for which the viscosity is known as a function of temperature.

An analytical parameter study of the leading edge flux was also developed which considers the effects of surface temperature, rock and melt thermal conductivities, and a finite radius of curvature for the leading edge. One significant result is that the infinite radius of curvature or flat plate limit holds for the flux at the leading edge for most penetrators and operating conditions achieved thus far. This result is valid for rocks with a melt thermal conductivity less than that of the solid rock, advance rates of $\sim$0.2 $mm \cdot s^{-1}$, and radii of curvature >5.0 mm. Models that predict the force-velocity relationship have been useful for scaling the penetrator thrust with the velocity and material properties. In one case the total force required for a penetrator moving in a medium with continuous properties is developed. In another the leading edge force is derived with a model that recognizes explicitly the discontinuous nature of the properties at the melt-rock interface. Other analytical approaches have examined the general effects of penetrator geometry on performance, stem cooling problems, and the power-velocity relation.

c. Status of the Calculations. Two phases of the analysis effort will be discussed: that directed at the production of specific penetrator designs and that directed at predicting penetrator performance as determined by the laboratory tests. AYER has been used to produce a number of melting body designs including the heater configurations and refractory metal body geometry for consolidators and extruders. These designs were accomplished with extensive parameter studies. The body geometries and heater configuration have been adjusted through many iterations to provide a good leading edge flux and to insure that material temperature limitations were met over a wide range of power and advance rates. The calculational procedure was generally for steady-state conditions and includes the melt layer and

surrounding rock. The HARE extruder has been tested extensively as designed, and its performance in basalt is well understood in terms of the analysis. The calculated temperature distribution and power losses have been compared with a calibration experiment for the 114-mm coring penetrator in an argon-filled quartz container. In an unusual application, the calculated azimuthal temperature distribution was correlated with the corrosion rates for the extended area penetrator.

The laboratory testing program generally provides data on instantaneous values of heater power, advance rate, total thrust, and temperature at one point in the refractory body during the course of approximately 1-m total penetration. Because of inhomogeneities in the natural rock samples, these quantities vary considerably. However, averages can be taken over short periods during which steady state has been achieved between programmed changes of thrust, rate, or power. These results can then be compared with the results of steady-state calculations. This comparison is most easily discussed in terms of the power-velocity and the thrust-velocity relationship.

For both consolidators and extruders the steady-state power as a function of velocity depends on the losses to the unmelted rock, the melt layer heat capacity, and the stem cooling losses. For extruders the energy carried off in the debris must also be included. The rock losses (energy conducted away from the penetrator beyond the melting isotherm), depend in turn on the heat capacity and thermal conductivity of the in situ rock and the temperature distribution. The melt layer and debris power are determined by the heat of fusion, melt heat capacity, and correct average debris and melt layer temperatures. The stem losses depend on penetrator geometry, cooling methods, and debris removal methods. Estimation of the stem losses, which are usually a small fraction of the total power, has not encountered any significant problems. Since the calculated and experimental powers agree fairly well, it can be assumed that the data for the important physical properties (in particular the thermal conductivity of the solid, the heat of fusion, and the heat capacities) are of sufficient accuracy for tuff and basalt that the AYER temperature distributions are correct.

With the power and temperature distributions determined, the steady-state force on the penetrator by a well-developed melt layer can be determined. The hydrodynamic forces applicable to the Subterrene geometries have been developed from the Navier-Stokes equations and applied to penetrators. The thrust values are also extremely sensitive to the other properties of the melt layer: the viscosity, the thermal conductivity which determines the critical thickness at the leading edge, the surface temperature distribution, and the melt velocity field. The inclusion of the hydrodynamics subroutine of VFQ in AYER has provided the temperature distribution and velocity field in the same calculation. Good approximations to the radiation and molecular thermal conductivities are provided by the theoretical calculations. For the HARE penetrator in basalt, this complete treatment has given reasonable thrust values on the assumption that the HARE is limited by the force on the leading edge.

2. The Thrust-Velocity Relationship for Extruding Penetrators.

a. Introduction. Calculations of the total thrust required to maintain a given advance rate for Subterrene penetrators are difficult for various reasons. For consolidating penetrators, the force retarding the penetrator does not necessarily result from the pressure required to move the viscous melt. If the leading edge is retarding the advance because of insufficient heat flux, the concentration of the force on a small area of the soil or rock can result in compaction and plowing of the unmelted material, and this further complicates the thrust-velocity relation. If the advance is being retarded by the consolidation requirement, this condition is satisfied by additional melting or by a combination of melting and compaction of the cold or heat-softened unmelted material. This latter effect has not been included in the hydrodynamics codes used for the thrust calculations. However, the thermal analysis of existing penetrators indicates that the consolidation condition is not always met at the velocities achieved in experiments. If this is the case, forces required for compaction could be the dominant contribution to the thrust. The situation for extruders in dense basalt is different with no compaction occurring and no consolidation requirement. The force

on the penetrator results from the pressures required to force the melt to the extruding ports. Considerable data has been accumulated for the thrust-velocity relationship for two extruders in basalt. However, the three-dimensional nature of the melting surface of the extended area penetrator precludes any detailed analysis. The HARE extruder has cylindrical symmetry throughout and is amenable to computer analysis. Since the exterior of the body is parallel to the axis of symmetry, most of the force is on the flat annular leading edge. This component of the force can be obtained approximately from a simple analytical model. Also, the two-dimensional geometry can be accommodated by the AYER heat conduction code. When used in conjunction with a subroutine based on the hydrodynamic analysis in VFQ, this code will calculate a steady-state temperature distribution, a melt velocity field, and a pressure distribution; and hence, determines a simultaneous power, advance rate, and thrust. In this report, one steady-state analysis of the HARE penetrator is discussed and compared with time-averaged operating conditions for the laboratory model in basalt.

b. Material Properties. The properties of the rock melt critical to the thrust calculations are the specific heat, heat of fusion, density, and the thermal conductivities, both molecular and radiative.

The radiative contribution to the flux is taken to be that given by the optically thin approximation. This flux is given by

$$F_R = E\, n^2\, \sigma(T_s^4 - T_m^4) \quad . \qquad \text{(V-1)}$$

The index of refraction is $n = 1.5$* and σ is the Stefan-Boltzmann constant. The effective emissivity is

$$E = \frac{\varepsilon_s\, \varepsilon_m}{\varepsilon_s + \varepsilon_m - \varepsilon_s\, \varepsilon_m} \quad .$$

The emissivity of the penetrator surface (ε_s) is taken to be an average over wavelength for molybdenum.* The emissivity for the rock at the melt interface (ε_m) is not known; if it is assumed to be near 1.0, then the effective emissivity is 0.25.

Experimental determinations of the thermal conductivity generally do not separate the radiative and conductive contributions.** Because the melt layers at the leading edge of most penetrators are so thin, the contribution due to molecular motion dominates and it must be estimated separately.

In Sec. C. 3, three theories are used to calculate the molecular thermal conductivity of an average rock (SiO_2) in the liquid phase. The phenomenological approach similar to that of Bridgeman was used to scale the conductivity from the solid to the liquid on the basis of the sound speed. The molecular collision theory of Horrocks and McLaughlin was used with basalt viscosities determining the parameters in the molecular potential. The phonon transport model of Liebfried and Schlömann for a perfect crystal was modified to a form appropriate to a liquid. All three models gave similar results and indicate an upper limit of 0.34 $W \cdot m^{-1} \cdot k^{-1}$ for the conductivity in the temperature range of 1500 to 2000 K. As will be seen, calculated values of the leading edge thrust can be brought into approximate agreement with the experimental values if the radiation flux is limited by Eq. (V-1) and if a value of 0.25 $W \cdot m^{-1} \cdot k^{-1}$ is used for the thermal conductivity of the melt.

The viscosities of the equilibrium melts of several basalts have been measured. In particular, that of Jemez basalt was obtained at Corning and the uniform melts of tholeiitic basalts were also examined during recrystallization by Shaw.*** These results are plotted in Fig. V-12. However, the behavior of basalt as it melts is not known. For the calculations considered here, it is assumed that it exhibits no significant liquid behavior below the melting temperature. In the melt layer a fit to the Corning data is used, and in the analytical model

*Hess, H. H., and A. Poldervaart, Basalts, (John Wiley & Sons, New York, 1968).

*Touloukian, Y. S., and D. P. DeWitt, Thermal Radiative Properties, Vol. 7, (Plenum Publishing Corp., New York 1970).

**Murase, T., and A. R. McBirney, "Thermal Conductivity of Lunar and Terrestrial Igneous Rocks in Their Melting Range," Science 170, 165-167 (1970).

***Shaw, H. R., "Rheology of Basalt in Melting Range," J. Petrology 10 (3), 510 (1969).

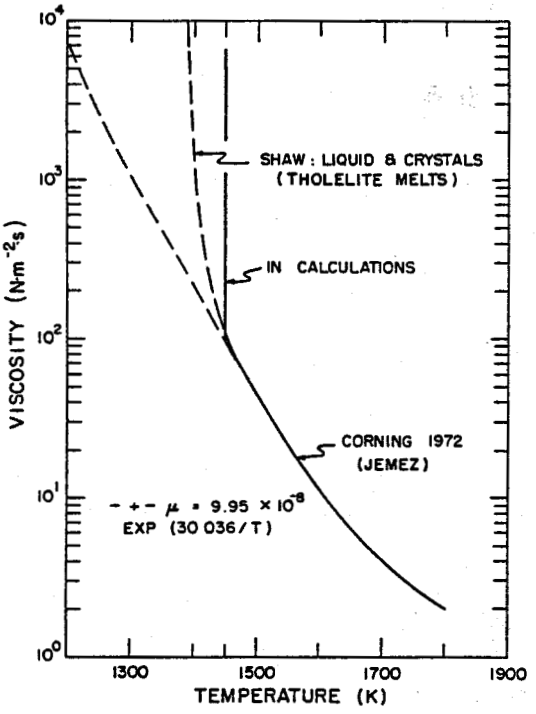

Fig. V-12. Viscosity of basalt as a function of temperature.

a value given by average melt temperature is used. The density, specific heat, and heat of fusion* represent typical basalts.

c. A Model for the Leading Edge Forces. A number of analytical models giving the various components of force on a rock-melting penetrator have been produced. The treatment detailed here determines the force resulting from the pressure gradient required to force the melt from between the melt-rock interface and the penetrator. It assumes the existence of a melting isotherm at which the material properties are discontinuous. The melt layer thickness and melting temperature appear explicitly in the results, and above the melting temperature the melt is represented by average uniform properties.

If a penetrator is operating in the correct mode its advance rate (v*) will be limited by the leading edge force. In blunt extruders this force will dominate and it will be convenient to have a

*Clarke, B., et al., "Rock Properties Related to Rapid Excavation," University of Missouri - Rolla, PB 184 767 (March 1969).

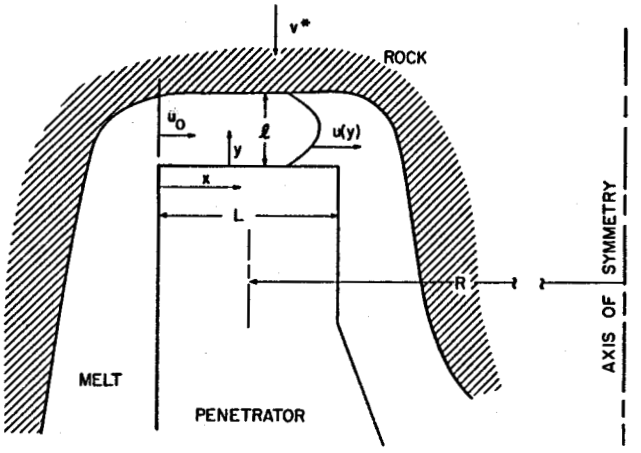

Fig. V-13. Geometry of HARE penetrator annular leading edge.

simple expression for the force-velocity relationship that explicitly recognizes the existence of the melt-rock interface and the discontinuities of the physical parameters at the melting temperature. Figure V-13 depicts a radial section through the melt layer for a penetrator with the HARE geometry. In this approximation the melt layer is characterized by a uniform thickness ℓ and an average viscosity $\bar{\mu} = \mu(\bar{T})$ determined by an average temperature. Consistent with these assumptions is the assumption that the velocity in the melt layer is parabolic in the radial direction

$$u = \hat{u} - \frac{4\,\hat{u}}{\ell^2}\left(y - \frac{\ell}{2}\right)^2$$

where $\hat{u} = \hat{u}(x)$. Then $u = \hat{u}$ at $\ell/2$ and $u = 0$ at $y = 0$ or ℓ. An average velocity can be defined as

$$\bar{u} = \frac{1}{\ell}\int_0^{\ell} u\,dy = \frac{\hat{u}}{3} \quad .$$

The shear rates at the penetrator and melt surface are

$$\left.\frac{\partial u}{\partial y}\right|_0 = \frac{4\,\hat{u}}{\ell} = \frac{12\,\bar{u}}{\ell}$$

$$\left.\frac{\partial u}{\partial y}\right|_{\ell} = -\frac{4\,\hat{u}}{\ell} = -\frac{12\,\bar{u}}{\ell} \quad .$$

The continuity equation gives approximately, for an annulus of effective radius R,

$$\rho_\ell \, \bar{u} \, (2\pi \, R\ell) = \rho_\ell \, u_o \, (2\pi \, R\ell) + \rho_i \, v^* \, (2\pi \, Rx) \quad ,$$

which for $\rho_i = \rho$ gives

$$\bar{u} = \frac{xv^*}{\ell} + u_o \quad ,$$

where u_o is the average melt velocity at the outside edge (see Fig. V-13). The pressure gradient required to move the melt at a constant velocity in the presence of a viscosity $\bar{\mu}$ is

$$\frac{dP}{dx} = \frac{d}{dy}\left(\bar{\mu} \frac{du}{dy}\right) \quad .$$

The pressure is taken to be a function of x only, since the velocity in the y direction is small.

$$\int_o^\ell \frac{dP}{dx} \, dy = \int_o^\ell d\left(\bar{\mu} \frac{\partial u}{\partial y}\right)$$

$$\frac{dP}{dx} = \frac{1}{\ell} \bar{\mu} \left(\left.\frac{\partial u}{\partial y}\right|_\ell - \left.\frac{\partial u}{\partial y}\right|_o\right) = - \frac{24 \, \bar{\mu}}{\ell^2}\left(\frac{x}{\ell} v^* + u_o\right)$$

The resulting pressure is

$$P = \frac{12 \, \bar{\mu} \, v^*}{\ell^2} x^2 + \frac{24 \, \bar{\mu} \, u_o}{\ell^2} x \quad ,$$

which gives rise to a force on an annulus of width L of,

$$F = \int_o^L P \, dA \approx 8\pi \, R \, \bar{\mu} \, v^* \frac{L^3}{\ell^3} + 24\pi \, R \, \bar{\mu} \, u_o \frac{L^2}{\ell^2} \quad .$$

If $u_o = 0$; that is, if no melt flows into the thin annulus between the flat tip and the unmelted rock, then the force on the advancing face is

$$F = 8\pi \, R \, \bar{\mu} \, v^* \left(\frac{L}{\ell}\right)^3 \quad . \qquad \text{(V-2)}$$

The melt layer thickness is related to the melt properties and temperature by

$$\ell = \frac{\lambda \, (T_s - T_m)}{\rho \, v^* \, (C_v \, \delta T + H) - F_R} \quad , \qquad \text{(V-3)}$$

which comes from the leading edge flux requirement.

$$F_c + F_R = \frac{\lambda \Delta T}{\ell} + F_R = \rho v^* \, (C_v \, \delta T + H)$$

Here $\delta T = T_m - T_a$, where T_a is the ambient temperature and H is the heat of fusion.

These equations are best suited for assessing the relative effects of penetrator tip geometry, average material properties, and operating conditions. The value of force obtained depends on v^{*4}, ΔT, and the third power of the material properties which makes the results sensitive to the choice of the appropriate average quantities. With the operating conditions of $v^* = 0.20 \times 10^{-3}$ m·s^{-1} and $T_s = 1900$ K and material properties $\lambda = 0.25$ W·m^{-1}·K^{-1}, $\rho = 2.7 \times 10^3$ kg·m^{-3}, $C_v = 1.25 \times 10^{-3}$ J·kg^{-1}·K^{-1}, $H = 420 \times 10^3$ J·kg^{-1}, and $\bar{\mu} = \mu(\bar{T}) = 5.0$ N·s·m^{-2}, we obtain for the radiation flux,

$$F_R = 0.24 \text{ W·m}^{-2} \quad ,$$

the melt layer thickness

$$\ell = 0.10 \text{ mm} \quad ,$$

and the force

$$F = 2.97 \text{ kN} \quad ,$$

which is in essential agreement with the ~4.0 kN used to obtain this velocity in the laboratory.

In addition to this simplified model, detailed steady-state computer analyses of the HARE penetrator were carried out. The thrust calculations were implemented with the addition of a hydrodynamics subroutine adapted from VFQ. During the iteration for the temperature solution, this subroutine uses the current melt temperatures to calculate the melt viscosities. From the conservation of mass and the Navier-Stokes equations, the velocity field in the melt is calculated. The forces on the penetrator due

to the melt pressure and viscous drag are then determined.

The procedure for one set of operating conditions required the manual adjustment of the melt-rock interface geometry between computer runs to obtain internal consistency. This was carried out for a velocity of $v^* = 0.15$ mm·s^{-1} and a maximum molybdenum temperature of $\sim$ 1900 K. At the mid-point (in the radial direction) of the leading edge, the resulting surface temperature and melt layer thickness were T_S = 1800 K and ℓ = 0.18 mm with an average temperature of $\sim$ 1600 K. The calculated leading edge force is 1.09 kN with an additional axial force of 0.22 kN on the conical throat. For these conditions the model of Eq. (V-2) gives 0.76 kN, again in fair agreement with the 2 to 3 kN needed to maintain this velocity in the laboratory. The situation is illustrated in Fig. V-14 which is a plot of force versus advance rate. The results of the calculations discussed above are compared to some of the experimental results. The solid closed curves bracket the experimental data envelope for various basalt samples and melting body powers. The points [M] are the results of the simple model of Eq. (V-2). The points (A) and [A] are the AYER results for a leading edge temperature of $\sim$ 1800 K. The dashed curve connects points scaled by v^{*4}. Unfortunately, these data were obtained before thermocouples were installed in the HARE melting body, and no correlations of calculations and experimental points with the same measured body temperatures can be made. However, a good agreement between melting body power and advance rate has been obtained, Fig. V-15, and a temperature distribution for a given velocity can be inferred from the AYER calculations. It should also be emphasized that the reduction of the experimental data required a judgement as to whether or not steady state had been reached and includes an average over an oscillating instantaneous velocity.

d. The Force on a Conical Section. The limiting effect of the leading edge flux has long been recognized and experimental verifications of higher velocities for penetrator designs that can eliminate this difficulty have been carried out. A conical consolidator with a diameter of 57 mm was

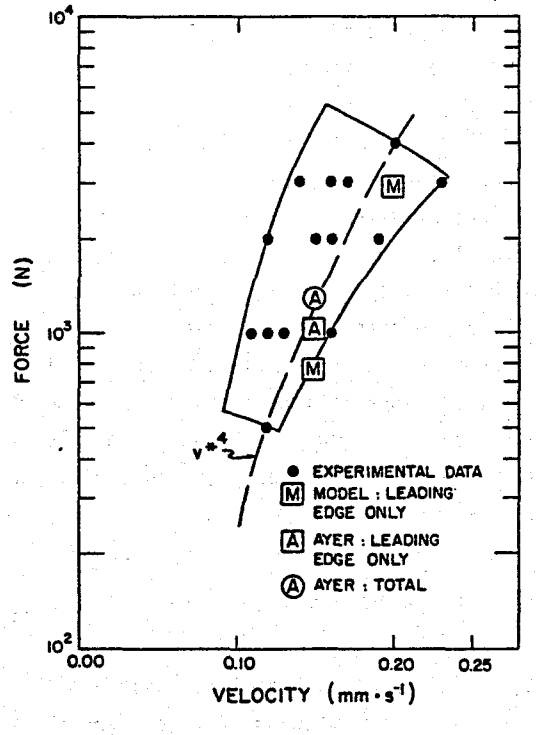

Fig. V-14. Required thrust as a function of advance rate for the HARE extruding penetrator.

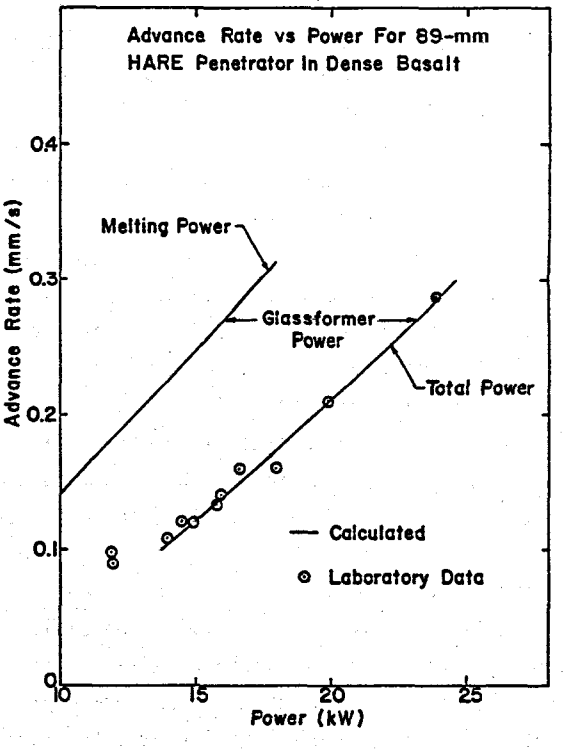

Fig. V-15. Advance rate - melting power and total power relationships for HARE extruding penetrator operating in basalt.

used in basalt with a predrilled hole to remove the rock that would normally be melted by the leading edge region of the penetrator. The leading edge advances unrestricted and the hole is melted to a larger diameter by the conical section with a length of 110 mm and half angle $\phi = \sin^{-1} 0.11$. If the surface of the penetrator is at an angle of ϕ to the direction of advance, then the mass flux perpendicular to the surface is reduced by the factor $\sin \phi$. The melt layer thickness is then given by Eq. (V-3) with v^* replaced by $v^* \sin \phi$. The expression for the force is further modified by the factor $\sin^2\phi$. One factor of $\sin \phi$ is for the effective velocity and one for the component of force parallel to the penetrator axis. If two penetrator elements occupy the same annular area projected on a plane perpendicular to the penetrator axis, then the force required to advance each at a given velocity will scale approximately as $\sin^2\phi$.

Table V-4 lists thrust calculated with this approximate model along with some experimental results. The average advance rates are considerably larger than the maximum ($\sim$0.25 mm·s^{-1}) observed for penetrators limited by the leading edge in basalt. The body temperature, taken to be the surface temperature in the calculations, is somewhat lower than that usually achieved. For 2000-K temperatures, the velocity could approach 1.0 mm·s^{-1} for this conical section. The calculational model includes many approximations and does not include physical effects such as glass-former drag and the variations of physical rock properties between samples; hence, only approximate agreement can be expected.

3. Liquid Basalt Thermal Conductivity Investigation. A number of circumstances combine to make the heat transfer due to molecular conduction dominate over radiation in the melt layer at the leading edge of Subterrene penetrators. These include the low emissivities of refractory metals, material temperature limitations, and the extreme thinness of the melt layer. Most high-temperature experimental measurements of liquid rock thermal conductivity combine the effects of conduction and radiation in fairly thick samples. Because the radiative properties of liquid rocks are not well known, the radiation contribution to the flux cannot be accurately subtracted out. This situation has prompted a comparison of theoretical estimates of the thermal

TABLE V-4

RESULTS OF CONICAL SECTION TESTS IN BASALT WITH PREDRILLED HOLE FOR LEADING EDGE

	Average Rate (mm·s^{-1})	Body Temperature (K)	Measured Thrust (kN)	Calculated Thrust (kN)
Basalt	0.85	1770	4	6.5
Basalt	0.5	1690	4	6.9

conductivity of liquid basalt due to molecular motion with that implied by the actual performance of Subterrene penetrators. The force required to maintain a given penetrator velocity is proportional to the inverse cube of the thermal conductivity of the surrounding melt. Since most of this force is accumulated in the thin layer at the leading edge where the conductive flux dominates, the calculated force is sensitive to the value assumed for the liquid thermal conductivity. The forces calculated by detailed computer simulation of the penetrator and the viscous melt best match laboratory values if 0.25 W/m·K is used for the thermal conductivity. The data of Murase and McBirney* for Columbia River basalt was used in the simulations for temperatures below melting (1450 K). This data is plotted in Fig. V-16 as the solid line labeled CRB. This basalt becomes transparent to radiation near the melting temperature and an abrupt rise in effective conductivity occurs. The contribution due to molecular motion is masked by the radiation at temperatures above 1450 K. The thermal conductivity of a liquid can be estimated with several theories, three of which are outlined here. In the discussions which follow, thermal conductivity represents only the molecular conduction and does not include any radiation contribution.

The first is a scaling based on the conductivity of the solid and the temperature dependence of the velocity of sound. The thermal conductivity can be written phenomenologically as

$$\lambda_B = C_v \frac{\bar{c}}{3} \bar{\ell} \ (\mathrm{W \cdot m^{-1} \cdot K^{-1}}) \ , \qquad \text{(V-4)}$$

where

C_v = an appropriate specific heat

$\bar{c}/3$ = velocity of sound averaged over three spatial directions.

$\bar{\ell}$ = the mean free path.

*Murase, T., and A. R. McBirney, "Thermal Conductivity of Lunar and Terrestrial Igneous Rocks in Their Melting Range," Science 170, 165-167 (1970).

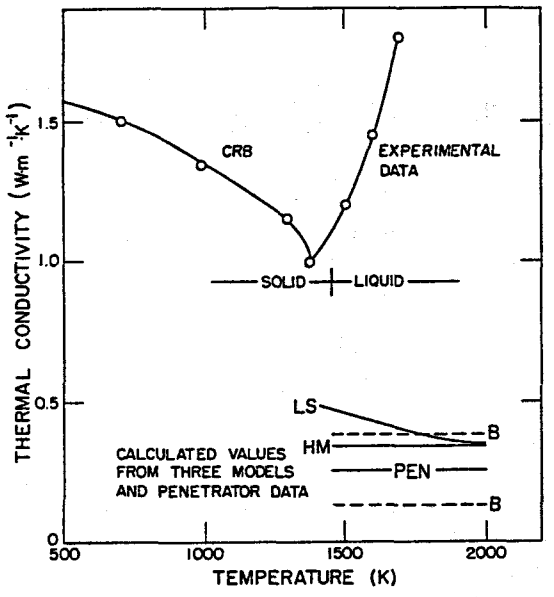

Fig. V-16. Liquid basalt thermal conductivity results.

This can be separated further into the contributions of longitudinal (ℓ) and transverse (t) modes.

$$\lambda_B = \frac{C_v}{3}\left(\frac{c_\ell}{3} + \frac{2}{3}c_t\right)\bar{\ell} \,. \qquad \text{(V-5)}$$

The sound velocities in basalt are given approximately in Table V-5. Liquid basalt will be considered to be composed of average triatomic molecules with molecular weight $\bar{A} = 60$ and which contain atoms of average weight $\bar{A} = 20$. These values are for SiO_2 and are close to the average for basalt. The density (ρ) of liquid basalt is 2.7×10^3 kg·m^{-3}. The classical specific heat is

$$C_v = \frac{3k}{m} = 1.25 \times 10^3 \ \text{J·kg}^{-1}\text{·K}^{-1} \,,$$

TABLE V-5

SOUND VELOCITIES IN BASALT (m·s^{-1})

	Solid (300 K)	Liquid
c_ℓ	5.0×10^3	3.0×10^3
c_t	3.7×10^3	0

where

$k = 1.38 \times 10^{-23}$ J·K^{-1} is Boltzmann's constant

$m = 20 \times 1.66 \times 10^{-27}$ kg is the atomic mass.

This value is close to the measured value of $C_p = 1.1 \times 10^3$ for some basalts. Also, this average liquid has a distance between molecules of

$$d = 3.25 \times 10^{-10} \ \text{m} \,.$$

If $\bar{\ell} = d$ is used for the solid, the thermal conductivity given by Eq. (V-5) is

$$\lambda_B \ (300 \ \text{K}) = 1.5 \ \text{W·m}^{-1}\text{·K}^{-1} \,,$$

which is close to the measured value for CRB at 300 K. So the average mean free path for the energy carriers (phonons) consistent with the measured thermal conductivity is the dimension of the space available to each molecule. If it is now assumed that this is also true for the liquid, then from Eq. (V-5)

$$\lambda_B \ (1500 \ \text{K}) = 0.38 \ \text{W·m}^{-1}\text{·K}^{-1} \,.$$

Two of the three longitudinal modes contributing to λ correspond to internal modes of the molecules, the remaining one to the translation of the molecules. If it is further assumed that in the liquid (but not in the tightly bound solid) the internal modes do not transfer energy during a collision, then a lower limit to λ_B is obtained:

$$\lambda_B \ (1500 \ \text{K}) = 0.13 \ \text{W·m}^{-1}\text{·K}^{-1} \,.$$

These values are indicated on Fig. V-16 by the dashed lines labeled B.

A second method is the molecular collision model of Horrocks and McLaughlin.* This utilizes information obtained from viscosity data, which is available for some basalts. Assumptions must be made concerning the type of packing of the molecules occurring in the liquid and the type of potential between molecules. They obtain for the thermal conductivity,

*Tye, R. P, Thermal Conductivity (Academic Press Inc., London, 1969).

$$\lambda_{HM} = \frac{\sqrt{2}\,\hat{C}_v}{2\pi\sqrt{M}\,a^2}\left[2z\varepsilon\left(L_1 v^{*4} - M_1 v^{*2}\right)\right]^{1/2} \quad .(V\text{-}6)$$

Here:

$\hat{C}_v = 3k$

$v^* = \sigma^3/v$

$a = \left(\sqrt{2}\,v\right)^{1/2}$

v = volume per molecule

ε and σ are the depth and zero crossing in the LJM potential:

$$\phi(r) = 4\varepsilon\left[\left(\frac{\sigma}{r}\right)^{12} - \left(\frac{\sigma}{r}\right)^{6}\right]$$

r = molecular separation

M = molecular mass

z = coordination number of lattice

L_1, M_1 are lattice summation constants.

The lattice constants are taken to be $Z = 12$, $L_1 = 22.11$ and $M_1 = 10.56$, corresponding to a face-centered cubic lattice. The estimation of σ and ε from viscosity can be complicated, and the following simplified procedure is used here. For the LJM potential

$$\sigma = R/2^{1/6} \quad ,$$

where R is the separation at minimum potential. Since the molecules of a liquid are bound $R \approx d = v^{1/3}$. The viscosity (η) of liquids can be written

$$\eta = \eta_o\, e^{\frac{E}{kT}} \quad ,$$

where E is the depth of the potential seen by a molecule moving through the lattice and results from binding to n neighbors; ε is the depth of the potential for binary interactions. Let ε be approximated by

$$\varepsilon = E/n \quad . \qquad (V\text{-}7)$$

For basalt $E = 41.5 \times 10^{-20}$ J and for closely packed spheres $n = 12$. Equation (V-7) then yields

$$\lambda_{HM} = 0.34\ W{\cdot}m^{-1}{\cdot}K^{-1} \quad ,$$

which is indicated in Fig. V-16 by the line labeled HM.

Another approach is to modify the theory of Leibfried and Schlömann* for a perfect crystal. They obtained for $T > \theta$

$$\lambda_{LS} = \frac{12}{5}\,4^{1/3}\left(\frac{k}{\hbar}\right)^3 \frac{Md}{(\gamma + 1/2)^2}\,\frac{\theta^3}{T} \quad , \qquad (V\text{-}8)$$

where:

$h = 6.62 \times 10^{-34}$ J·s is Planck's constant

M = mean atomic mass

$d = v^{1/3}$

v = volume per atom

θ = Debye temperature

T = absolute temperature

$\gamma = -\partial\,(\ell n\,\theta)/\partial\,(\ell n\,v)$ is the Grüneisen anharmonicity parameter.

The Debye temperature is

$$\theta = \frac{h}{k}\,\nu_L \quad ,$$

where ν_L is the highest vibrational frequency of the lattice. This is obtained by integrating over the Debye spectrum

$$g(\nu) = 4\pi V\,\nu^2\,(2\,c_t^{-3} + c_\ell^{-3}) \quad .$$

In the liquid there are only longitudinal modes with N degrees of freedom; so on integration

$$\nu_L = \left(\frac{3N\,c_\ell^{-3}}{4\pi V}\right)^{1/3} \quad ,$$

where $V/N = v$, the volume per atom. For liquid basalt $\theta \approx 385$ K; so the condition is met on Eq. (V-8). The anharmonicity parameter can be written

*Tye, R. P., Thermal Conductivity (Academic Press Inc., London, 1969).

$$\gamma = -\frac{d}{3\theta}\left(\frac{\partial\theta}{\partial v}\frac{\partial v}{\partial d} + \frac{\partial\theta}{\partial c_\ell}\frac{\partial c_\ell}{\partial d}\right)$$

$$\gamma = \gamma_1 + \gamma_2$$

The first term is equal to 1/2; the second reduces to

$$\gamma_2 = \frac{-\rho}{c_\ell}\cdot\frac{\partial c_\ell}{\partial \rho} \quad ,$$

where $\rho = \frac{M}{V}$ is the density. Data to evaluate γ_2 for a liquid basalt was not available. A rough estimate based on the solid data is $\gamma_2 \approx 3.75$. The thermal conductivity can now be estimated as

$$\gamma_{LS} = 0.67 \times \frac{10^3}{T}\ W\cdot m^{-1}\cdot K^{-1}$$

and is labeled LS in Fig. V-16. It must be emphasized that this method in particular is extremely sensitive to the longitudinal sound speed and its dependence on density.

All of the above methods involve gross assumptions and would profit from more data for the fundamental parameters (c_ℓ, ε, σ, etc.). However, they exhibit reasonable agreement with the thermal conductivity implied by the performance of Subterrene penetrators as indicated by the line labeled PEN in Fig. V-16.

Using a value of 0.25 $W\cdot m^{-1}\cdot K^{-1}$ for the thermal conductivity of molten basalt in the computer simulation program, it becomes evident that the penetration rate of an extruding penetrator is limited by the heat flux that can be provided at the leading edge (flow stagnation point). Based on allowable temperatures in the molybdenum body, the calculations indicate that the leading edge heat flux will restrict penetration rates in basalt to approximately 0.25 mm/s. Away from the leading edge, however, the conical shape of the melting body provides a significant geometrical enhancement, and much higher penetration rates are possible. This concept was demonstrated in the laboratory test using a conical shaped penetrator melting into a basalt sample that was predrilled to remove the rock that would normally be melted by the leading edge region of the penetrator. With the penetrator body temperature below the operating maximum, sustained rates of just under 1 mm/s were attained. This represents a factor of 4 to 5 times the rate that would have been expected if the leading edge heat flux were controlling the rate. Experimental confirmation of this analytically predicted result led to a major research program to introduce techniques for increasing the available leading edge heat flux.

4. Stem Cooling with Particle Transport. One of the analytical approaches to the general problem of the effects of penetrator performance on stem cooling has been the development of an analytical model and computer program to calculate stem cooling characteristics with a centrally extruding penetrator. This model includes the transport of, and heat transfer from, highly idealized melt/solid particles in the extrudate carry-off tube. A particular concern has been that the wall of the central extrudate tube gets hot enough to cause melt sticking near the "tip" or penetrator end. A flow schematic of the system modeled is shown in Fig. V-17. In this particular

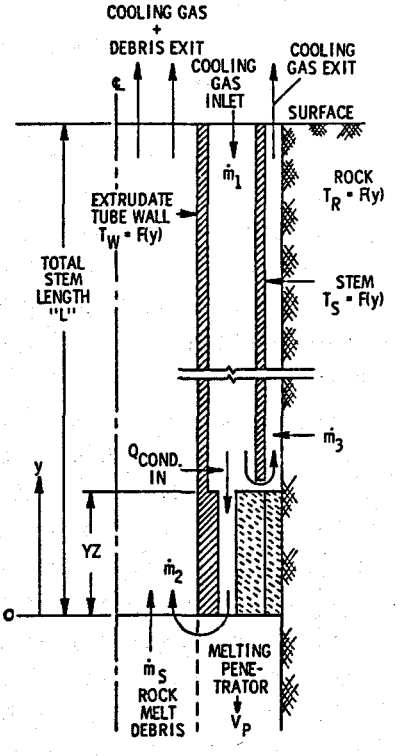

Fig. V-17. Flow schematic for stem model calculations.

model, a short section of stem near the tip end ($0 \leq y \leq YZ$) has a different flow geometry and wall material than the remainder of the stem. At the station $y = YZ$ a heat load referred to as "tip conduction" is assumed to be added to the total cooling gas flow coming down channel 1 (the "downcomer"). This represents heat conducted from the melting penetrator and from the hot rock in the region $0 \leq y \leq YZ$. After the tip conduction heat is added, the flow is split into two streams. One stream continues down a revised channel 1 and becomes the central "upcomer" flow in channel 2 at $y = 0$ where the rock-melting debris is introduced. The other becomes the outer annulus "upcomer" flow in channel 3 at $y = YZ$. The flow balance and downcomer pressure are controlled by sonic restrictions at $y = 0$ for flow into channel 2 and at $y = YZ$ for flow into channel 3. Melt is assumed to be introduced already formed in solid-like particles moving at a low velocity at the tip end, $y = 0$. These particles are assumed to be rigid, spherical, and of uniform size both at a given axial station and throughout the length of the stem. This is obviously a simplification of the true particle characteristics, but by varying the particle diameter parametrically it can be assumed that any significant effects of particle irregularity will be observed.

At any axial station the steady-state heat balance is a result of convective heat transfer from the particles (which are assumed to be at a uniform temperature), to the fluid in channel 2; combined radiative heat transfer from the particles and convective heat transfer from the fluid in channel 2 to the counterflowing fluid in channel 1; and for $y > YZ$ there is heat transfer from channel 1 to channel 3, and from channel 3 to (or from) the surrounding rock. In addition, as stated above, a lumped heat load is added to the total flow at $y = YZ$. Equations for the heat balance and particle velocity are developed and are integrated numerically starting at $y = 0$ with an assumed gas temperature at the tip end. Integrations are terminated when the gas temperature in channel 1 (the downcomer) is reduced to the prescribed gas inlet temperature. The value of y at this point, then, is the total stem length corresponding to the assumed tip-end gas temperature.

Calculations were made of the 86-mm extruding penetrator over a range of particle diameters and tip-end gas temperatures (or total stem lengths) for gas flow rates of 40 g/s (70.7 SCFM) and 100 g/s (176.6 SCFM) for nominal conditions. These results indicate that as the net heat transfer to the fluid is reduced by conduction into the rock, the tip-end gas temperature quickly approaches a limit, and further increases in stem length do not increase this gas temperature. This tip-end temperature is approximately the maximum gas temperature, and the maximum inner tube wall temperature closely follows this gas temperature. This is true even when a thermal resistance corresponding to a relatively thick layer of rock deposited on the tube wall is included.

Calculations for conditions different from these can be made quite easily for stem geometries of the general type of the 86-mm penetrator. Changes can be made to the program for other geometry types, such as a single upcomer stem.

5. Melt-Heating Analysis.

a. Introduction. The concept of increasing the advance rate of rock-melting penetrators by the direct deposition of energy in the melting rock with ohmic heating holds technical promise if certain fundamental difficulties can be overcome. Higher advance rates can be expected if power is deposited in the melt layer to mitigate the effect of the low melt thermal conductivity in isolating the hot penetrator from the unmelted rock. In principle it would be advantageous to deposit the energy directly in the unmelted rock; however, all penetrator electrode configurations considered here result in deposition in the higher temperature molten rock. This is due to the highly nonlinear dependence of the resistivity of rock on temperature in the melting range. In this report a simple model is presented which estimates the velocity enhancement that can be expected with direct melt heating for a leading edge limited annular penetrator. Some of the problem areas are the selection of a leading edge insulator, materials compatibility, the stability of the melt current distribution, and the effects of natural inhomogeneities on the current distribution. Only the current distribution will be considered here. Small amplitude perturbation theory is used to examine the conditions under which the current distribution becomes unstable in the thin annulus of rock melt at the leading edge.

b. Leading Edge Analysis. It is necessary to resort to the computer model to determine the

temperature profile across the melt layer during steady-state advance and energy deposition. The temperature dependence of the electrical resistivity of the melt is given by

$$\rho = \rho_o \, e^{\left(+\frac{\beta}{T}\right)} .$$

Velocity effects make the one-dimensional model intractable unless simplifying assumptions are made. An energy deposition routine was installed in AYER to deposit power in the melt layer at the leading edge of an insulated penetrator. The assumption is made that the voltage gradients are parallel to the surface of the insulated tip. Then, with the total melt current specified, the current density distribution across the melt layer and the local power density, $i^2\rho$, can be determined. The calculations then include the effects of the temperature-dependent power deposition and melt velocity field on the heat transfer and hydrodynamic force solutions. For direct comparison with a conventional penetrator, the HARE geometry was used. An insulating nose insert with the properties of boron nitride replaces the conventional molybdenum leading edge. This geometry is illustrated in Fig. V-18 where item A is the boron nitride insert.

The case to be considered first is that of an adiabatic leading edge. In these calculations the heater was adjusted to provide a zero temperature gradient at the surface of the boron nitride. This can be seen in Fig. V-19 where the calculated temperature is plotted as a function of distance from the penetrator surface at the position labeled B in Fig. V-18. Curves 2 through 5 in Fig. V-19 are for the velocities indicated, and the melt power has been adjusted to give a maximum temperature at B of approximately T_s = 1950 K. The outside of the melt layer is at T_m = 1450 K, the center of the melting range of basalt. Curve 1 of Fig. V-19 is for a velocity of 0.15 mm·s^{-1} with no melt heating. Here the maximum molybdenum temperature (~1900 K) occurs at the inside surface of the metal body, and the temperature is close to linear with position. To facilitate a comparison of the two cases it is noted that with melt heating the AYER temperature profiles can be fitted closely with the parabola

$$T = T_S - (T_S - T_m)\left(\frac{y}{\ell}\right)^2 ,$$

which is plotted as the dashed curves in Fig. V-19. Then, approximately

$$\left.\frac{dT}{dy}\right|_{y=\ell} = -\frac{2(T_S - T_m)}{\ell} , \qquad (V\text{-}9)$$

and the conductive flux is twice that of the almost linear, no melt-heating case at the melt-rock interface. The mass-averaged temperature is

$$\bar{T} = T_S - \frac{(T_S - T_m)}{3} , \qquad (V\text{-}10)$$

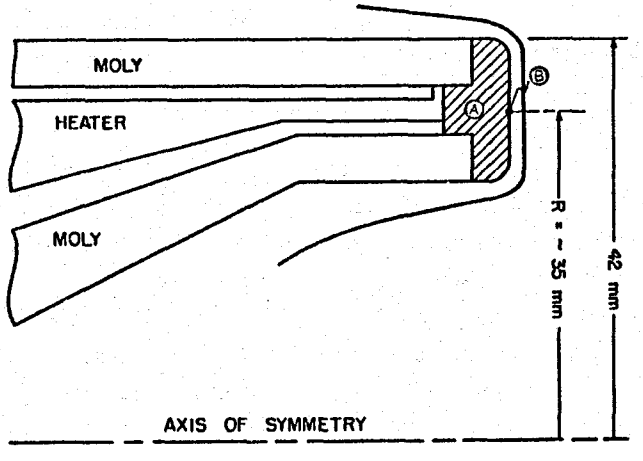

Fig. V-18. Penetrator geometry for melt-heating analysis.

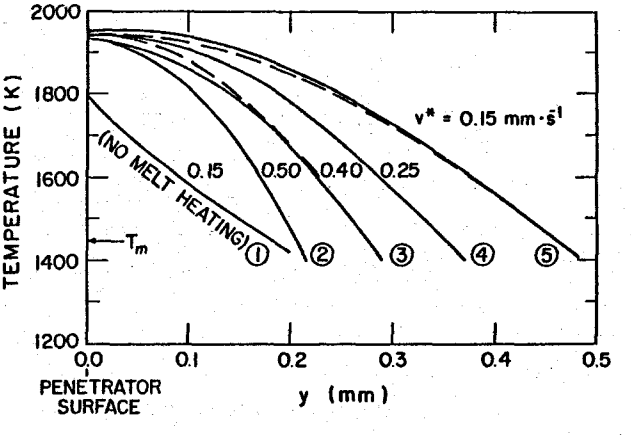

Fig. V-19. Calculated melt layer temperature profiles as a function of penetration velocity with and without melt heating.

whereas, for the linear case it is

$$\bar{T} = T_S - \frac{(T_S - T_m)}{2} \quad , \qquad (V\text{-}11)$$

which is somewhat lower. With the use of Eqs. (V-9), (V-10), and (V-11) the expected reduction in the leading edge force at a given velocity can be obtained. For example, consider the curves 1 and 5 of Fig. V-19 for a penetrator velocity of $v^* = 0.15$ mm·s^{-1}. From Eq. (V-10) we have for the melt heat case, $\bar{T} \sim 1800$; for curve 1, Eq. (V-11) gives $\bar{T} \sim 1625$. The effective viscosity for melt heating can be a factor of 4 down from the conventional case. Also, Eq. (V-9) shows that for a given flux at the melt-rock interface, and hence for a given velocity, the melt layer is approximately twice as thick for the melt-heating case. Since the force scales as ℓ^{-3} and as $\bar{\mu}$, a given velocity with melt heating could require a thrust force as little as 1/32 of that required without melt heating. In fact, AYER and simple model calculations predict even lower thrusts.

The situation is illustrated in Fig. V-20, which is a plot of force versus advance rate. The performance map for the conventional HARE penetrator is repeated in the upper left corner. The closed curve brackets the experimental performance for various basalt samples and melting body powers. The points [M] are calculated with the simple model of Sec. C. 2 and include only the leading edge component of the force, given by

$$F = 8\pi R\, \bar{\mu} \left(\frac{L}{\ell}\right)^3 \quad . \qquad (V\text{-}12)$$

The points [A] and (A) are the AYER results for the leading edge and total forces corresponding to the melt temperature profile of curve 1 in Fig. V-19. For most conditions the leading edge force is proportional to the fourth power of the velocity for a constant leading edge temperature. The dashed lines in Fig. V-20 connect points scaled by $F \propto v^{*4}$. The calculated performance of a HARE with melt heating in basalt is also plotted in Fig. V-20 with the same nomenclature as the conventional case. A second result of AYER at $v^* = 0.5$ mm·s^{-1} for a lower surface temperature (1850 K) is shown. For the melt heating

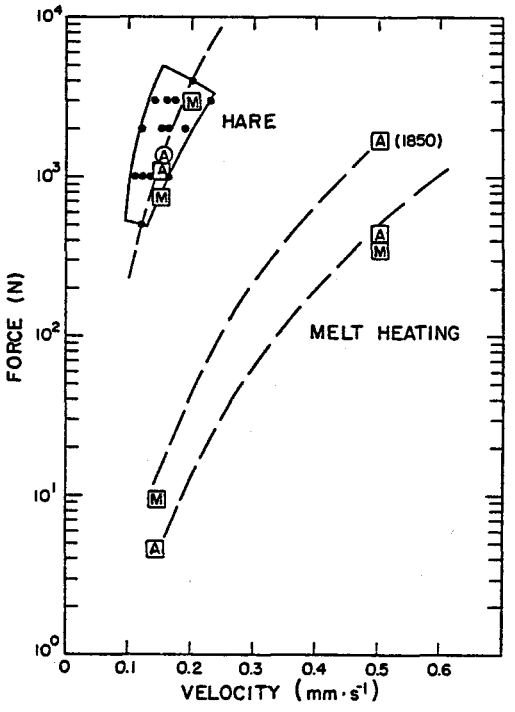

Fig. V-20. Thrust force as a function of penetration velocity with and without melt heating.

case the values of ℓ used in Eq. (V-12) are taken from the AYER calculations. Because of the broad maximum in the temperature curve, ℓ is not as sensitive to the surface temperature as in the linear case. In practice, maintaining any given velocity requires an accurate control of thrust and internal and melt powers. The upper dashed curve was obtained by scaling the point [A] (1850 K) with $F \propto v^{*4}$ and represents a more conservative operating temperature. If a uniform melt layer and power deposition can be maintained, it should be possible to obtain performance between the two curves without overheating the penetrator tip.

c. Instabilities in the Current Distribution.

The temperature dependence of the resistivity gives rise to a power density in the melt that is sensitive to the temperature. If the voltage gradient is constant, the power density increases with increasing temperature. If the current density is constant, the power density ($p = i^2 \rho$) decreases with increasing temperature. We are now concerned with the effects of this on the current and temperature distribution in a thin melt layer bounded by the insulating penetrator leading edge, the rock-melt interface, and

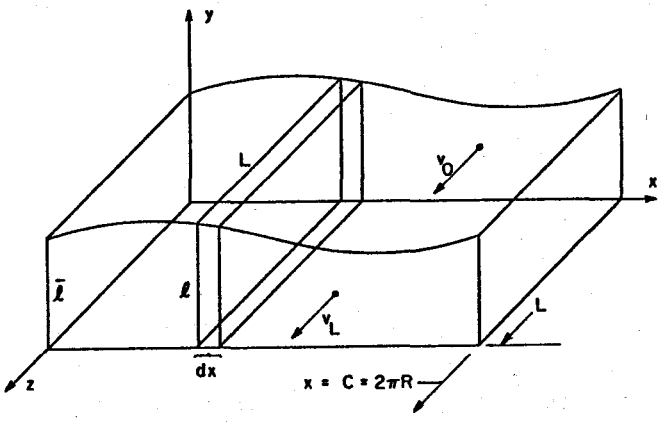

Fig. V-21. Rectangular model used for current stability analysis.

the electrodes. We will consider a rectangular model which applies to the annular penetrator with R >> L. In Fig. V-21 the penetrator surface is at y = 0, the melting interface at y = $\bar{\ell}$, and the electrodes are at z = 0 and z =L. For any such pair of electrodes only the voltage V and the total current I can be regulated.

By an instability we mean a local change τ in temperature, whose magnitude increases with the time, from the value $\bar{T}$ of the average melt layer temperature required for a steady-state velocity of v*. $\bar{T}$ is an average over the melt layer

$$\bar{T} = \frac{1}{m}\int_{\text{melt layer}} T\, dm \quad .$$

These instabilities can occur since a local increase in temperature lowers the resistivity, which results in higher current density and power density, which in turn continues the increase in temperature. This can cause an uncontrolled increase of temperature throughout the melt layer (thermal runaway) or the occurrence of local high-current channels. As will be seen, for voltage control both thermal runaway and channeling will be more likely than for current control. If the total current is constant, the local current density can vary and produce channeling; however, thermal runaway is prevented. To determine the quantitative conditions for the onset of the growth of instabilities for the condition of constant total current, we will use small-amplitude temperature perturbation theory; that is $\tau << \bar{T}$.

Such a treatment applies only when the instabilities begin but provides no information on the large amplitude limit. The conditions for growth will depend on the power deposition and the damping effects of the conduction and convection losses.

The following assumptions are made:

1. Sinusoidal perturbations
2. Conduction losses from sides (z = 0, L) are neglected
3. Adiabatic condition at melt-rock interface
4. Melt layer has no inhomogeneities.

The conservation of energy gives, for the volume element $\ell L\, dx$

$$\int \rho C \frac{\partial T}{\partial t}\, dV = \int \dot{q}\, dV + \int F \cdot dA + \int \rho C\, Tv \cdot dA$$

$$d\dot{E} = d\dot{Q} + dP_f + dP_v \quad . \qquad \text{(V-13)}$$

We assume the temperature is of the form

$$T = \bar{T} + T_1\, e^{\alpha t} \sin \omega x = \bar{T} + \tau \qquad \text{(V-14)}$$

where

$$\tau << T \quad .$$

The growth rate α can then be evaluated. From Eq. (V-14)

$$\alpha = \frac{1}{\tau}\frac{\partial T}{\partial t} \quad .$$

Writing $d\dot{E}$ approximately as

$$d\dot{E} = \rho C \frac{\partial T}{\partial t}\, \ell L\, dx$$

we obtain from Eq. (V-13)

$$\alpha = \frac{1}{\tau \rho C}\left(\frac{d\dot{Q}}{dV} + \frac{dP_f}{dV} + \frac{dP_v}{dV}\right) \quad . \qquad \text{(V-15)}$$

Each term on the right will consist of a steady-state term and a contribution to the growth rate: so

$$\alpha = \alpha_q + \alpha_f + \alpha_v \quad ,$$

and the steady-state terms must cancel,

$$\left(\frac{d\dot{Q}}{dV} + \frac{dP_f}{dV} + \frac{dP_v}{dV}\right)_{SS} = 0 \quad .$$

The growth rates and the steady-state terms are determined by an expansion of each term of Eq. (V-15) in a power series in τ. The zero-order terms represent the steady state, and the remaining terms give the growth rates. For small-amplitude theory only the first-order terms in τ are retained. Generally, α_q resulting from the power deposition will be positive; α_f and α_v resulting from conduction and convection losses will be negative. The procedure is straightforward and will only be outlined here.

For the power deposition term the temperature-dependent resistivity is expanded, and it is assumed that the total current can be held constant by external control. This results in a growth rate of

$$\alpha_q = \frac{nv^*}{\ell}\left(1 - \frac{2\lambda}{C}\right) \quad . \qquad \text{(V-16)}$$

Here $n = \beta/\overline{T}$, $\lambda = 2\pi/\omega$ is the perturbation wavelength, v^* is the advance rate, ℓ is the melt layer thickness, and C is the circumference of the annulus. The second term in Eq. V-16 is the damping provided by the constant-current condition. It is not significant for perturbations small in extent compared to the circumference of the penetrator. The melt layer thickness (ℓ) can be determined by equating the conductive flux to the mass-velocity flux at the melt-rock interface. Then, for basalt with T_m = 1450 K and a penetrator surface temperature of T_s = 2000 K

$$\alpha_q = \frac{n\rho C v^{*2}}{K_\ell} \quad ,$$

where K_ℓ is the thermal conductivity of the melt.

The power density in the element due to heat flux can be separated into conductive and radiative parts and into x and y components. For the power loss by conduction to the rest of the melt layer (x-direction),

$$\frac{dP}{dV} = \nabla\cdot F_x = K_\ell \frac{d^2T}{dx^2} = - K_\ell \omega^2 \tau \quad .$$

This is the only term sensitive to the shape of the instability. There is no steady-state contribution, and the growth rate, in this case negative, is

$$\alpha_K = - \frac{\omega^2 K_\ell}{\rho C} \quad .$$

It can also be shown that the inclusion of a radiation conductivity results in no additional first-order terms, and the equilibrium value of the radiation conductivity can be included in K_ℓ. Even though the penetrator temperature is maintained so that there is no heat exchange with the melt layer in steady state, conduction from the instability to the penetrator can provide some damping. The power density loss is

$$\frac{dP_p}{dV} = \frac{F_p(\tau)}{\ell} \quad .$$

The flux $F_p(\tau)$ depends on the y-dependence of τ and on the properties of the penetrator tip. However, the thermal resistance of the penetrator tip will dominate, and for an appropriately chosen conduction length (Λ) for the insulator, the damping rate becomes

$$\alpha_p \simeq - \frac{9}{4}\frac{K_p}{K_\ell}\frac{v^*}{\Lambda} \quad .$$

The next significant term results from the mass flow (in the z-direction) across the layer

$$dP_v = \rho C(v_L T_L - v_o T_o)\ell dx \quad . \qquad \text{(V-17)}$$

Considering first the HARE geometry, v_o = 0, and assuming that the same perturbation applies to T_L as to T, we have

$$\alpha_v \simeq - \frac{3}{2}\frac{\rho C}{K_\ell} v^{*2} \quad .$$

To this point only temperature perturbations have been considered. However, since temperature profiles can be established across the gap in a time short compared to the risetime of temperature perturbations, it will be assumed that ℓ and T_s retain the relationship

$$\ell = \frac{2K_\ell\,(T_s - T_m)}{\rho C\; v^*\; \delta T} \quad .$$

This results in a positive contribution to α of

$$\alpha_{v\ell} \simeq \frac{9}{2}\,\frac{v^*}{\ell} \quad ,$$

which for basalt and v* in mm·s^{-1} is

$$\alpha_{v\ell} = 81\; v^{*2} \quad .$$

This is the only term resulting from this combined mode; however, as seen in the graph of Fig. V-22, it contributes significantly to the onset of instabilities.

If the geometry of the penetrator is such that v_o in Eq. (V-17) is not zero, two other effects need be considered. For a constant $v_o = \bar{v}_o$ the power lost per unit volume becomes

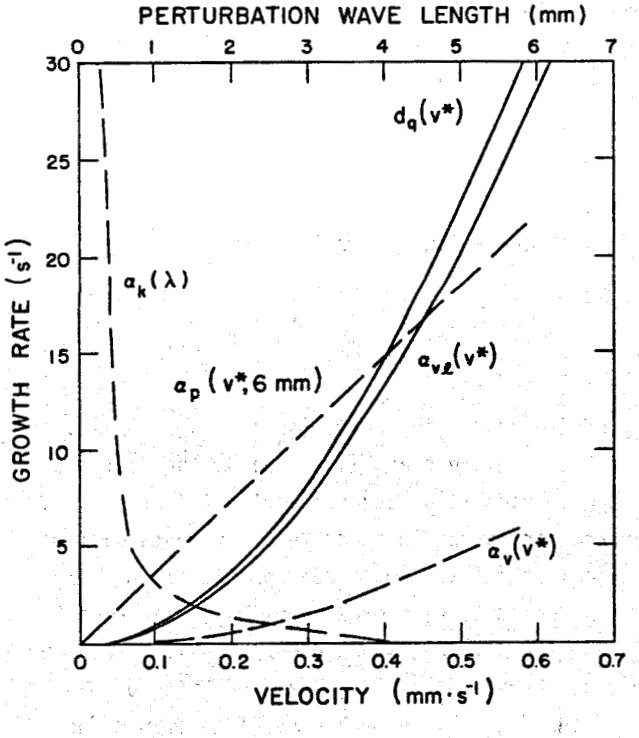

Fig. V-22. Small-amplitude instability growth rates --HARE configuration in basalt.

$$\frac{dP_v}{dV} = -\frac{\rho C}{L}\,(v_L\,\bar{T} - \bar{v}_o\,T_o) - \frac{\rho C}{L}\,v_L\,\tau \quad .$$

The additional term in $dP_v/dV\big|_{SS}$ necessitates an increase in dQ/dV to maintain the steady-state velocity v*. The corresponding increase in α_q is

$$\Delta\alpha_q = n\,\frac{\bar{v}_o}{L}\,\frac{\bar{T} - T_o}{\bar{T}} \quad .$$

Further damping is provided by the new term in α_v. The size of these terms is determined by v_o, which depends on the geometry and the advance rate. For convenience m is defined as

$$m = A_R/2\pi\; R\; L \quad ,$$

where A_R is the area through which rock enters the reservoir and 2π R L is the approximate frontal area of the leading edge. Then

$$\alpha_v = -\frac{v^*}{\ell}\,(1 + m)$$

and

$$\Delta\alpha_q = nm\,\frac{v^*}{\ell}\,\frac{\bar{T} - T_o}{\bar{T}} \quad .$$

If the melt enters the gap at a high temperature, where $T_o \sim \bar{T}$, then $\Delta\alpha_q \sim 0$, and considerable damping is provided by the new term in α_v for geometries with $m > 1$.

Another damping effect can occur because of the temperature dependence of the viscosity. As the local temperature rises the decreased viscosity will result in an increase of melt velocity if the pressure drop across the melt layer is constant. An upper limit to the size of this effect can be obtained if it is assumed that the pressure in the reservoir is constant. This can be true if the dimensions of the reservoir are large enough and the flow velocities and viscosity in the reservoir are low enough. In this case the upper limit to the

damping rate contributed by the viscosity is, with s = 15 for basalt,

$$\alpha_\mu \approx - \frac{smv^*}{\ell} \frac{\bar{T} - T_o}{\bar{T}} ,$$

where

$$\mu = \mu_o e^{\frac{S\bar{T}}{\bar{T}}}$$

and

$$S = \frac{\alpha}{\bar{T}} .$$

For $\hat{T}$ = 2000 K and since $T_o \sim T_m$, $(\bar{T} - T_o)/\bar{T} \simeq 1/6$. The sum of the contributions to the growth rate due to velocity would then be

$$\alpha_v = - \frac{v^*}{\ell} \left(1 + m + \frac{1}{6} sm - nm\right) = - \frac{v^*}{\ell} \left(1 + \frac{11}{6} m\right) . \quad \text{(V-18)}$$

The size of the various growth rates in basalt are compared in the graph of Fig. V-22. The solid curves are the positive rates that lead to instability, and the dashed curves are the negative or damping terms. The conduction damping term $\alpha_K(\lambda)$ is significant only for small wavelengths ($\sim$ 1.0 mm). Only the velocity damping for v_o = 0 is plotted and is small compared to the positive term for all v*. The damping $\alpha_p(v^*, \Lambda)$ due to the conductivity of the penetrator tip, here taken to have the properties of boron nitride, depends on the choice of the conduction length, Λ. In Fig. V-22 Λ = 6 mm is chosen as a reasonable thickness for the boron nitride, which connects the melt layer to the molybdenum penetrator, which is at a uniform temperature because of the high thermal conductivity. For this case the sum of the positive terms, $\alpha_q(v^*)$ and $\alpha_{v\ell}(v^*)$, dominate the sum of the negative terms for some range of λ and for $v^* \sim 0.3$ mm·s^{-1}. The second term in α_v as given by Eq. (V-18) can, in principle, provide stability under most circumstances. However, this equation represents only an upper limit.

A number of experiments have been performed which examine the characteristics of electrical energy deposition in a basalt melt flowing through an annular gap between two pieces of boron nitride. The application of the foregoing theory to the stability of the current configuration in such experiments requires that certain modifications be made. Since the melt layer cannot grow in thickness, we have $\alpha_{v\ell} = 0$. The only positive contribution to the growth rate is

$$\alpha_q = \frac{n}{\rho C \bar{T}} \frac{dQ}{dV} .$$

However dQ/dV is not determined by the melting power relation but is given by

$$\frac{\dot{dQ}}{dV} = \frac{\rho C v_L}{L} (\bar{T} - T_o) ,$$

so that

$$\alpha_q = n \frac{v_L}{L} \frac{\bar{T} - T_o}{\bar{T}} .$$

However, in the temperature range applicable to penetrators in basalt n $\approx$ 5, T_o > 1450 K and $\bar{T} \sim$ 2000 K. Then

$$\alpha_q \approx \frac{v_L}{L}$$

and, with the velocity damping term

$$\alpha_q + \alpha_v \approx \frac{v_L}{L} - \frac{v_L}{L} = 0 .$$

Any of the conduction terms ($\alpha_K < 0$, $\alpha_p < 0$) and $\alpha_\mu < 0$ can insure stability. Unless the melt is heated to high temperatures such that $\bar{T} >> T_o$, the current configuration in these experiments will be stable in the small-amplitude approximation.

A second type of experiment was an attempt to examine the melt-heating process visually. Concentric graphite electrodes, separated by a boron nitride insulator, were heated by rf to 1770 K and were brought in contact with a stack of transparent Pyrex disks. A 60-Hz voltage was impressed across the electrodes, and when current flow in the melt was indicated, a slow penetration was started. The action

at the electrodes was photographed through the Pyrex disks. Since the rather slow (0.1 $mm \cdot s^{-1}$) forward velocities achieved were probably determined by the electrode temperatures and not the melt heating in front of the boron nitride, and since the melt layer thickness was not determined, a quantitative application of the foregoing theory cannot be made. However, during some of these experiments, bright, radial, high-temperature filaments were observed and photographed between the electrodes. It is possible that this was a high-amplitude phase of an unstable discharge in the melt. Further experiments of this type are needed.

6. Power Transmission Analysis of Subterrene Stem. The properties of the Subterrene drill stem that affect the electrical power transmission to the penetrator heater have been investigated. This consisted of a consideration of material properties, the resulting electrical properties of two stem configurations, and sample calculations of the fraction of transmitted power available to heat the penetrator. Because of the generally high currents resulting from the low resistances of existing and proposed heaters, only stem designs in which the structural members are also conductors were considered. One such configuration is illustrated in Fig. V-23. It consists of concentric aluminum cylinders insulated from one another and providing downward and return conduction paths. In the other configuration the center conductor was replaced by a number of copper cables.

For each type of stem, the direct- and alternating-current (to 10^4 Hz) transmission properties were determined. These analyses included the following effects:

- Temperature-dependent electrical properties of the conducting structural members (aluminum, copper, and steel).
- Effects of ground conduction in parallel with the outer return conductor.
- Contact resistance at the drill stem joints.
- Properties of possible insulators and drilling fluids and the effects on the leakage conductance.

These considerations resulted in an expected range of distributed parameters, characteristic impedances, and attenuation constants. The efficiency of a number of combinations of drill stems and melting body heaters were calculated as a function of hole depth. An example of the efficiency versus depth for the configuration depicted in Fig. V-23 is shown in Fig. V-24. Here the alternating-current

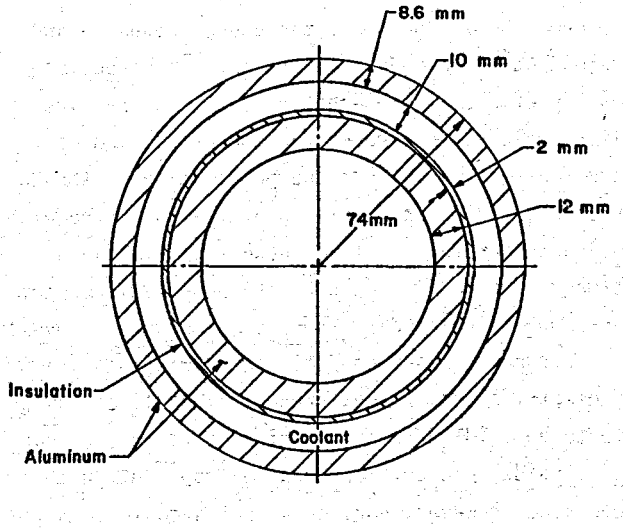

Fig. V-23. Cross section of proposed Subterrene drill stem utilizing concentric aluminum conductors.

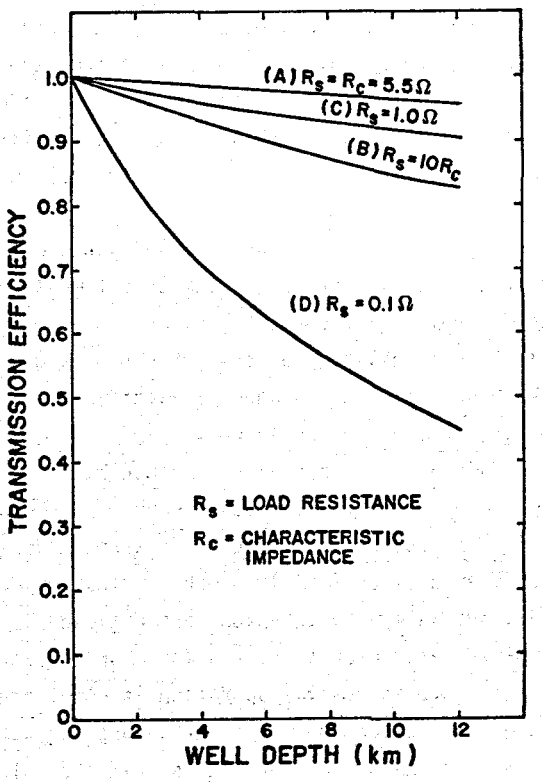

Fig. V-24. Power transmission characteristics of a Subterrene stem as a function of depth and load resistance.

characteristics have been used, and good insulation and negligible contact resistance were assumed. If the characteristic impedance (R_c) and the load (R_s) are matched, perhaps through a downhole transformer, negligible transmission losses result (curve A) even at depths of 12 km. For higher or lower loads the efficiency lessens (curves B and C). At heater resistances below 0.1 Ω, which is typical of present laboratory penetrators, the efficiency is below 0.5 at 10 km. The design direction for deep Subterrene systems would dictate the need for higher resistance heating elements with the prospects of high transmission efficiencies for load resistances above 1 Ω.

D. Applications and Technology Transfer

The basic notion of developing an excavation tool based upon the melting of rocks and soils was generated by the need for very deep drilling as proposed in the original Mohole Project. The rock-melting idea recognized that very deep in the earth extremely high temperatures -- approaching rock melting points -- would be encountered. Therefore a tool that formed the borehole by melting could uniquely solve this problem.

For the general field of drilling and excavation technology, clearly delineating some of the major problem areas was a straightforward task. To name only a few, the following problems seemed significant:

- High costs associated with geothermal energy drilling.
- High costs associated with drilling deep wells, particularly as a result of trip time spent making downhole equipment changes.
- Hole stability problems in weak caving ground.
- High cutter costs and low lifetime when boring in very hard abrasive rock.
- Maintaining a sustained advance rate when boring in wet and variable loose ground.

With the Subterrene concept the three major facets of excavation, namely, rock fracturing, debris removal, and wall stabilization, are attacked in a single, integrated operation. In loose or porous formations the debris removal operation is eliminated by density consolidation. Another unique advantage of the Subterrene system concept is that the holes are automatically lined with a hard glass-like material. It may thus be possible to eliminate the costly and time-consuming procedure of inserting and cementing metal casings typically associated with wells drilled with rotary bits.

Studies made at Los Alamos combined with a survey of potential users in industry have revealed a large number of potential applications of the Subterrene. The system's inherent ability to make holes of precise diameter could be utilized in producing holes for anchoring structures such as bridges, TV towers, and transmission line towers. Emplacement holes for anchoring pipeline supports could be readily melted in difficult materials such as Alaskan permafrost. Loose gravel and other unconsolidated formations are difficult to drill and stabilize with conventional rotary equipment. The Subterrene, which would leave a glass-lined hole, provides a solution to this difficulty. Conversely, hard, abrasive rocks can also be penetrated because the melting temperature, not the hardness or abrasiveness, determines the usefulness of the Subterrene.

Particular interest in small-diameter, horizontal, glass-lined holes motivated a separate study, which has been completed. These small horizontal borings can be used as underground utility conduits for the installation of telephone, gas, water, and television lines; as glass-lined holes for high-explosive shot emplacement; and as drainage holes to stabilize roadcuts and embankments. The study indicates that hole straightness requirements can be met by adding deviation sensors and alignment-control units to the hole-forming assembly.

From the viewpoint of the energy research and development programs at Los Alamos, two potential uses are of special interest. The first involves melting holes in hot rocks for the extraction of geothermal energy. Since the penetration of the Subterrene depends on the melting of the rock, the high *in situ* temperatures will be beneficial in saving thermal energy and increasing the penetration rate. The second is related to the LASL program for developing underground superconducting transmission lines for electrical power. At present, such lines would have to be laid in trenches which could only be dug with considerable environmental disruption. With a Subterrene, however, horizontal holes could be melted with a minimum disturbance of the ground surface.

The technology dissemination efforts expended by members of the Subterrene program at Los Alamos have

been extensive in both scope and depth. Approximately 60 technical papers and reports have been written by the project staff on all phases of Subterrene activities for distribution and presentation at various technical society meetings. These reports continue to be in demand and are forwarded to all interested organizations and individuals. A substantial number of technical briefings have been presented to interested individuals and groups by the Subterrene staff throughout the program. Interested individuals and groups include members of the United States Congress, representatives of major industrial concerns, representatives of the armed forces, utility and power distribution specialists, drilling and oil-field specialists, university professors, professional engineers, and college students. For use at meetings which cannot be attended by a member of the staff, a short documentary color film on the Subterrene concept has been produced which utilizes technical animation to illustrate the basic operating concepts.

Initial impact in the area of public demonstrations has been achieved through the use of a mobile Subterrene field-demonstration unit which performed successfully before several groups in Washington, DC. The demonstrations were held at the U.S. Army's Engineering Proving Grounds quarry area at Fort Belvoir, VA. Among the estimated 300 persons who attended one of the four scheduled demonstrations were representatives from Congress, U.S. Government agencies, the news media, equipment manufacturers, and excavation firms. A similar demonstration was conducted shortly thereafter at the Denver Federal Center in Denver, CO. A Subterrene field-demonstration unit was sent to the city of Tacoma, WA, to participate in their Technology Transfer Field Days Demonstration at their request. After performing for the general public, the unit was viewed and operated by personnel associated with underground utility emplacements. Such demonstrations, particularly when they involve the production of useful holes by nonlaboratory work crews, are felt to be significant advances in the technology transfer arena. A brief summary of these activities is presented in Table V-6.

TABLE V-6
LASL INITIATIVES IN TECHNOLOGY
DISSEMINATION AND TRANSFER

Documentation	Briefings	Advisory Panels	Demonstrations
LASL reports	Technical society presentations	Geosciences advisory panel	Rock melting demonstrations for visitors at LASL
Technical society reports	All interested visitors to LASL	Industrial staff members	Washington, DC field demonstrations
Extensive mailing list for reports	Visiting lecture tours	National Science Foundation program managers	Denver Federal Center field demonstrations
Applications survey letters	Prospective funding agency briefings	ERDA program managers	Tacoma, WA Technology Transfer Field Days
Journal covers and articles		Internal LASL staff reviews	Drainage holes at Bandelier National Monument
Subterrene films			
Replies to industrial inquiries			

Displays exhibiting examples of Subterrene rock-melting penetrator systems, glass-lined holes, rock-melted debris samples, and technical reports were prepared for the First Houston Technology Transfer Conference in Houston, TX, and the 1974 Annual Meeting of the Association of Engineering Geologists in Denver, CO. Technical papers on Subterrene technology were presented at each of these meetings. Permanent display samples were prepared for the American Museum of Atomic Energy in Oak Ridge, TN, and Subterrene hardware and posters were included in the current ERDA traveling exhibit on geothermal energy.

In conclusion it appears that all of the preliminary steps in achieving the transfer of a new technology have been accomplished by the Subterrene staff. The technical needs were identified in depth, the applicable technology was directed toward the development and testing of a new system, and a vast program in technology dissemination was implemented. To complete this process, a large-scale commercial utilization of the technology is required.

VI. TECHNICAL REPORTS AND PRESENTATIONS

Copies of the reports listed below can be obtained from:

National Technical Information Service (NTIS)
U.S. Department of Commerce
5285 Port Royal Road
Springfield, VA 22151;

the completed reports are identified by their LA-MS number by NTIS.

Discussions of the technical reports can be directed to individual authors at:

University of California
Los Alamos Scientific Laboratory
P. O. Box 1663
Group Q-DO, MS-570
Los Alamos, NM 87545
Telephone: (505) 667-6722

A. COMPLETED LASL TECHNICAL REPORTS

LASL Report No.	Title	Author(s)
LA-5354-MS	Systems and Cost Analysis for a Nuclear Subterrene Tunneling Machine - A Preliminary Study. (September 1973).	J. H. Altseimer
LA-5422-MS	A Versatile Rock-Melting System for the Formation of Small-Diameter Horizontal Glass-Lined Holes (October 1973).	D. L. Sims
LA-5423-MS	Carbon Receptor Reactions in Subterrene Penetrators (October 1973).	W. A. Stark, Jr. M. C. Krupka
LA-5435-MS	Rock Heat-Loss Shape Factors for Subterrene Penetrators (October 1973).	G. E. Cort
LA-5459-SR	Rapid Excavation by Rock Melting -- LASL Subterrene Program -- December 31, 1972 to September 1, 1973 (November 1973).	R. J. Hanold
LA-5211-MS	Subterrene Electrical Heater Design and Morphology (February 1974).	P. E. Armstrong
LA-5502-MS	Heat Transfer and Thermal Treatment Processes in Subterrene-Produced Glass Hole Linings (February 1974).	A. C. Stanton
LA-5517-MS	Conceptual Design of a Coring Subterrene Geoprospector (February 1974).	J. W. Neudecker
LA-5540-MS	Selected Physiochemical Properties of Basaltic Rocks, Liquids and Glasses (March 1974).	M. C. Krupka
LA-5573-MS	Development of Mobile Rock-Melting Subterrene Field Unit for Universal Extruding Penetrators (April 1974).	J. E. Griggs
LA-5608-MS	Numerical Solution of Melt Flow and Thermal Energy Transfer for the Lithothermodynamics of a Rock-Melting Penetrator (May 1974).	R. D. McFarland
LA-5613-MS	The AYER Heat Conduction Computer Program (May 1974).	R. G. Lawton
LA-5621-MS	PLACID: A General Finite-Element Computer Program for Stress Analysis of Plane and Axisymmetric Solids (May 1974).	R. G. Lawton
LA-5689-MS	Geothermal Well Technology and Potential Applications of Subterrene Devices - A Status Review (August 1974).	J. H. Altseimer
LA-5826-MS	Characterization of Rock Melts and Glasses Formed by Earth-Melting Subterrenes (January 1975).	L. B. Lundberg

LASL Report No.	Title	Author(s)
LA-5857-MS	Chemical Corrosion of Molybdenum and Tungsten in Liquid Basalt, Tuff, and Granite with Application to Subterrene Penetrators (February 1975).	W. A. Stark, Jr. M. C. Krupka
LA-5838	Petrography and Chemistry of Minerals and Glass in Rocks Partially Fused by Rock-Melting Drills (September 1975).	S. N. Ehrenberg Priscilla Perkins M. C. Krupka
LA-6038-MS	Unique Refractory Techniques for Fabricating Subterrene Penetrators (September 1975).	W. C. Turner
LA-6135-MS	Rock Property Measurements Pertinent to the Construction of Drainage Systems at Archeological Sites in Arizona by Subterrene Penetrators (November 1975).	G. M. Pharr
LA-6265-MS	Development of Coring, Consolidating, Subterrene Penetrators (March 1976).	H. D. Murphy J. W. Neudecker G. E. Cort W. C. Turner R. D. McFarland J. E. Griggs
LA-6555-MS	Technical and Cost Analysis of Rock Melting Systems for Producing Geothermal Wells (November 1976).	J. H. Altseimer

B. TECHNICAL PRESENTATIONS AND JOURNAL ARTICLES

	Conference on Research in Tunneling and Excavation Technology (Abstract and Presentation)	
J. C. Rowley	Rapid Excavation by Rock Melting	NSF, Wayzata, MN, September 14-15, 1973
	15th Symposium on Rock Mechanics (Presentation and Paper)	
R. J. Hanold	The Subterrene Concept and its Role in Future Excavation Technology	U.S. National Committee on Rock Mechanics, Custer, SD, September 17-19, 1973
	26th Pacific Coast Regional Meeting (Abstract and Presentation)	
M. C. Krupka	Refractory Material and Glass Technology Problems Associated with the Development of a Rock Melting Drill.	American Ceramic Society, San Francisco, CA, October 31-November 2, 1973
	Tunnels & Tunnelling Magazine (Invited Article)	
J. H. Altseimer	Subterrene Rock Melting Devices	British Tunnelling Society, January-February 1974
	University of Wyoming (Invited Presentation)	
J. C. Rowley	Rock Melting and Geothermal Energy	Laramie, WY, April 25, 1974
	Geotechnical Eng. Group & Association of Eng. Geologists Joint Meeting (Invited Presentation)	
R. J. Hanold	The LASL Subterrene Concept	Los Angeles, CA, May 30, 1974

	Rapid Excavation & Tunneling Conference (Presentation and Paper)	
J. C. Rowley R. J. Hanold C. A. Bankston J. W. Neudecker	Rock Melting Subterrenes - Their Role in Future Excavation Technology	American Inst. of Mining Engineering, San Francisco, CA, June 24-27, 1974
	Petroleum Engineer (Journal Article)	
D. L. Sims	Melting Glass-Lined Holes: New Drilling Technology	July 1974
	Journal of Vacuum Science and Technology (Article)	
W. A. Stark, Jr., et al	Application of Thick Film and Bulk Coating Technology to the Subterrene Program	American Vacuum Society, Vol. 11, No. 4, July-August 1974
	3rd International Congress ISRM (Presentation and Paper)	
J. C. Rowley	Rock Melting Applied to Excavation and Tunneling	International Society for Rock Mechanics, Denver, CO, September 2-7, 1974
	NATO Committee on Challenges of Modern Society (Presentation)	
C. A. Bankston	The Los Alamos Scientific Laboratory Subterrene Project and It's Applications to Geothermal Energy	NATO, Los Alamos, NM, September 18, 1974
	Conference on Research for Development of Geothermal Resources (Presentation and Paper)	
J. C. Rowley	Rock-Melting Technology and Geothermal Drilling	NSF, JPL, CIT, Pasadena, CA, September 23-25, 1974
	NASA - Houston Technology Transfer Conference (Presentation and Paper)	
R. J. Hanold C. A. Bankston J. C. Rowley W. W. Long	The Initiatives of the Los Alamos Scientific Laboratory in the Transfer of a New Excavation Technology	Houston, TX, September 24-25, 1974
	Earth & Planetary Sciences Group-Johnson Space Flight Center (Presentation)	
R. J. Hanold	The Los Alamos Subterrene Program and its Role in Geothermal Energy Development	NASA, Houston, TX, September 26, 1974
	17th Annual Meeting, Association of Engineering Geologists (Abstract and Presentation)	
C. A. Bankston J. H. Altseimer	The Rock Melting Subterrene and its Potential Role in Geothermal Energy	AEG, Denver, CO, October 18, 1974
	AIAA/SAE 10th Propulsion Conference (Presentation and Paper)	
J. H. Altseimer J. D. Balcomb W. E. Keller W. A. Ranken	Nuclear Propulsion Technology Transfer to Energy Systems	AIAA/SAE, San Diego, CA, October 21-23, 1974
	1974 ASME Winter Annual Meeting (Presentation and Paper)	
R. D. McFarland R. J. Hanold	Viscous Melt Flow and Thermal Energy Transfer for a Rock-Melting Penetrator	ASME, New York, NY, November 18-22, 1974
	Tunnels & Tunnelling Magazine (Article)	
R. E. Williams	Soil Melting - A Practical Trial	British Tunnelling Society, January-February 1975
	1975 ASME Winter Annual Meeting (Presentation and Paper)	
H. N. Fisher	Thermal Analysis of Some Subterrene Penetrators	ASME, Houston, TX, November 30-December 4, 1975
	University of Colorado (Invited Presentation)	
J. H. Altseimer	The Subterrene Program and Geothermal Energy	Boulder, CO, December 2, 1975

C. REPORTS RELATED TO SUBTERRENE TECHNOLOGY PUBLISHED BY OTHER ORGANIZATIONS

1. Black, D. L., "Basic Understanding of Earth Tunneling by Melting," Prepared for U.S. Department of Transportation by Westinghouse Astronuclear Laboratory, July 1974.

2. Bledsoe, J. D., Hill, J. E., and Coon, R. F., "Cost Comparison Between Subterrene and Current Tunneling Methods," Prepared for National Science Foundation by A. A. Mathews, Inc., May 1975.

3. Black, D. L., "A Study of Borehole Plugging in Bedded Salt Domes by Earth Melting Technology," Westinghouse Astronuclear Laboratory, June 1975.

4. Nielsen, R. R., Abou-Sayed, A., and Jones, A. H., "Characterization of Rock-Glass Formed by the LASL Subterrene in Bandelier Tuff," Terra Tek, November 1975.

5. Muan, A., "Silicate-Metal Reactions with a Bearing on the Performance of Subterrene Penetrators," The Pennsylvania State University, August 1976.

6. St. John, C. M., "Stresses and Displacements Around Deep Holes in Hot Rocks," University of Minnesota, September 1976.

☆ U.S. GOVERNMENT PRINTING OFFICE 1977—777-018/14